AN AXON'S JOURNEY TO FIND ITS PATH: *IN VIVO* CHARACTERIZATION OF THE MODULATORS AND EFFECTORS OF THE RAC GTPASE SIGNALING PATHWAY INVOLVED IN AXON GUIDANCE

By

Rafael Sênos Demarco

Submitted to the graduate degree program in Molecular Biosciences
and the Graduate Faculty of the University of Kansas
in partial fulfillment of the requirements for the degree of
Doctor of Philosophy.

_____
Chairperson – Erik Lundquist

_____
Brian Ackley

_____
Victoria Corbin

_____
Stuart Macdonald

_____
Kristi Neufeld

_____
Lisa Timmons

_____
Jennifer Gleason

Date Defended: April 06, 2011

The Dissertation Committee for Rafael Sênos Demarco
certifies that this is the approved version of the following dissertation:

AN AXON'S JOURNEY TO FIND ITS PATH: *IN VIVO* CHARACTERIZATION OF THE MODULATORS AND EFFECTORS OF THE RAC GTPASE SIGNALING PATHWAY INVOLVED IN AXON GUIDANCE

_____
Chairperson – Erik Lundquist

Date approved: April 06, 2011

Abstract

The molecular mechanisms leading to axonal guidance are vital for the proper wiring of the nervous system. Many psychiatric disorders may arise from the improper development of the brain. If an axon does not form, or is extended to a place where it is not supposed to be, proper synapses will not form and communication between neurons and neighbor cells will be affected. An axon is extended after the migration of the growth cone. Filopodia and lamellipodia are extended from the growth cone in order to sense the environment for guidance cues. Once signaled, the growth cone migrates to its final target and the axon is developed. A class of proteins called the Rac GTPases is essential for the process of axon pathfinding.

In the model nematode *Caenorhabditis elegans*, MIG-2/RhoG and CED-10/Rac1 are the two redundant Rac GTPases involved in growth cone migration. The main role of Rac GTPases in axon guidance is due to its control over the actin cytoskeleton. The actin-binding UNC-115/abLIM acts downstream of CED-10/Rac1 in axon pathfinding. In Chapters II and III, I describe how Rac signaling activates UNC-115/abLIM. I propose that the scaffolding protein RACK-1 recruits UNC-115/abLIM to the plasma membrane and brings other molecules, such as PKC, for its modulation.

Rac GTPases switch between an inactive, GDP-bound form, to an active, GTP-bound form. Activation can be aided by guanine-nucleotide exchange factors (GEFs), and inactivation is enhanced by GTPase activating proteins (GAPs). UNC-73/Trio is a GEF that acts with both MIG-2/RhoG and CED-

10/Rac1 in axon guidance. Nevertheless, mutations that disrupt the Rac GEF activity of UNC-73/Trio do not affect axon pathfinding to the same levels as the abolishment of Rac activity seen in the double mutant of *mig-2* and *ced-10*. Along with other evidence, this suggested that there were other molecules involved in the control of Rac GTPases in this process.

I performed a candidate-based genetic screen in the *C. elegans* genome in order to find other DH-containing GEFs that could potentially interact with MIG-2/RhoG and CED-10/Rac1. In Chapter IV, I show that the Rac GEF TIAM-1 acts upstream of MIG-2/RhoG and CED-10/Rac1 as a linker between these GTPases and CDC-42, another member of the Rho subfamily of small GTPases. Moreover, previous studies have implicated Rac GTPases, but not UNC-73/Trio, in the UNC-6/Netrin attractive signaling system. I show that TIAM-1 is the GEF recruited for this system. In Chapter V I show that other GEFs are also involved in this process. The Rac GEF PIX-1/βPIX, and two CDC-42 GEFs, UIG-1/Clg and EXC-5/FGD1, are also involved in the control of Rac GTPases during axon development.

In summary, my work has shown how Rac GTPases control the activity of the actin-binding protein UNC-115/abLIM, and how Rac GTPases themselves are controlled during the process of axon guidance.

Acknowledgements

To pursue my dream of becoming a scientist, I had to give up on a lot. I had to leave my country and my family, and come to a place where I did not know anyone. I had to develop my language skills in order to better communicate, and I had to learn to become an independent person. My journey to the U.S. was only possible thanks to the immense love and support from my family and friends in Brazil. My mother, Silvia, and my father, Mauro, provided me with the emotional and financial support needed to live abroad. I also had to miss on most of the childhood/teenage years of my siblings, Fábio and Beatriz, in order to be away for so long. Though I missed them deeply, they cared for me throughout this time and I am very happy to see they have been very successful in their lives as well. My grandmothers, Carminha and Iracy, and great-aunt Laís, among with the rest of my family, were also constant supporters of this quest.

I also need to acknowledge the University of Kansas for providing me with the initial scholarship via which I came to study abroad in the U.S. In particular, I would like to thank Dr. Erik A Lundquist for his believe in my potential as a graduate student and for developing my research skills to a point in which I could think critically by myself and defend my doctorate. To all the members of the Lundquist lab – specially my class- and roommate Adam Norris – and members of Brian Ackley's lab, I would like to present my immense gratitude for all the great times together and helpful discussions. Finally, I would like to thank my graduate advisory committee members for all the helpful input they have provided me in my carreer.

Table of Contents

List of Figures

List of Tables

Chapter I

Introduction

Neurons are the main type of cells that constitute the nervous system. They are responsible for the storage and conduction of the electrical and chemical information necessary for the coordination and survival of an organism (Ghysen 2003). Neuronal cells are born out of neuroblasts, which are neuronal precursors that often migrate to a final destination and extend processes called neurites in order to contact other neurons or cells. Neurons typically consist of one or more dendrites (the neurites that typically receive information via chemical and electrical synapses), a cell body (which processes such information for further action), and one or more axons (which are the neurites that often conduct the processed information to synapse into a target cell) (Ghysen 2003). Neurites are formed early in neuron development. Neuroblasts typically polarize their intracellular machinery to determine where dendrites and axons will be formed. Once polarized, structures called growth cones are formed, and axons and dendrites start to develop (Marin, Valiente et al. 2010). In axon development and guidance, the growth cone protrudes lamellipodia (from Latin, sheet-like feet) and filopodia (thread-like feet) that are essential for its migration. These protrusions act as sensory and motile forces that guide the growth cone to its destination, leaving an extended neurite behind – the axon (Small, Stradal et al. 2002; Mattila and Lappalainen 2008).

In order to create lamellipodia and filopodia, neurons have to rearrange their peripheral actin cytoskeletons. Actin monomers can be assembled together in different fashions: in filopodia, actin filaments are bundled together (Mattila and Lappalainen 2008), while in lamellipodia these filaments are arranged in a 70^{o}

angle, creating an actin filament meshwork (Small, Stradal et al. 2002). Several actin-binding proteins, such as the Arp2/3 complex, Formins, UNC-115/abLIM, Capping and Anti-Capping proteins (i.e., UNC-34/Enabled) and many others have been previously implicated in protrusion formation and or dynamics (Korobova and Svitkina 2008; Matusek, Gombos et al. 2008; Norris, Dyer et al. 2009). These actin-modulating proteins contribute to axon development and guidance in overlapping or specific ways. Actin nucleators, such as the Arp2/3 complex, formins and possibly UNC-115/abLIM, contribute to protrusion formation by the polymerization of actin filaments. Arp2/3 nucleates actin filaments in a 70^{o} angle from the sides of previously assembled filaments (Suetsugu, Miki et al. 2002; Korobova and Svitkina 2008). Formins associate with the fast growing end of actin filaments, promoting their extension (Evangelista, Zigmond et al. 2003). Though the precise role of the actin-binding protein UNC-115/abLIM has not yet been determined, some evidence suggests it is a putative *de novo* actin filament nucleator (Lundquist, Herman et al. 1998; Garcia, Abbasi et al. 2007; Norris, Dyer et al. 2009; Demarco and Lundquist 2010). Capping and anti-capping proteins contribute to protrusion dynamics by regulating actin assembly in the growing tips of the filaments (Bashaw, Kidd et al. 2000; Aguda, Burtnick et al. 2005).

A class of molecules that is vital for growth cone migration and the control of the actin cytoskeleton is the Rac GTPases (Dickson 2001). Racs are members of the Rho subfamily of small GTPases. This family consists of Rac (Ras-related C3 botulinium toxin substrate), Rho (Ras homology) and Cdc-42 (Cell division

control protein 42), and every member is active when bound to a guanosine triphosphate (GTP) molecule, and inactive when bound to a guanosine diphosphate (GDP) molecule (Hall 1992; Bishop and Hall 2000). Activation can be aided by Guanine-nucleotide Exchange Factors (GEFs), molecules that typically contain a Double Homology (DH) domain (which are often followed by a Pleckstrin Homology [PH] domain). The DH domain of these molecules facilitates the exit of GDP from the GTP-binding pocket. Because the intracellular concentration of GTP is typically much higher than of GDP, a GTP molecule can enter the GTP-binding pocket of the GTPase and activate it. Rho GTPase inactivation can be aided by GTPase-Activating Proteins (GAPs), which enhance the intrinsic GTPase activity of Rho proteins, yielding in the hydrolysis of GTP into GDP and inorganic phosphate (Pi) (Schmidt and Hall 2002).

Proper regulation of Rac GTPase activity is crucial for lamellipodial and filopodial formation (Dickson 2001). *In vitro* studies have demonstrated the role of these molecules and some of their effectors in cell migration and neuronal development (Dickson 2002). However, these studies often use dominant negative proteins, and they lack the relevant physiological environment that surrounds neurons as they grow. Therefore, an *in vivo* analysis of the modulators and effectors of Rac GTPases in the journey axons take to find their path could benefit our knowledge of what happens during this process. I took a cell biological, biochemical and genetic approach to characterize the molecules involved in the Rac signaling pathway used for axon guidance. The nematode *Caenorhabditis elegans* was used as a model organism for my genetic studies

for its several advantages (Brenner 1974; Coulson, Sulston et al. 1986; White, Southgate et al. 1986). These animals are relatively cheap to maintain, have a very brief generation cycle (of about 3 days), have hermaphrodite and male sexes (which enable geneticists to easily cross and maintain strains), are transparent (which allow for the use of microscopy without the need of fixation and dissection), and have their genomes sequenced and available on the Wormbase database, among other positive facts. In addition, the stereotyped *C. elegans* nervous system consists of virtually the same types of neurons higher organisms have (including humans), and the molecules involved in neuronal development (for instance, Rac GTPases) are quite well conserved among species . Figure 1.1 demonstrates what was known about Rac GTPase modulators and effectors in *C. elegans* axon pathfinding prior and after this work. I was able to elucidate some of the mechanisms utilized by Rac GTPases to modulate the activity of the novel actin-binding protein UNC-115/abLIM (Chapters II and III). In addition, we also uncovered the roles of different activators of the Rac GTPase pathway during growth cone migration (Chapters IV and V).

Prevalent human neurological disorders such as autism, epilepsy and dyslexia could have their roots in the improper wiring of the nervous system. Small changes in expression of ROBO1, a guidance receptor involved in neurite guidance, are implicated in human dyslexia (Hannula-Jouppi, Kaminen-Ahola et al. 2005). The ROBO family of transmembrane receptors has also been involved in the modulation of the serotonin receptor SerT, a molecule in which

polymorphisms have been associated with the development of autism (Anitha, Nakamura et al. 2008). Changes in the expression levels of netrin-G2, a membrane-bound guidance molecule, have been implicated in temporal lobe epilepsy in rats and humans (Pan, Liu et al.). Hence a better understanding of the molecular pathways involved in modulating the actin cytoskeleton is of extreme importance for the study of neurodevelopment.

Figure 1.1

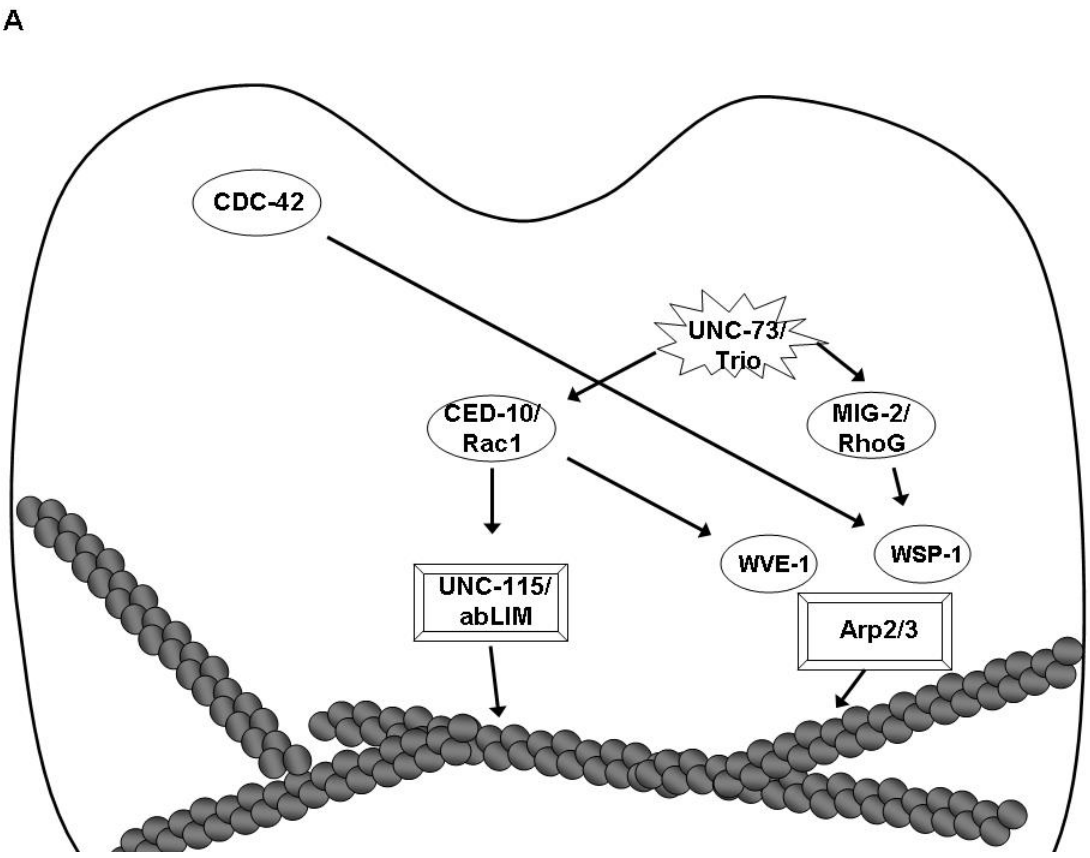
A
CDC-42
UNC-73/
Trio
CED-10/
Rac1
MIG-2/
RhoG
WVE-1
WSP-1
UNC-115/
abLIM
Arp2/3

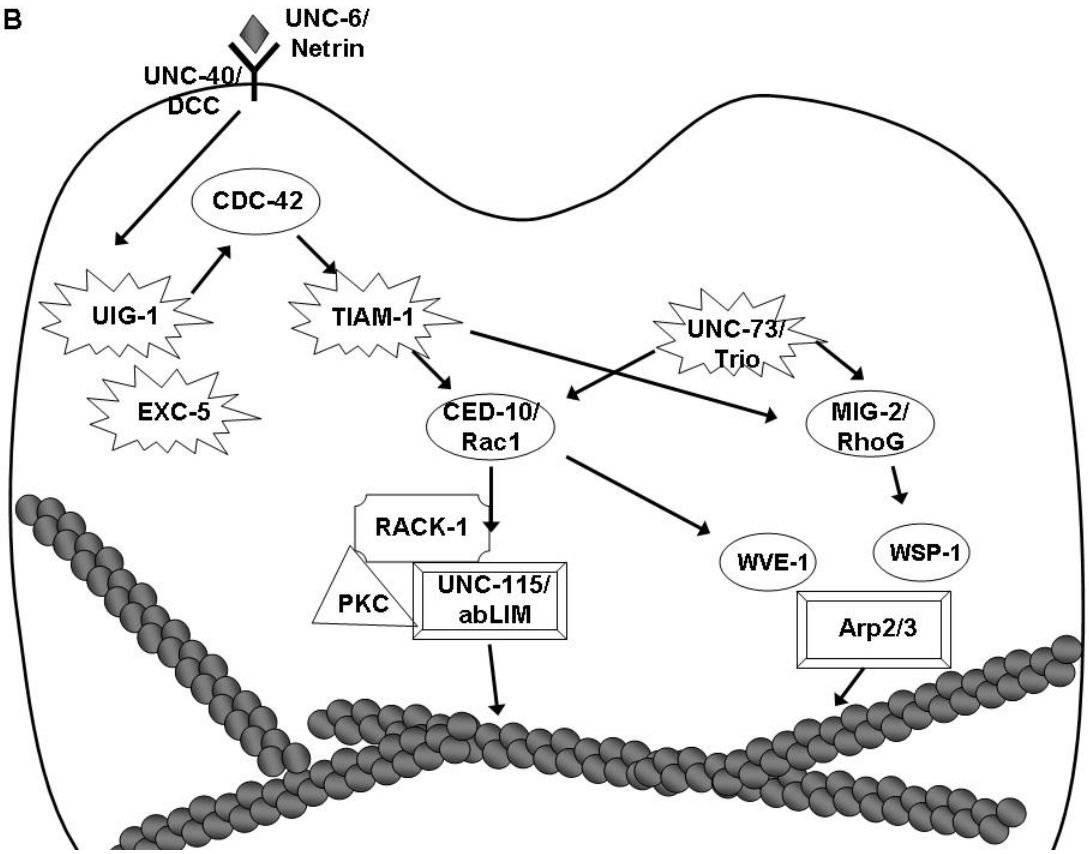
B
UNC-6/
Netrin
UNC-40/
DCC
CDC-42
UIG-1
TIAM-1
UNC-73/
Trio
EXC-5
CED-10/
Rac1
MIG-2/
RhoG
RACK-1
WVE-1
WSP-1
PKC
UNC-115/
abLIM
Arp2/3

Figure 1.1. A representation of the molecules known to participate in the reassembly of the actin cytoskeleton during growth cone migration. A. Before our work, the only GEF known to regulate MIG-2/RhoG and CED-10/Rac was UNC-73/Trio. Not much was known about how CDC-42 interacts with Racs, nor how CED-10/Rac activated UNC-115/abLIM. **B.** After our work, new molecules were involved in the proper control of axon guidance. In both drawings, actin filaments are represented by small gray circles bundled together. The plasma membrane of the growth cone is surrounding all molecules.

Chapter II

RACK-1 acts cell autonomously with Rac GTPase signaling and UNC-115/abLIM in *C. elegans* axon pathfinding and cell migration

2.1 Abstract

Migrating cells and growth cones extend lamellipodial and filopodial protrusions that are required for outgrowth and guidance. The mechanisms of cytoskeletal regulation that underlie cell and growth cone migration are of much interest to developmental biologists. Previous studies have shown that the Arp2/3 complex and UNC-115/abLIM act redundantly to mediate growth cone lamellipodia and filopodia formation and axon pathfinding. While much is known about the regulation of Arp2/3, less is known about regulators of UNC-115/abLIM. Here we show that the *C. elegans* counterpart of the Receptor for Activated C Kinase (RACK-1) interacts physically with the actin-binding protein UNC-115/abLIM, and that RACK-1 is required for axon pathfinding. Genetic interactions indicate that RACK-1 acts cell autonomously in the UNC-115/abLIM pathway in axon pathfinding and lamellipodia and filopodia formation, downstream of the CED-10/Rac GTPase and in parallel to MIG-2/RhoG. Furthermore, we show that RACK-1 is involved in migration of the gonadal distal tip cells, and that the signaling pathways involved in this process might be distinct from those involved in axon pathfinding. In sum, these studies pinpoint RACK-1 as a component of a novel signaling pathway involving Rac GTPases and UNC-115/abLIM, and suggest that RACK-1 might be involved in the regulation of the actin cytoskeleton and lamellipodia and filopodia formation in migrating cells and growth cones.

2.2 Introduction

The actin cytoskeleton is necessary for the formation of cellular protrusions, lamellipodia and filopodia, that underlie morphogenetic events such as cell migration and axon pathfinding (Welch, Mallavarapu et al. 1997; Borisy and Svitkina 2000; Pollard and Borisy 2003; Gallo and Letourneau 2004). Unraveling the complex molecular events that regulate actin structure and dynamics in migrating cells and growth cones will be central to understanding the development of multicellular organisms and the nervous system in particular. Migrating cells and growth cones display dynamic lamellipodial and filopodial protrusions consisting of a meshwork of actin filaments and bundles of actin filaments, respectively (Welch and Mullins 2002; Svitkina, Bulanova et al. 2003; Gallo and Letourneau 2004; Korobova and Svitkina 2008; Pak, Flynn et al. 2008). Lamellipodia and filopodia serve to guide cells and growth cones and also provide in part the motile force necessary for cell migration and growth cone advance (Zhou and Cohan 2004). A complex interplay of filopodial and lamellipodial dynamics controlled by guidance receptors and their ligands is the basis for guidance outgrowth and migration.

In cultured cells, the actin-nucleating Arp2/3 complex controls the formation of lamellipodial networks (Svitkina and Borisy 1999; Borisy and Svitkina 2000; Beltzner and Pollard 2007), whereas the anti-capping protein Enabled controls filopodial formation (Lebrand, Dent et al. 2004; Barzik, Kotova et al. 2005). Enabled also affects axon pathfinding in *C. elegans* (Withee, Galligan et al. 2004; Shakir, Gill et al. 2006). In migrating growth cones in *C.*

elegans, the Arp2/3 complex is required for both lamellipodial and filopodial formation (Norris, Dyer et al. 2009), likely due to the contribution of Arp2/3-nucleated actin filaments to filopodial bundles (Korobova and Svitkina 2008). The actin-binding protein UNC-115/abLIM (Lundquist, Herman et al. 1998) also controls lamellipodial and filopodial formation in *C. elegans* growth cones (Norris, Dyer et al. 2009), and acts in parallel to the Arp2/3 complex in axon pathfinding (Lundquist, Herman et al. 1998; Shakir, Jiang et al. 2008; Norris, Dyer et al. 2009), indicating that UNC-115/abLIM may be contributing to both lamellipodial and filopodial formation in growth cones. The signaling pathways that control Arp2/3 activation are well documented. The Arp2/3 activators WASP and WAVE act downstream of Cdc42 and Rac GTPases respectively to regulate Arp2/3 activity (Miki, Suetsugu et al. 1998; Eden, Rohatgi et al. 2002; Miki and Takenawa 2003; Innocenti, Zucconi et al. 2004; Beltzner and Pollard 2007). In *C. elegans* axon pathfinding, WVE-1/WAVE acts downstream of CED-10/Rac and WSP-1/WASP acts downstream of the MIG-2/RhoG GTPase to regulate Arp2/3 (Shakir, Jiang et al. 2008).

While much is known about the Arp2/3 signaling pathway, less is known about the control of UNC-115/abLIM in lamellipodia and filopodia formation. The conserved UNC-115/abLIM proteins have multiple LIM domains at the N terminus and an actin-binding villin headpiece domain at the C terminus (Roof, Hayes et al. 1997; Lundquist, Herman et al. 1998; Garcia, Abbasi et al. 2007). The central region of the molecule contains a short region of similarity shared with the dematin protein, which also contains a C terminal actin-binding villin

headpiece domain. Previous studies in *C. elegans* showed that UNC-115/abLIM acts downstream of the CED-10/Rac GTPase in neuronal lamellipodia and filopodia formation (Struckhoff and Lundquist 2003). The conserved seven-WD repeat molecule SWAN-1 physically interacts with the UNC-115 LIM domains and with Rac GTPases, and is normally required to attenuate Rac GTPase signaling (Yang, Lu et al. 2006), indicating that SWAN-1 might be a link between Rac signaling and UNC-115/abLIM.

A two-hybrid screen with the central region of UNC-115 identified the *C. elegans* Receptor for Activated C Kinase molecule (Rack1), called RACK-1 in *C. elegans* (Mochly-Rosen, Khaner et al. 1991; Ai, Poole et al. 2009). Rack1 molecules are composed of seven WD repeats, which form a seven-bladed beta propeller structure that serves as a scaffold for protein-protein interactions (Neer, Schmidt et al. 1994). Rack1 was first identified as a molecule that bound to activated protein kinase C and mediated its plasma membrane translocation (Ron, Chen et al. 1994; Besson, Wilson et al. 2002). Further studies have shown that Rack1 acts with a very diverse set of signaling complexes and can mediate their sub cellular distributions and shuttling (reviewed in (Sklan, Podoly et al. 2006)). This diversity of interaction leads to a diversity of function for Rack1, including transcriptional and translational regulation, regulation of membrane trafficking, regulation of signal transduction, and cell adhesion (Sklan, Podoly et al. 2006). Interestingly, Rack1 controls cell motility via its interaction with the Src tyrosine kinase (Liliental and Chang 1998; Besson, Wilson et al. 2002). Rack1 is a substrate for Src tyrosine phosphorylation and acts as a repressor of Src in

response to active PKC (Chang, Conroy et al. 1998; Buensuceso, Woodside et al. 2001; Schechtman and Mochly-Rosen 2001; Besson, Wilson et al. 2002; Chang, Harte et al. 2002). Rack1 inhibits Src-induced cell motility in cultured 3T3 fibroblasts, and inhibits Src phosphorylation of p190RhoGAP (Miller, Lee et al. 2004), a modulator of Rho GTPase signaling and actin organization. Rack1 is also phosphorylated on tyrosine 52 by c-Abl, which is involved in Rack1 regulation of focal adhesion kinase and integrin function (Kiely, Baillie et al. 2009). In *C. elegans,* RACK-1 has been shown to be involved in embryonic cytokinesis (Ai, Poole et al. 2009). *C. elegans* RACK-1 regulates membrane trafficking and recycling endosome distribution via interaction with dynactin, and thus might regulate the microtubule motor dynein. As a consequence, *rack-1* loss of function leads to defects in cytokinesis and chromosome separation in the early embryo.

Here we show that RACK-1 interacts with the actin-binding protein UNC-115/abLIM, and that RACK-1 is required for axon pathfinding. Genetic interactions indicate that RACK-1 acts in the UNC-115/abLIM pathway in axon pathfinding, downstream of the CED-10/Rac GTPase and in parallel to MIG-2/RhoG and the UNC-34/Enabled. Neuron-specific expression of RACK-1 is sufficient to rescue the axon pathfinding defects of *rack-1* mutants, indicating that RACK-1 acts cell autonomously in axon pathfinding. Furthermore, we show that RACK-1 is involved in migration of the gonadal distal tip cells, and that the signaling pathways involved in this process might be distinct from those involved in axon pathfinding. In sum, these studies pinpoint RACK-1 as a component of a

signaling pathway involving Rac GTPases and UNC-115/abLIM, and suggest that RACK-1 might be involved in the regulation of the actin cytoskeleton and lamellipodia and filopodia formation in migrating cells and growth cones.

2.3 Results

RACK-1 interacts with UNC-115/abLIM in a yeast two-hybrid screen. The actin-binding protein UNC-115/abLIM has three LIM domains in the N-terminus, a villin headpiece domain (VHD) in the C-terminus, and a middle region with unknown function that contains a highly conserved region across species, the UAD domain (UNC-115, abLIM, dematin) (Figure 1A) (Lundquist, Herman et al. 1998). The VHD physically interacts with F-actin (Roof, Hayes et al. 1997; Struckhoff and Lundquist 2003), while the LIM domains are thought to mediate protein-protein interactions. Previous studies showed that the seven WD-repeat protein SWAN-1, a negative regulator of UNC-115 activity, interacts with the LIM domains of UNC-115 (Yang, Lu et al. 2006).

In order to identify molecules that interact physically with the non-LIM-domain region UNC-115, the central region of UNC-115 (residues 243 to 553 of the F09B9.2b molecule as described on Wormbase) was used as bait in a yeast two-hybrid screen (Figure 1A). This two-hybrid screen was performed at the Molecular Interaction Facility at the University of Wisconsin-Madison. The screen involved activation of β-galactosidase activity and *HIS5* expression in a liquid-based microtiter screening procedure (see Materials and Methods). From a total of 36 million *C. elegans* poly-A primed cDNAs screened, seven cDNAs that corresponded to the K04D7.1 gene (as annotated on Wormbase) were found. All seven cDNAs were found to activate when retested, and all seven cDNAs displayed bait-dependence and did not activate in the absence of the UNC-115 bait (data not shown).

The seven cDNAs represented five independent isolates (i.e. represented five different 5' ends), with two of the isolates having two representatives each (Figure 1E). Three of the cDNAs contained the entire predicted K04D7.1 open reading frame, and two were missing some of the predicted 5' open reading frame. All five cDNAs were in frame to the GAL4 activation domain in the pACT two-hybrid vector.

The K04D7.1 cDNAs were predicted to encode a molecule similar to vertebrate Receptor for Activated C Kinase (Rack1), called RACK-1 in *C. elegans* (Figures 1D and E) (Ai, Poole et al. 2009). RACK-1 is predicted to contain seven WD repeats that form a seven-bladed beta-propeller similar to the beta subunit of G proteins (Sondek, Bohm et al. 1996). Rack1 molecules define a conserved family of seven-WD repeat proteins, and are distinct from other families such as Gβ and AN11/SWAN-1 (Sondek, Bohm et al. 1996; Yang, Lu et al. 2006). Rack1 molecules are defined by two conserved regions that interact with protein kinase C, a conserved tyrosine residue that is phosphorylated by the Src tyrosine kinase, and a tyrosine residue at position 52 that is phosphorylated by c-Abl. The PKC interaction sites and the Src phosphorylated tyrosine are conserved in the *C. elegans* RACK-1 protein, but the c-Abl phosphorylated tyrosine at position 52 in human Rack1 is not present in *C. elegans* RACK-1 (Figure 1E). Two of the cDNAs isolated in the two-hybrid screen were missing coding region for the first predicted WD repeat and one of them was missing part of the second predicted WD repeat (Figure 1E).

UNC-115 co-immunoprecipitated with RACK-1. To confirm that RACK-1 and UNC-115 interact in a complex, we determined if RACK-1 and UNC-115 co-immunoprecipitated from *C. elegans* extracts. We generated a transgene expressing MYC-tagged RACK-1 under its endogenous promoter and made animals transgenic for this construct. This transgene produced functional RACK-1::MYC, as it rescued the sterility, gonadal distal tip cell migration defects, and axon pathfinding defects caused by the *rack-1(tm2262)* deletion (see below). We immunoprecipitated MYC-tagged RACK-1 (RACK-1::MYC) using an anti-MYC antibody from animals harboring a *rack-1::myc* integrated gene (see Materials and Methods). Using anti-MYC western blots, we found that RACK-1::MYC (36 kD) was expressed in *C. elegans* extracts and that it was immunoprecipitated by this treatment (Figure 1B). Western blots using anti-UNC-115 antibody (Yang, Lu et al. 2006) showed the specific co-immunoprecipitation of UNC-115 (72 kD) with RACK-1::MYC (Figure 1B). In the absence of the anti-MYC antibody, RACK-1::MYC did not precipitate, and neither did UNC-115 (Figure 1B). Furthermore, we could detect no UNC-115 when extracts from *C. elegans* not expressing RACK-1::MYC were immunoprecipitated with the MYC antibody (data not shown). We repeated this co-immunoprecipitation two additional times, and the results of one representative experiment are shown in Figure 1.

***rack-1* is required for axon pathfinding.** *C. elegans* RACK-1 is a 325 amino-acid protein that has two regions similar to the PKC binding sites of vertebrate RACK and a conserved tyrosine that is phosphorylated by Src in vertebrate

RACK. *C. elegans* PKC and Src isoforms are expressed in the nervous system, and both PKC and Src have been implicated in growth cone pathfinding and cell migration (Tabuse 2002; Itoh, Hirose et al. 2005). Furthermore, we show above that RACK-1 interacts with UNC-115, a molecule that controls axon pathfinding in *C. elegans* (Lundquist, Herman et al. 1998). Thus, we determined if RACK-1 was also involved in axon pathfinding in *C. elegans*.

The VD and DD motor neurons are GABAergic neurons that control the coordination and movement of the nematode (White, Southgate et al. 1986; McIntire, Jorgensen et al. 1993). The VD and DD cell bodies reside on the right side of the ventral nerve cord. Axons extend anteriorly, branch, and extend dorsally to form axon commissures (Figure 2). Upon reaching the dorsal cord, the axons branch again and extend posteriorly and anteriorly. We used an *unc-25::gfp* transgene (*juIs76)* to image the VD/DD neurons and their axons (Jin, Jorgensen et al. 1999). *unc-115(ky275)* disrupts axon pathfinding in these neurons, yielding in an uncoordinated movement phenotype (Lundquist, Herman et al. 1998). We perturbed *rack-1* function using RNAi by injection (see Materials and Methods). In 22% of injected animals (n > 100), *rack-1(RNAi)* disrupted the proper pathfinding of the VD and DD commissural axons (Figures 2A and B). The defects seen, such as axon misguidance, branching and premature termination, resembled the defects observed in *unc-115(ky275)* (Lundquist, Herman et al. 1998) and were never observed in wild-type animals. These results suggest that RACK-1 might be involved in axon pathfinding, similar to UNC-115.

A deletion of the *rack-1* locus, called *tm2262,* was isolated and kindly provided by the National Bioresource Project for the Experimental Animal "Nematode C. elegans" (S. Mitani). The *tm2262* deletion was an in-frame deletion that removed part of the first WD repeat, all of the second, and most of the third, including the predicted PKC interaction site in WD3 (Figures 1C-E). Since *tm2262* is an in-frame deletion, *tm2262* animals might still produce truncated RACK-1 protein and *rack-1(tm2262)* might be a hypomorph. However, RNAi did not worsen the low brood size or axon defects of *rack-1(tm2262)* (see below; data not shown), indicating that it might be a strong loss of function allele.

Similar to RNAi of *rack-1*, the deletion allele *rack-1(tm2262)* caused pathfinding defects in the VD and DD motor neurons (Figure 2). Normally, all VD/DD commissures extend on the right side of the animal except DD1/VD2, which form a single commissure in the anterior (arrow in Figure 2C). *rack-1(tm2262)* displayed VD/DD commissures aberrantly extending up the left side of the animal (Figure 1D), and VD/DD axons that were misguided on their dorsal migrations (Figure 1D). In our hands, 27% of wild type animals harboring the *unc-25:gfp* transgene *juIs76* had VD/DD commissures on the left side in addition to DD1/VD2. However, 60% of *rack-1(tm2262); juIs76* showed VD/DD commissures on the left side ($p < 0.001$) (Figure 3). In *juIs76* animals, generally only one or two left-side VD/DD were observed, whereas multiple axons on the left side were often observed in *rack-1(tm2262); juIs76* animals (Figure 2D). In addition, 42% of *rack-1(tm2262); juIs76* animals displayed VD/DD axon guidance and outgrowth defects such as axonal wandering, branching or termination

(Figure 3), whereas *juIs76* alone showed no strong defects but did display some minor axon wandering.

To ensure that the axon guidance defects observed in *rack-1(tm2262)* were due to *rack-1* perturbation and not a background mutation, we rescued the VD/DD axon defects with a *rack-1::myc* transgene. *rack-1::myc* rescued both left-right defects and commissural guidance defects (60% to 32% ($p < 0.001$) and 42% to 10% ($p < 0.001$)) (Figure 3). Together, these results indicate that RACK-1 is required for VD/DD axon pathfinding.

***rack-1(tm2262)* caused reduced brood size.** *rack-1(tm2262)* animals were slow growing and had very low brood size. In a progeny count, ten wild-type and ten *rack-1(tm2262)* animals were individually plated and then transferred to a new plate every day until egg-laying ceased. The number of viable adult progeny resulting from each animal were counted and averaged. The average progeny count for a wild-type N2 animal was of 278.4 (s.d.=32.72), while for *rack-1(tm2262)* the count dropped to 23.3 (s.d.=9.9) ($p < 0.0001$). A transgene containing the *rack-1* gene under its native promoter fused to the *gfp* coding region (*rack-1::gfp*) (see Materials and Methods) increased brood size in *rack-1(tm2262)* animals to 73.78 (s.d.=17.18) ($p < 0.0001$), suggesting that *rack-1::gfp* was functional and could rescue the brood size defect in *rack-1* animals. *rack-1::myc* could also rescue the low brood size of *rack(tm2262)* (data not shown). Thus, the reduction in brood size was due to *rack-1* and not due to genetic background in the *tm2262* strain.

The reduced brood size of *rack-1(tm2262)* seems to be predominantly due to decreased production of fertilized embryos. *rack-1* might affect oogenesis or spermatogenesis, but the nature of this sterility has not been explored. Previous studies indicate that *rack-1* also affects embryogenesis by regulating membrane trafficking and recycling endosome distribution via interaction with dynactin to control cytokinesis and chromosome separation in the early embryo (Ai, Poole et al. 2009).

***rack-1::gfp* was expressed in most tissues, including neurons and the distal tip cells.** In order to determine where the *rack-1* gene is expressed, we constructed a reporter transgene consisting of the promoter region of *rack-1* fused to the *gfp* coding region (see Materials and Methods). *rack-1 promoter::gfp* was expressed in most if not all tissues. Due to mitotic loss of the transgene-bearing extrachromosomal array, we were able to analyze *rack-1 promoter::gfp* expression in mosaic animals in which we could discern specific cell types. *rack-1 promoter::gfp* was expressed in neurons as well as the distal tip cells of the gonad (Figures 4A and B).

In order to determine the subcellular localization of RACK-1 protein, we constructed a full-length *rack-1::gfp* fusion. This transgene is predicted to encode a full-length RACK-1 protein with GFP at the C-terminus (RACK-1::GFP). *rack-1::gfp* rescued the sterility and gonadal distal tip cell migration defects of *rack-1(tm2262)* mutants. RACK-1::GFP was present in the cytoplasm of cells and showed little if any nuclear accumulation (Figures 4C and D), although low

levels of RACK-1::GFP in the nucleus cannot be excluded. RACK-1::GFP was present in the growth cones of extending VD commissural axons, but was present in the axons and cell bodies as well (Figure 5A and B).

***rack-1* acts cell-autonomously in the VD/DD neurons to control axon pathfinding.** *rack-1* was expressed in most if not all tissues in the animal, including neurons. To determine if RACK-1 is required in the VD/DD neurons themselves for axon pathfinding, we drove expression of *rack-1::gfp* specifically in the VD/DD neurons using the GABAergic neuron-specific *unc-25* promoter. The wild-type *rack-1(+)* coding region lacking the upstream promoter region was fused to *gfp* downstream of the *unc-25* promoter. The *Ex[unc-25 promoter::rack-1::gfp]* transgene was expressed specifically in the GABAergic neurons including the VD/DD neurons and nowhere else (Figure 5A). This transgene did not rescue the fertility defects and DTC migration defects of *rack-1(tm2262)* as did the genomic *rack-1(+)* transgene (data not shown), indicating that expression was specific to the VD/DD neurons. *Ex[unc-25 promoter::rack-1(+)]* rescued the lateral asymmetry defects and axon wandering defects of *rack-1(tm2262)* animals (Figure 3) (60% to 33% for lateral asymmetry defects and 16% to 8% for axon wandering defects; $p < 0.001$ in both cases). In this experiment, individual axons were scored, due to the mosaic nature of the *Ex[unc-25 promoter::rack-1(+)]* transgene. These data indicate that *rack-1* acts cell autonomously in neurons in axon pathfinding.

***rack-1(tm2262)* enhanced *mig-2(mu28)* and *unc-34(e951)* but not *unc-115(ky275)* or *ced-10(n1993)* in PDE axon pathfinding**. The above results show that RACK-1 physically interacted with UNC-115/abLIM and that *rack-1* loss of function caused axon pathfinding defects similar to *unc-115*. Previous studies showed that UNC-115/abLIM acts downstream of the Rac GTPase CED-10/Rac and in parallel to MIG-2/RhoG in axon pathfinding (Lundquist 2003; Struckhoff and Lundquist 2003). We next set out to determine if RACK-1 interacts with UNC-115/abLIM and the Rac GTPases in axon pathfinding. To analyze genetic interactions between these molecules, we used the PDE neurons, which are located at the post-deiridic region of the animal. These neurons are a good model for axon pathfinding since the reporter construct *osm-6::gfp* is expressed only in the PDEs in the post-deirid (Collet, Spike et al. 1998; Struckhoff and Lundquist 2003), allowing unambiguous identification and scoring of the simple PDE axon morphology. Furthermore, the defects in PDE axon pathfinding in single mutants were weak, allowing for discrimination of genetic interactions in double mutants.

In wild-type, the PDE cell body extends an axonal projection toward the ventral nerve cord in a straight line, where the axon then branches and extends anteriorly and posteriorly (Figure 6A) (White, Southgate et al. 1986). Pathfinding defects were defined as axons that were prematurely terminated or that wandered at a greater than 45 degree angle relative to the normal PDE axon (for example, Figure 6B). As shown previously, *mig-2(mu28)*, *ced-10(n1993)*, and *unc-115(ky275)*, alone had low-penetrance defects in PDE axon pathfinding on

their own (3%-7%; Figure 6C). We found that *rack-1(tm2262)* also had very few defects in PDE axon pathfinding (1%; Figure 6C).

Previous results show that CED-10/Rac and MIG-2/RhoG act redundantly in PDE axon pathfinding, and UNC-115/abLIM works downstream of CED-10/Rac, in parallel to MIG-2/RhoG in PDE pathfinding (Lundquist, Reddien et al. 2001; Struckhoff and Lundquist 2003). If RACK-1 works in the same pathway as UNC-115/abLIM, we expect that loss of function of both *rack-1* and *unc-115* would be no more severe than either mutant alone. Indeed, *rack-1(tm2262M+); unc-115(ky275)* double mutants (M+ denotes that the homozygous animal was derived from a balanced heterozygote and has wild-type maternal contribution) displayed levels of PDE axon pathfinding defects (6%; Figure 6C) that were not significantly different from *unc-115(ky275)* and *rack-1(tm2262)* alone, suggesting that UNC-115/abLIM and RACK-1 might act in the same pathway. In contrast, *rack-1(tm2262M+); mig-2(mu28)* double mutants showed significantly increased levels of defects compared to either single alone (28%; Figure 6C). This result demonstrates that *rack-1(tm2262)* can synergize with other mutants to cause axon defects, and that RACK-1 and MIG-2/RhoG might act in parallel pathways in axon pathfinding.

CED-10/Rac and UNC-115/abLIM have previously been shown to act in the same pathway in parallel to MIG-2/RhoG (Struckhoff and Lundquist 2003). *rack-1(tm2262M+) ced-10(n1993M+)* double mutants displayed no significant increase in PDE defects compared to either single alone (6%; Figure 6C), consistent with the idea that RACK-1, CED-10/Rac, and UNC-115/abLIM act in a

common pathway in parallel to MIG-2/RhoG in axon pathfinding. If this is the case, we would expect the *rack-1(tm2262M+) ced-10(n1993M+); unc-115(ky275)* triple mutant to be no more severe than any double mutant combination alone. As previously reported, *ced-10(n1993); unc-115(ky275)* double mutants were significantly more severe than either single alone (35%; Figure 6C) (Lundquist, Reddien et al. 2001; Struckhoff and Lundquist 2003). This is likely due to the fact that CED-10/Rac also regulates the Arp2/3 complex in parallel to UNC-115/abLIM (Shakir, Jiang et al. 2008; Norris, Dyer et al. 2009). *rack-1(tm2262M+) ced-10(n1993M+)* mutants did not show this interaction. Possibly, RACK-1 is not the only molecule regulating UNC-115 and has a weaker effect. In any case, the *rack-1(tm2262M+) ced-10(n1993M+); unc-115(ky275)* triple mutant was not significantly more severe than *ced-10(n1993); unc-115(ky275)* alone (34% compared to 35%; Figure 6C). Taken together, these results are consistent with the idea that RACK-1, CED-10/Rac, and UNC-115/abLIM act in a common pathway in axon pathfinding in parallel to MIG-2/RhoG.

UNC-34/Enabled has been shown to act in parallel to both CED-10/Rac and MIG-2/RhoG in axon pathfinding (Shakir, Gill et al. 2006). Indeed, *rack-1(tm2262M+); unc-34(e951M+)* double mutants displayed significantly increased pathfinding defects compared to *unc-34(e951)* alone (35% compared to 19%; Figure 6C). This result indicates that RACK-1 acts in parallel to UNC-34/Enabled and is consistent with RACK-1 acting with CED-10/Rac and UNC-115/abLIM in axon pathfinding.

***rack-1(tm2262)* partially suppressed axon pathfinding defects and ectopic lamellipodia induced by activated CED-10(G12V).** Loss-of-function studies described above provide evidence that RACK-1 might act with CED-10/Rac and UNC-115/abLIM in axon pathfinding. In order to further test the relationship between RACK-1 and the Rac GTPases we next asked what effect *rack-1(tm2262)* loss of function might have on overactive Rac GTPases. Constitutively-activated Rac GTPases transgenes harbor a guanine-12-valine mutation in the GTPase binding pocket, which favors the active GTP-bound state of the GTPases. Previous studies showed that CED-10(G12V) and MIG-2(G16V) (the G12V equivalent) both caused axon pathfinding defects and drove the formation of ectopic neurites, lamellipodia, and filopodia when expressed in PDE neurons (Figure 7A), and that UNC-115/abLIM was required for ectopic lamellipodia and filopodia induced by CED-10(G12V) but not MIG-2(G16V) (Struckhoff and Lundquist 2003).

We determined if RACK-1 was required for the effects of CED-10(G12V) and MIG-2(G16V). CED-10(G12V) alone caused 66% of PDE neurons to have ectopic lamellipodia and filopodia in young adults (Figure 7B). *rack-1(tm2262); ced-10(G12V)* animals displayed 45% ectopic lamellipodia and filopodia, a significant reduction ($p = 0.004$) from CED-10(G12V) alone (Figure 7B). These data indicate that *rack-1(tm2262)* partially suppressed activated CED-10(G12V) and that functional RACK-1 might be required for the formation of ectopic lamellipodia and filopodia induced by activated CED-10. In contrast, *rack-1(tm2262)* did not suppress ectopic lamellipodia and filopodia associated with

MIG-2(G16V) and in fact slightly enhanced these defects (Figure 7B; p = 0.03), indicating that this suppression is specific to CED-10(G12V). These effects are similar to those observed with the *wve-1/WAVE* mutant, which suppressed CED-10(G12V) and slightly enhanced MIG-2(G16V) (Shakir, Jiang et al. 2008). These data are consistent with the idea that RACK-1 acts downstream of CED-10/Rac in parallel to MIG-2/RhoG in axon pathfinding, similar to UNC-115/abLIM.

rack-1(tm2262)* did not suppress defects induced by activated *myr::unc-115. Previous studies showed that UNC-115 tagged with an N-terminal myristylation sequence (MYR) caused activation of the molecule (Yang and Lundquist 2005). MYR::UNC-115 localized to the plasma membrane and other membranes as expected for a myristylated protein and induced the formation of ectopic lamellipodia, filopodia and neurites in *C. elegans* neurons and in cultured mammalian fibroblasts (Yang and Lundquist 2005). The formation of these ectopic lamellipodia and filopodia was dependent upon the actin-binding domain of UNC-115, suggesting that the molecule was constitutively active (Yang and Lundquist 2005).

To further dissect the interaction of RACK-1 with UNC-115, we assayed the effects of MYR::UNC-115 in a *rack-1(tm2262)* loss of function background. MYR::UNC-115 was expressed from the *unc-115* promoter (the *lqIs62* transgene), which drives expression in most neurons including PDE and the VD/DDs (Yang and Lundquist 2005). The *myr::unc-115* transgene scored in (Yang and Lundquist 2005) was maintained as an extrachromosomal array. We integrated this transgene into the genome for these studies (*lqIs62)*. We found

that *lqIs62[MYR::UNC-115]* caused 8% ectopic lamellipodia and filopodia in PDE neurons (Figure 7B), similar to but weaker than the extrachromosomal array effects reported in (Yang and Lundquist 2005). The ectopic lamellipodia and filopodia induced by MYR::UNC-115 were not significantly altered by *rack-1(tm2262)* mutation (Figure 7B), indicating that RACK-1 is not required for lamellipodia and filopodia induced by MYR::UNC-115. This result suggests that RACK-1 might act upstream of UNC-115 or together with UNC-115, or that the MYR::UNC-115 molecule acts independently of RACK-1 activity.

To study the interactions of *rack-1* with *myr::unc-115* in more detail, we analyzed the VD/DD motor neurons as described above. *myr::unc-115* expression caused left-right lateral asymmetry defects and commissural axon pathfinding defects as described for *rack-1(tm2262)* in Figures 2 and 3 (Figure 8A). *rack-1(tm2262); myr::unc-115* animals displayed lateral asymmetry defects similar to each alone (Figure 8A; 45%-55%, not significant). This is consistent with RACK-1 acting upstream of or together with UNC-115 in the same pathway. In VD/DD commissural axon pathfinding, *rack-1(tm2262); myr::unc-115* displayed significantly increased defects compared to the additive effects of each alone (Figure 8A). Thus, *rack-1(tm2262)* might enhance *myr::unc-115* in VD/DD pathfinding.

In summary, we detected no strong suppression of *myr::unc-115* by *rack-1(tm2262)* in the PDE neurons and the VD/DD neurons. The results are consistent with RACK-1 acting upstream of or together with UNC-115 in axon pathfinding. Some context-specific interactions were observed, such as *rack-*

1(tm2262) enhancing VD/DD commissural axon pathfinding, indicating that RACK-1 and UNC-115 might have distinct interactions in different contexts or developmental events.

UNC-115 is required for the ectopic lamellipodia induced by MYR::RACK-1. The above results indicate that RACK-1 is not required for the effects of MYR::UNC-115, suggesting that RACK-1 might act upstream of UNC-115. To test this idea, we constructed a myristylated version of RACK-1, similar to MYR::UNC-115. We reasoned that constitutive membrane localization might activate RACK-1 as it does UNC-115. *myr::rack-1::gfp* was expressed in the PDE neurons by the *osm-6* promoter. MYR::RACK-1::GFP displayed a membrane-associated distribution (arrowhead in Figure 9A), as did MYR::UNC-115 (Yang and Lundquist 2005). MYR::RACK-1 animals displayed ectopic lamellipodial protrusions along the cell body, dendrite, and axon, similar to MYR::UNC-115 and activated Rac GTPases (arrow in Figure 9A). The putative null *unc-115* alleles *ky275* and *ky274* suppressed this effect (11% in *myr::rack-1* reduced to 0% and 4% in *unc-115(ky275); myr::rack-1* and *unc-115(ky274); myr::rack-1*, respectively) (Figure 9B). The hypomorphic *unc-115(mn481)* allele (Lundquist, Herman et al. 1998), which retains some UNC-115 activity, did not suppress *myr::rack-1*, indicating that possibly only a small amount of UNC-115 activity is required for MYR::RACK-1 to drive ectopic lamellipodia. These studies support the model that RACK-1 acts upstream of UNC-115 in lamellipodia formation.

Despite the strong genetic interactions of *rack-1* and *unc-115*, we could detect no change in distribution of UNC-115::GFP in loss of function *rack-1(tm2262)* or in the activated *myr::unc-115* transgenics (data not shown). In each case, UNC-115::GFP was present uniformly throughout the cytoplasm, similar to wild-type animals, and showed no membrane localization.

***rack-1(tm2262)* suppresses *myr::unc-115* in VD cell body position.**

Activated *myr::unc-115* caused lateral displacement of GABAergic motor neuron cell bodies such that they often were found outside of the ventral nerve cord (Figure 8B). The VD GABAergic neurons are descendants of the P cells. The P cells are born laterally and the P nuclei migrate ventrally to the ventral nerve cord, where the P cells divide to produce ventral hypodermal cells including the vulva and the ventral VD neurons (Sulston and Horvitz 1977; White, Southgate et al. 1986). Failure of the ventral migration of the P nuclei can result in laterally displaced VD neuron cell bodies. This phenotype is observed in *mig-2; ced-10* double mutants, but not in *unc-115* mutants (Lundquist, Reddien et al. 2001). Possibly, ectopic activity from MYR::UNC-115 impedes P nucleus migration. *rack-1(tm2262)* suppressed the displaced VD cell body defect of *myr::unc-115* (Figure 8A): 30% of *myr::unc-115* animals had misplaced VD cell bodies compared to 15% of *rack-1(tm2262); myr::unc-115* ($p = 0.011$). This result suggests that RACK-1 might act downstream of or participate with MYR::UNC-115 in impeding P nucleus migration, again suggesting context-dependent interactions of UNC-115 and RACK-1.

***rack-1(tm2262)* caused gonadal distal tip cell migration defects.** The *C. elegans* gonad is derived from two somatic cells (Z1 and Z4) surrounding the two germ cells (Z2 and Z3) (Kimble and Hirsh 1979). Z1 and Z4 divide to produce the somatic cells of the gonad. Before morphogenesis, the gonad is oval shaped and located ventrally in the middle of the animal. The distal tip cells (DTCs) at the anterior and posterior tips of the gonad begin migration, and as they migrate they lead the gonad behind them. The DTCs migrate anteriorly and posteriorly, turn dorsally and migrate to the dorsal region of the animal, and then migrate posteriorly and anteriorly back toward the middle of the animal. DTC migration results in the U-shaped bi-lobed gonad of *C. elegans* (Figure 10A). If DTC migration is perturbed, misrouted and misshapen gonads result. The gonads of 32% of *rack-1(tm2262)* animals were misrouted (Figures 10B and C). Misrouting defects included failure to turn dorsally as well as extra turns, such as turning back ventrally after the dorsal migration. We did not observe gonads that had extended past their normal stopping point near the middle of the animal, as has been observed in other mutations that affect DTC migration (Tannoury, Rodriguez et al. ; Meighan and Schwarzbauer 2007). A *rack-1::gfp* transgene rescued gonad misrouting defects in *rack-1(tm2262)* (32% to 5%; $p < 0.005$) (Figure 10C), indicating that the gonad defects were due to *rack-1* perturbation. It should be noted that *rack-1(tm2262)* homozygotes from a heterozygous mother *(rack-1(tm2262M+))* had less severe DTC migration defects compared to the *rack-1(tm2262)* animals without maternal contribution (21% compared to 32%; $p = 0.03$). This indicates that DTC migration defects were partially rescued by wild-

type maternal *rack-1(+)* activity. *unc-115* mutants displayed no defects in DTC migration, and the gonad defects of *rack-1* were not affected by *unc-115* (data not shown). *rack-1::myc* also rescued the DTC migration defects of *rack-1(tm2262)* (data not shown). Thus, DTC migration is controlled by RACK-1 and is independent of UNC-115/abLIM.

CED-10/Rac and MIG-2/RhoG have previously been shown to control gonad distal tip cell migration (Lundquist, Reddien et al. 2001), and we have shown here that RACK-1 also controls DTC migration. To determine if RACK-1 interacts with Rac signaling in DTC migration, we analyzed DTC migration in double mutants.

As reported previously, both *ced-10(n1993)* and *mig-2(mu28)* mutations caused defects in DTC migration (27% for *mig-2(mu28)*, 12% for *ced-10(n1993)*) (Figure 10C) (Lundquist, Reddien et al. 2001). We found that double mutants of *ced-10* and *mig-2* with *rack-1* showed no significant difference in defects compared to the stronger singles alone. *rack-1(tm2262M+); mig-2(mu28)* showed no significant difference (26%) compared to *mig-2(mu28)* (27%), and *rack-1(tm2262M+) ced-10(n1993)* showed no significant difference compared to *rack-1(tm2262M+)* (21% in each case).

CED-10/Rac and MIG-2/RhoG interact differently in the DTCs than they do in other tissues such as axons, in which they act in parallel redundant pathways. *ced-10; mig-2* double mutants did not display enhanced DTC migration defects compared to either single alone (Lundquist, Reddien et al. 2001), suggesting that they might act in the same pathway or in independent

pathways that each control a distinct aspect of DTC migration. Our results suggest the same for RACK-1, that it might act in a pathway independent of CED-10 and MIG-2, or that CED-10, MIG-2 and RACK-1 might all act in the same pathway in DTC migration.

2.4 Discussion

In summary, we have presented data indicating that RACK-1 is required cell autonomously for axon pathfinding, and that RACK-1 is required for migration of the distal tip cells of the gonad. We show that RACK-1 interacts physically with UNC-115/abLIM, and that RACK-1 and UNC-115/abLIM might act in the same pathway in axon pathfinding. Consistent with this idea, RACK-1 was required for ectopic lamellipodia and filopodia induced by the activated CED-10/Rac GTPase, similar to UNC-115/abLIM. RACK-1-like molecules have been implicated in a wide variety of cellular events and have been shown to interact with a large number of distinct protein complexes, consistent with the idea of RACK molecules as scaffolds and integrators (Sklan, Podoly et al. 2006). RACK molecules have been shown to control cell adhesion and migration and interact with Src, c-Abl, Rho GTPase regulators, and integrins in these events (Liliental and Chang 1998; Besson, Wilson et al. 2002; Kiely, Baillie et al. 2009). Our studies here suggest that RACK-1 interacts with the actin-binding protein UNC-115/abLIM and Rac GTPases in the control of axon pathfinding and cell migration.

Previous studies showed that in *C. elegans*, RACK-1 depletion by RNAi resulted in embryos with cytokinesis defects, including shorter astral microtubules, defects in chromosome separation, and defects in membrane organization and recycling endosome distribution (Ai, Poole et al. 2009). We found that the deletion *rack-1(tm2262)* was very sick and slow-growing, and gave very few progeny. *rack-1(tm2262)* produced very few embryos, suggesting that

the animals had defects in sperm and/or oocyte production. Indeed, *rack-1* RNAi resulted in defects in germline membrane organization (Ai, Poole et al. 2009), consistent with the sterility that we observed in the *rack-1(tm2262)* mutant.

RACK-1 is cell autonomously required for axon pathfinding. *rack-1(tm2262)* mutants displayed a variety of axon pathfinding defects, including left-right choice and guidance defects of the VD and DD commissural motor axons and guidance defects of the PDE axons. VD/DD axons are dorsally directed, and PDE axons are ventrally directed, indicating that *rack-1* is not specific for any particular guidance direction. VD/DD axon pathfinding defects were rescued when *rack-1(+)* was expressed under a promoter that specifically drives expression in the GABAergic neurons including VD/DD and nowhere else, demonstrating that RACK-1 is required cell-autonomously for axon pathfinding. As RACK-1 is likely involved in many different developmental events, this result shows that the effects of RACK-1 on axon pathfinding are due to defects in the neuron itself and not a substrate or guidepost tissue such as the hypodermis or other neurons. Indeed, RACK-1 was expressed in neurons, and functional RACK-1::GFP fusion protein accumulated in the growth cones of neurons, consistent with a role of RACK-1 in growth cone cytoskeletal regulation. RACK-1::GFP also accumulated in the cell bodies and axons of neurons.

RACK-1 controls distal tip cell migration. We have shown that *rack-1(tm2262)* mutants display defects in the structure of the gonad arms consistent

with a defect in distal tip cell migration. *rack-1* is expressed in the migrating distal tip cells. The Rac GTPases CED-10/Rac and MIG-2/RhoG also each affect distal tip cell migration, but do not show the phenotypic synergy in DTC migration as is observed in axon pathfinding (Lundquist, Reddien et al. 2001). Thus, CED-10/Rac and MIG-2/RhoG might act in independent pathways that control distinct aspects of DTC migration.

DTC migration defects in *mig-2; rack-1* and *ced-10 rack-1* double mutants were not significantly different than the stronger single mutants alone. This result suggests that RACK-1 might act in a pathway independent of MIG-2 and CED-10, or that all three act in a comon pathway. This again points to context dependent differences in the function of RACK-1 and suggests that RACK-1 might interact with different effectors in different ways in different cells and cellular events. Indeed, the effect of RACK-1 on DTC migration is likely to be independent of UNC-115/abLIM, as *unc-115* mutants have no effect on DTC migration alone or in any double mutant combination analyzed so far, including *ced-10* and *mig-2*.

RACK-1 acts in the CED-10/Rac and UNC-115/abLIM pathway in axon pathfinding. A model of RACK-1 interaction with CED-10/Rac and UNC-115/abLIM is shown in Figure 10A. Double mutant analysis showed that *rack-1(tm2262)* synergized with *mig-2/RhoG* and *unc-34/Enabled* in PDE axon pathfinding, similar to *unc-115/abLIM* and *ced-10/Rac*. *rack-1(tm2262)* did not

synergize with *unc-115/abLIM* or *ced-10/Rac*, consistent with the idea that they act in the same pathway in parallel to *mig-2/RhoG* and *unc-34/Enabled*.

Activated CED-10(G12V) drives the formation of ectopic lamellipodia and filopodia in PDE neurons, and *unc-115* loss of function suppresses this effect (Struckhoff and Lundquist 2003). We show here that *rack-1(tm2262)* also partially suppressed ectopic lamellipodia and filopodia caused by CED-10(G12V), indicating that RACK-1 is required downstream of CED-10/Rac in lamellipodia and filopodia formation (Figure 10A). This result suggests that RACK-1 might normally be required for lamellipodia and filopodia formation. This is in contrast to the seven-WD repeat protein SWAN-1, which physically interacts with the UNC-115 LIM domains and with CED-10/Rac but which is normally required to inhibit CED-10/Rac signaling in lamellipodia and filopodia formation (Yang, Lu et al. 2006). Thus, these two seven-WD repeat proteins SWAN-1 and RACK-1 might have opposite effect on CED-10/Rac signaling: SWAN-1 inhibits it, and RACK-1 is required downstream of it to form lamellipodia and filopodia. That RACK-1 is required for lamellipodia and filopodia formation downstream of CED-10/Rac suggests that RACK-1 might be acting directly in cytoskeletal regulation. It is also possible that RACK-1 exerts its effects downstream of Rac GTPases through transcriptional or translational control, but the fact that RACK-1 interacts physically with the actin-binding protein UNC-115/abLIM supports the idea that RACK-1 directly controls cytoskeletal signaling.

RACK-1 physically interacts with UNC-115/abLIM and genetically acts in the same pathway in axon pathfinding. UNC-115 can be activated constitutively

by the addition of an N-terminal myristylation sequence (Struckhoff and Lundquist 2003), which mediates the covalent attachment of a fatty acid myristyl residue to the protein and drives localization to membranes, including the plasma membrane. MYR::UNC-115 also drives the formation of ectopic lamellipodia and filopodia, similar to but weaker than CED-10(G12V) (Struckhoff and Lundquist 2003). No strong suppression or enhancement of axon pathfinding defects were observed in double mutants of *rack-1(tm2262)* and *myr::unc-115*. One interpretation of these data is that RACK-1 does not act downstream of UNC-115/abLIM and instead might act together with or upstream of UNC-115/abLIM. Indeed, *unc-115* mutations suppressed the ectopic lamellipodia caused by MYR::RACK-1, indicating that UNC-115 acts downstream of RACK-1. These results are consistent with a model in which RACK-1 acts downstream of CED-10/Rac and upstream of UNC-115/abLIM in axon pathfinding (Figure 11).

RACK-1 and MYR::UNC-115 display context-specific interactions. RACK-1 and UNC-115 displayed context-dependent interactions in addition to those described in the PDE neurons above. First, *rack-1* slightly but significantly increased VD/DD commissural pathfinding defects caused by *myr::unc-115*. We do not understand the nature of the VD/DD axon pathfinding defects caused by MYR::UNC-115, but it is possible that they are due to excessive lamellipodial and filopodial protrusion, possibly in the growth cone. If this is the case, these effects were enhanced by *rack-1* loss of function, suggesting that RACK-1 might

negatively regulate MYR::UNC-115 in this context, possibly by excluding MYR::UNC-115 from regions in which it induces lamellipodia and filopodia.

Second, *rack-1(tm2262)* suppressed the lateral displacement of VD cell bodies caused by *myr::unc-115*. Laterally misplaced VD cell bodies are indicative of a defect in the ventral migration of the nuclei of the P cells. UNC-115 is not normally involved in P nucleus migration, but *ced-10/Rac* and *mig-2/RhoG* act redundantly in the process (Lundquist, Reddien et al. 2001). Possibly, *myr::unc-15* ectopically interferes with P nucleus migration, and RACK-1 is required for this effect. In this case RACK-1 might normally positively regulate MYR::UNC-115. In any case, these data indicate that RACK-1 and UNC-115 might have distinct interactions in different cellular contexts.

In summary, these studies suggest that RACK-1 acts in a common pathway with CED-10/Rac and UNC-115/abLIM in axon pathfinding (Figure 11). These studies implicate the Receptor of Activated C Kinase as a new Rac GTPase effector molecule, as RACK-1 acts downstream of CED-10 and upstream of UNC-115/abLIM in axon pathfinding. Future studies will be directed at understanding the roles of plasma membrane localization and phosphorylation in the regulation of this pathway.

2.5. Materials and Methods

***C. elegans* genetics and culture**: *C. elegans* culture and techniques were performed using standard protocols (Brenner 1974; Sulston and Hodgkin 1988). All experiments were performed at 20^{o}C. The *rack-1(tm2262)* allele was provided to us by the National Bioresource Project for the Experimental Animal "Nematode C. elegans" (S. Mitani), and was outcrossed to wild-type N2 animals three times before analysis. Polymerase chain reaction (PCR) was used to verify the homozygosity of *rack-1(tm2262)* in strains. The following mutations and genetic constructs were used: *LGII: juIs76[unc-25::gfp]; LGIV: ced-10(n1993), rack-1(tm2262), nT1 IV:V, lqIs3[osm-6::gfp]; LGV: unc-34(e951); LGX: unc-115(ky275), mig-2(mu28), lqIs2[osm-6::gfp]; LG?: lqIs62[myr::unc-115(+)]. C. elegans* transformation was performed by standard techniques using DNA microinjection into the syncytial germline of hermaphrodites (Epstein and Shakes 1995). Transgenes were integrated into the genome using trimethylpsoralen and standard techniques (Mello, Kramer et al. 1991; Anderson 1995).

All micrographs were obtained on a Leica DMRE microscope with a Qimaging Rolera MGi EMCCD camera or a Qimaging Retiga CCD camera. Openlab and IPlab software were used to obtain images.

Molecular biology: All coding regions amplified by PCR were sequenced to ensure the absence of mutations in the sequence. PCR, recombinant DNA and other molecular biology techniques were performed according to standard

techniques (Sambrook 1989). Primer and plasmid sequences are available upon request.

Scoring of VD, DD and PDE axon defects: Axon pathfinding defects were scored with fluorescence microscopy of hermaphrodite animals in the fourth larval stage (L4) or young adults expressing a green fluorescent protein transgene for specific cells. To visualize and score the axons of VDs and DDs, animals harboring an *unc-25 promoter::gfp* integrated transgene (*juIs76 II*) were used (Jin, Jorgensen et al. 1999). To visualize and score PDE axons, animals harboring an *osm-6 promoter::gfp* integrated transgene (*lqIs2 X* or *lqIs3 IV*) were used (Collet, Spike et al. 1998; Struckhoff and Lundquist 2003). VD/DD Lateral asymmetry: VD/DD commissural axons normally extend up the right side of the animal (except the VD1/DD2 commissure, which extends on the left). The number of animals with aberrant left-side extension of commissural axons was scored. VD/DD axon pathfinding: A VD/DD commissural axon that failed to reach the dorsal nerve cord or that wandered laterally before reaching the dorsal nerve cord was considered mutant. The percent of animals with pathfinding defects was noted, and the percentage of defective axons was noted. VD cell body displacement: The VD neurons are descendants o the P cells. If the P nuclei fail to migrate ventrally, the resulting VD cell bodies can be laterally displaced out of the ventral nerve cord. The percentage of animals with laterally displaced VD cell bodies was scored. PDE axon pathfinding: The cell bodies of the PDE neurons (PDEL and PDER) are situated in the posterior lateral post-

deirid ganglion. PDEs extend an axon ventrally to the ventral nerve cord, which then bifurcates and extends anteriorly and posteriorly in the ventral nerve cord. If the axon failed to reach the ventral nerve cord or wandered beyond a 45^{o} angle from a straight line ventrally from the cell body, it was considered mutant. Significance was determined using Fisher Exact Analysis.

Activated *ced-10(G12V)*, *mig-2(G16V),* and *myr::unc-115* transgenes. *ced-10(G12V)* and *mig-2(G16V)* transgenes under the control of the *osm-6* promoter were used as described previously (Struckhoff and Lundquist 2003). A *myr::unc-115* transgene under the control of the *unc-115* promoter was used as described previously (Yang and Lundquist 2005).

Scoring of distal tip cell migration defects: Gonadal distal tip cell migration defects were scored by Differential Interference Microscopy in young adult hermaphrodite animals. Any deviation from the normal U-shape of gonad arms was scored as defective, including failure to migrate fully, failure to make a dorsal turn, failure to make an anterior or posterior turn, or extra dorsal-ventral or anterior-posterior turns. Significances of differences (p values) were determined using Fisher Exact Analysis.

RACK-1 transgenes. A full-length *rack-1(+)* transgene was generated by PCR from genomic DNA (based on the Wormbase gene model K07D7.1) and included the entire upstream *rack-1* region (~2.5 kb), the coding region, and the

downstream region past the poly-A addition site (Figure 1E). *rack-1::gfp* and *rack-1::myc* fusion constructs were generated by amplifying the entire *rack-1* upstream region and coding region lacking the stop codon fused in frame to *gfp* or *myc*. The *unc-25 promoter::rack-1::gfp* fusion protein was generated by amplifying the *rack-1* coding region lacking the upstream region. This fragment was placed downstream of the *unc-25* promoter and fused in frame to *gfp* at the 3' end.

UNC-115 yeast-two-hybrid screen: The two-hybrid screen was conducted at the Molecular Interaction Facility at the University of Wisconsin-Madison (thanks to E. Maher). In a liquid multi-well format, approximately 36 million *C. elegans* cDNA clones representing both oligo dT and random-primed libraries were screened via mating. UNC-115 was fused to the GAL4 DNA-binding domain in the pBUTE plasmid and the prey cDNAs were fused to the GAL4 activation domain in the pACT plasmid. In the yeast strain, the bacterial *lacZ* gene and the *HIS5* gene were under the control of a GAL4-regulated promoter. The interaction screen consisted of assaying β-galactosidase (β-gal) activity (for *lacZ)* and growth on 25mM 3-aminotriazole (3-AT) (for *HIS5)*. This analysis identified 244 potential interacting cDNAs that had β-gal activity and grew on 25mM 3-AT. From these 244, 142 isolates activated both *lacZ* and *HIS5* similarly when re-tested. Of these, 124 were bait-specific and did not activate when the bait plasmid was removed. These cDNAs were sequenced, and seven of these were

found to represent the K07D7.1 gene in Wormbase (*rack-1)* (Ai, Poole et al. 2009).

RACK-1::MYC Immunoprecipitation. In order to obtain large amounts of *C. elegans* protein extract, animals carrying an integrated *rack-1::myc* transgene were raised at room temperature in a liquid culture containing 2.5mg cholesterol, 0.05mg/mL streptomycin, *Escherichia coli* strain HB101 and M9 buffer (up to 500mL). After about a week, these animals were harvested and snap-frozen in liquid nitrogen. We then added lysis buffer (1X PBS, 10% glycerol, 0.1% NP40, 0.1% Tween) in a 1:1 ratio, and then 1mM of phenylmethanesulphonylfluoride. We lysed the animals with glass beads in a beater for two cycles of 1 minute each. The supernatant was then collected and stored at –80^{o}C for further experiments. We based our immunoprecipitation assays in Clonetech Laboratories' protocol No. PT3407-1 (Clonetech). We performed the standard immunoprecipitation assays as described in (Yang, Lu et al. 2006) using protein G (Zymed) and anti-Myc monoclonal antibody (Clontech). The anti-UNC-115 antibody is described in (Yang, Lu et al. 2006).

Figure 2.1

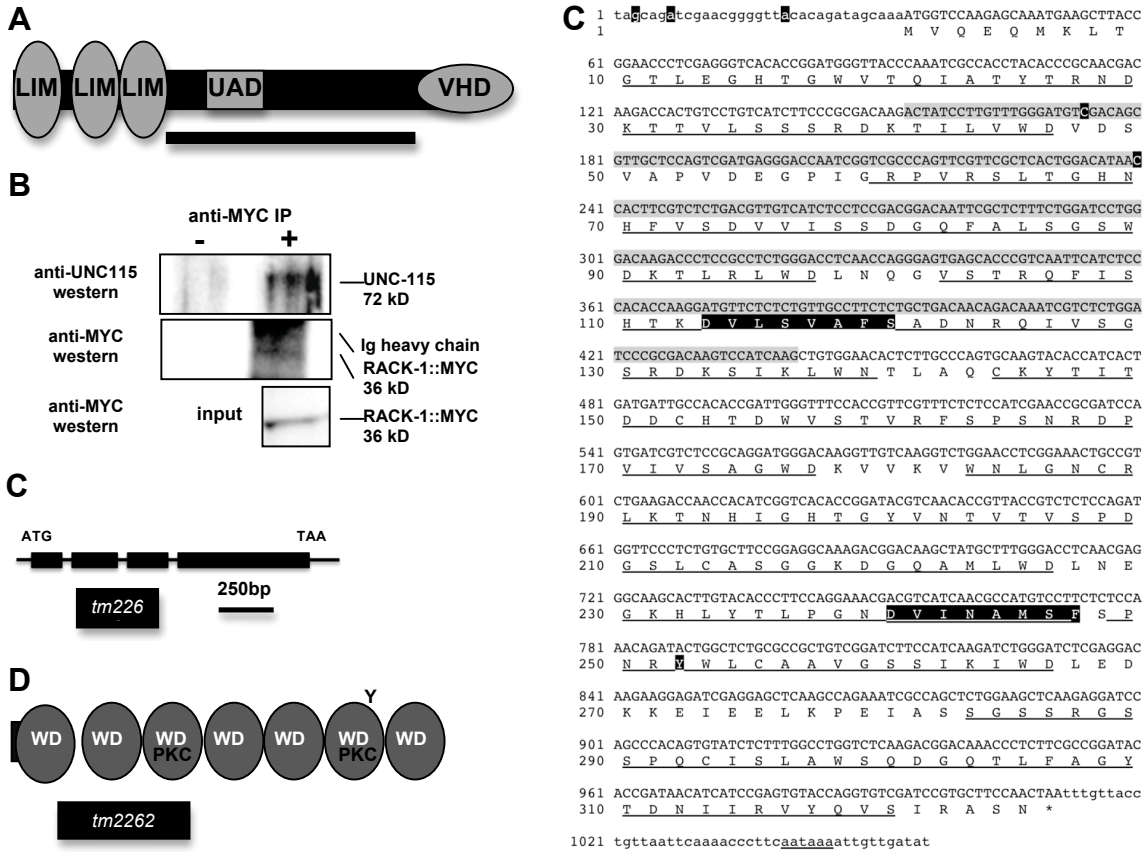
A
LIM
LIM
LIM
UAD
VHD
B
anti-MYC IP
-
+
anti-UNC115 western
UNC-115 72 kD
anti-MYC western
Ig heavy chain
RACK-1::MYC 36 kD
anti-MYC western
input
RACK-1::MYC 36 kD
C
ATG
TAA
250bp
tm226
D
WD
WD
WD PKC
WD
WD
WD PKC
Y
WD
tm2262
C
1 tagcagatcgaacggggttacacagatagcaaaaATGGTCCAAGAGCAAATGAAGCTTACC
1 M V Q E Q M K L T
61 GGAACCCTCGAGGGTCACACCGGATGGGTTACCCAAATCGCCACCTACACCCGCAACGAC
10 G T L E G H T G W V T Q I A T Y T R N D
121 AAGACCACTGTCCTGTCATCTTCCCGCGACAAGACTATCCTTGTTTGGGATGTCGACAGC
30 K T T V L S S S R D K T I L V W D V D S
181 GTTGCTCCAGTCGATGAGGGACCAATCGGTCGCCCAGTTCGTTCGCTCACTGGACATAAC
50 V A P V D E G P I G R P V R S L T G H N
241 CACTTCGTCTCTGACGTTGTCATCTCCTCCGACGGACAATTCGCTCTTTCTGGATCCTGG
70 H F V S D V V I S S D G Q F A L S G S W
301 GACAAGACCCTCCGCCTCTGGGACCTCAACCAGGGAGTGAGCACCCGTCAATTCATCTCC
90 D K T L R L W D L N Q G V S T R Q F I S
361 CACACCAAGGATGTTCTCTCTGTTGCCTTCTCTGCTGACAACAGACAAATCGTCTCTGGA
110 H T K D V L S V A F S A D N R Q I V S G
421 TCCCGCGACAAGTCCATCAAGCTGTGGAACACTCTTGCCCAGTGCAAGTACACCATCACT
130 S R D K S I K L W N T L A Q C K Y T I T
481 GATGATTGCCACACCGATTGGGTTTCCACCGTTCGTTTCTCTCCATCGAACCGCGATCCA
150 D D C H T D W V S T V R F S P S N R D P
541 GTGATCGTCTCCGCAGGATGGGACAAGGTTGTCAAGGTCTGGAACCTCGGAAACTGCCGT
170 V I V S A G W D K V V K V W N L G N C R
601 CTGAAGACCAACCACATCGGTCACACCGGATACGTCAACACCGTTACCGTCTCTCCAGAT
190 L K T N H I G H T G Y V N T V T V S P D
661 GGTTCCCTCTGTGCTTCCGGAGGCAAAGACGGACAAGCTATGCTTTGGGACCTCAACGAG
210 G S L C A S G G K D G Q A M L W D L N E
721 GGCAAGCACTTGTACACCCTTCCAGGAAACGACGTCATCAACGCCATGTCCTTCTCTCCA
230 G K H L Y T L P G N D V I N A M S F S P
781 AACAGATACTGGCTCTGCGCCGCTGTCGGATCTTCCATCAAGATCTGGGATCTCGAGGAC
250 N R W W L C A A V G S S I K I W D L E D
841 AAGAAGGAGATCGAGGAGCTCAAGCCAGAAATCGCCAGCTCTGGAAGCTCAAGAGGATCC
270 K K E I E E L K P E I A S S G S S R G S
901 AGCCCACAGTGTATCTCTTTGGCCTGGTCTCAAGACGGACAAACCCTCTTCGCCGGATAC
290 S P Q C I S L A W S Q D G Q T L F A G Y
961 ACCGATAACATCATCCGAGTGTACCAGGTGTCGATCCGTGCTTCCAACTAAtttgttacc
310 T D N I I R V Y Q V S I R A S N *
1021 tgttaattcaaaacccttcaataaaattgttgatat

Figure 2.1. RACK-1 and UNC-115 interact by two-hybrid and co-immunoprecipitation. A) A schematic diagram of the 639-residue UNC-115 molecule. LIM = LIM domains; VHD = villin headpiece domain; UAD = unc-115/abLIM/dematin domain. The bar represents the region of the molecule used as bait in a two-hybrid screen. B) UNC-115 co-immunoprecipitated with MYC-tagged RACK-1. Lysates of worms expressing MYC-tagged RACK-1 were used in immunoprecipitation experiments with and without anti-Myc antibody. Western blots using anti-UNC-115 antibody (Yang, Lu et al. 2006) (top) showed that UNC-115 co-immunoprecipitated with RACK-1::MYC. Western blots using anti-Myc showed that RACK-1::MYC was expressed (input) and was immunoprecipitated. RACK-1::MYC ran just below the Ig heavy chain of the anti-Myc antibody used in the immunoprecipitation. C) The *rack-1* gene and *tm2262* allele. This model is based on the K07D7.1 gene model in Wormbase and on the cDNAs sequenced from the two-hybrid screen. *tm2262* is a 331-bp deletion. (D) Schematic diagram of the 325-residue RACK-1 protein. WD = WD repeat; PKC = conserved protein kinase C interaction sites; Y = conserved tyrosine phosphorylated by Src in mammalian RACK. The region removed by the *tm2262* deletion is indicated. D) Sequence of the *rack-1* cDNA and protein. cDNA sequence: The sequence of the RACK-1 cDNA is based upon sequencing seven cDNAs isolated from the two-hybrid screen and on cDNA sequences in Wormbase. The predicted open reading frame is upper case, and the 5' and 3' untranslated regions are lower case. A predicted poly-A addition site is underlined, and poly A residues are present in the cDNAs at the end of the

sequence shown here. The nucleotides removed by the *tm2262* deletion are shaded in grey. The starting points of the five independent cDNAs isolated in the two-hybrid screen are highlighted in black. Amino acid sequence: The predicted amino acid sequence is shown below the cDNA sequence. The WD repeats are underlined; the two conserved PKC interaction sites are highlighted in black; and the conserved tyrosine residue that is phosphorylated by Src in mammalian RACK is highlighted in black.

Figure 2.2

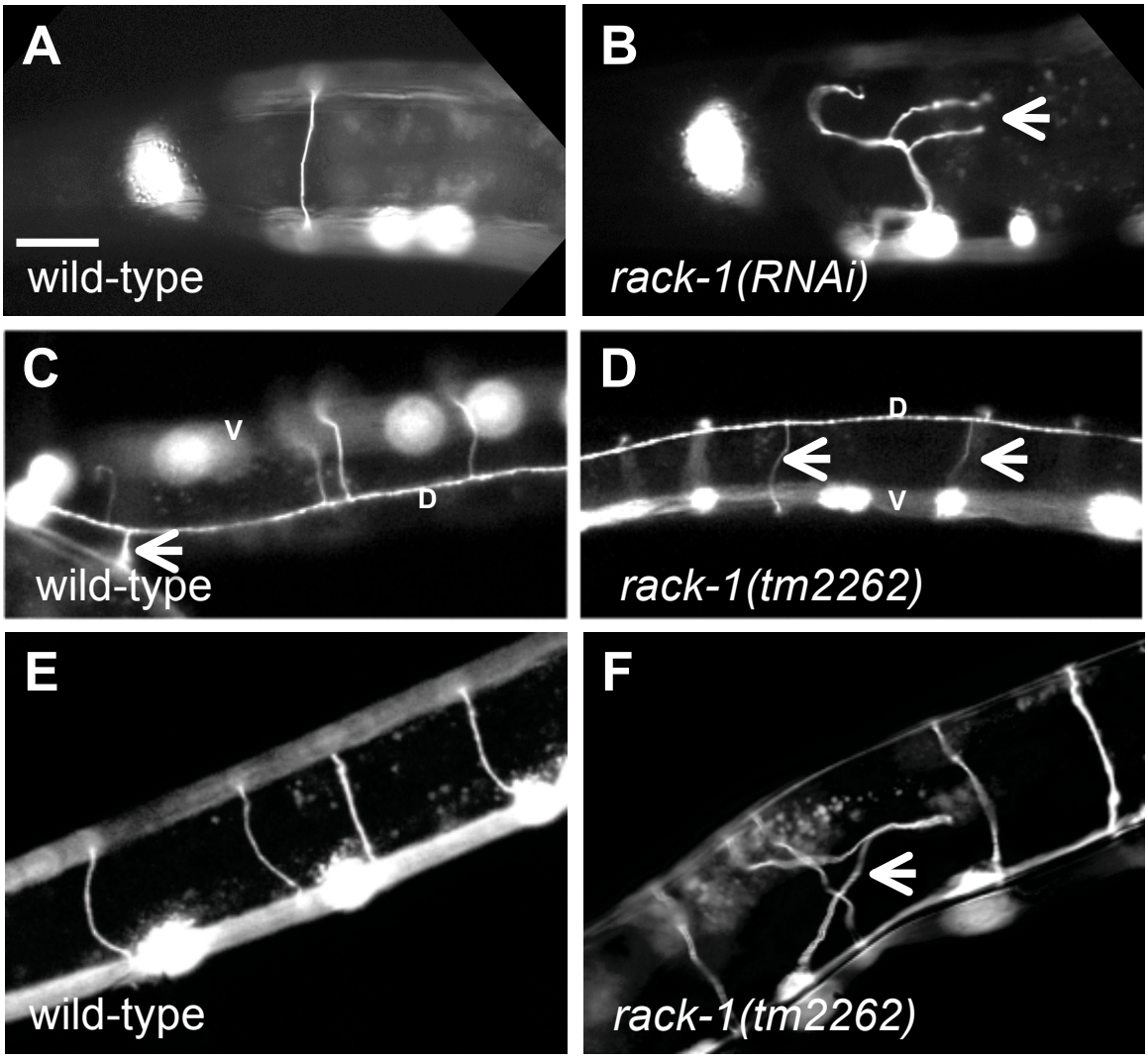
A
wild-type
B
rack-1(RNAi)
C
V
D
wild-type
D
D
V
rack-1(tm2262)
E
wild-type
F
rack-1(tm2262)

Figure 2.2. RACK-1 is required for VD/DD motor axon pathfinding. All panels are micrographs of animals with *unc-25promoter::gfp* expression (*juIs76* transgene) in the VD/DD GABAergic motor neurons. The scale bar in A represents 10μm for all panels. (A and B) Wild-type and *rack-1(RNAi)* showing the DD1/VD2 commissure on the left side of the animal. Misrouted and branched axons are indicated by an arrow. Dorsal is up, and anterior is left. (C and D) Dorsal views of the dorsal nerve cords (marked by a D) of wild-type and *rack-1(tm2262)*. This dorsal view allows for demonstration of the sidedness of axon pathfinding. The cell bodies in the ventral nerve cord are out of focus (marked by a V). The arrow in C points to the DD1/VD2 commissure on the left side of the animal. All other VD/DD commissures go up the right side. Arrows in D point to VD/DD commissures that aberrantly extend up the left side of the animal in *rack-1(tm2262)*. (E and F) VD/DD commissures in wild-type and *rack-1(tm2262)*. The arrow in F points to a misguided axon.

Figure 2.3

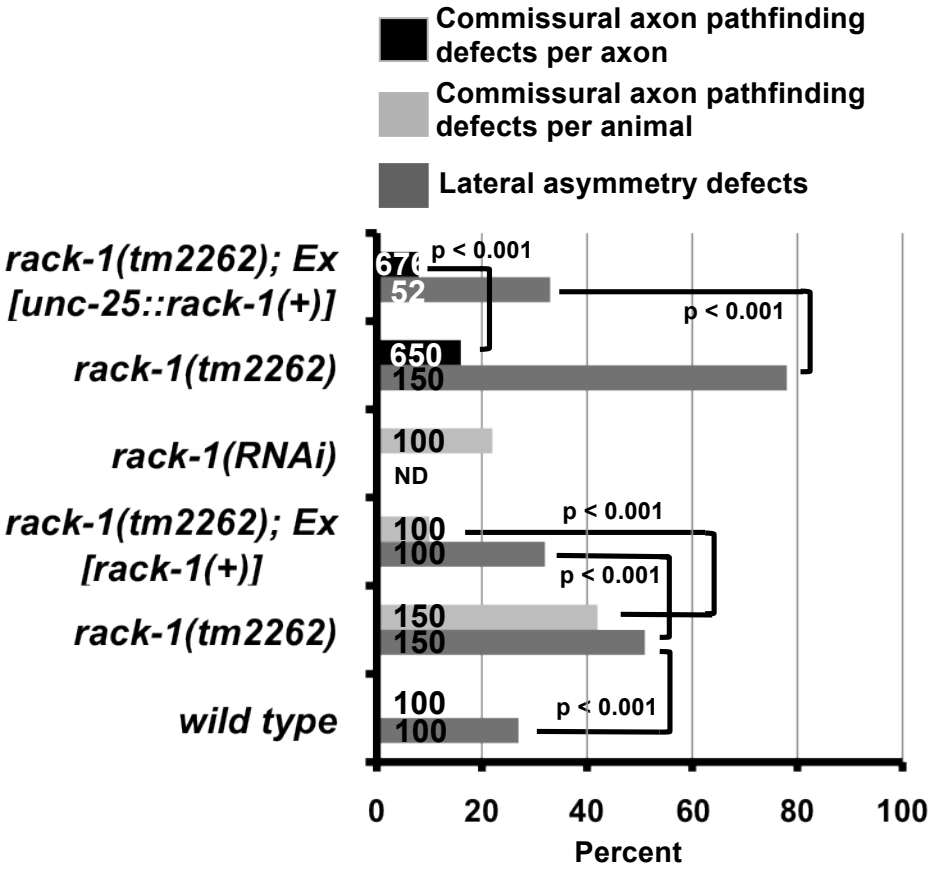
Commissural axon pathfinding defects per axon
Commissural axon pathfinding defects per animal
Lateral asymmetry defects
rack-1(tm2262); Ex [unc-25::rack-1(+)]
rack-1(tm2262)
rack-1(RNAi)
rack-1(tm2262); Ex [rack-1(+)]
rack-1(tm2262)
wild type
p < 0.001
p < 0.001
p < 0.001
p < 0.001
p < 0.001
52
650
150
100
ND
100
100
150
150
100
100
0
20
40
60
80
100
Percent

Figure 2.3. RACK-1 acts cell autonomously in VD/DD motor axon pathfinding. The Y axis denotes genotype, and the X axis represents percentage of defects of the sort described in the legend. *Ex[rack-1(+)]* is the full-length *rack-1::myc* transgene under the *rack-1* endogenous promoter, and *Ex[unc-25::rack-1(+)]* is a transgene with *rack-1::gfp* expression driven by the *unc-25* promoter specifically in the GABAergic neurons, including the VD/DDs. VD/DD commissural axon pathfinding defects were scored by animal (the percent of animals with defective axons) or by axon (the percent of defect axons). Number of animals or axons scored is indicated in the bars. P-values for significance were determined by Fisher Exact Analysis.

Figure 2.4

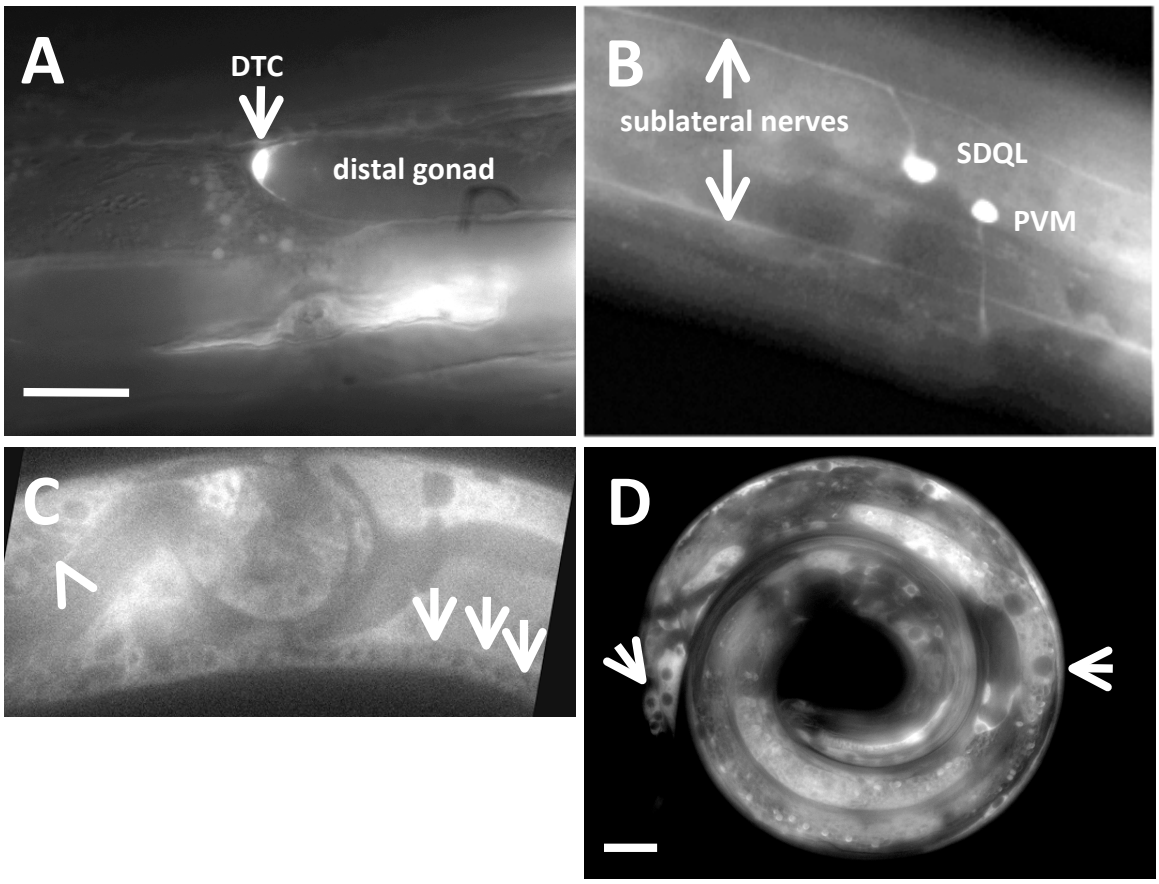

Figure 2.4. RACK-1 is expressed in most cells, including neurons and the gonadal distal tip cells. Panels are fluorescent micrographs of animals harboring *rack-1::gfp* transgenes. (A and B) are fusions of the *rack-1* promoter to *gfp*; and (C and D) are fusions of the entire full-length *rack-1* coding region to GFP. A) A distal tip cell expressed *rack-1::gfp*. B) Neurons expressed *rack-1::gfp*. C) Full-length RACK-1::GFP was expressed in neurons in the ventral nerve cord (arrows) and in the amphid (arrowhead). D) Full-length RACK-1::GFP was excluded from nuclei in tail hypodermis and gut (arrows). The scale bar in A represents 5μm for A-C, and the scale bar in D represents 5μm.

Figure 2.5

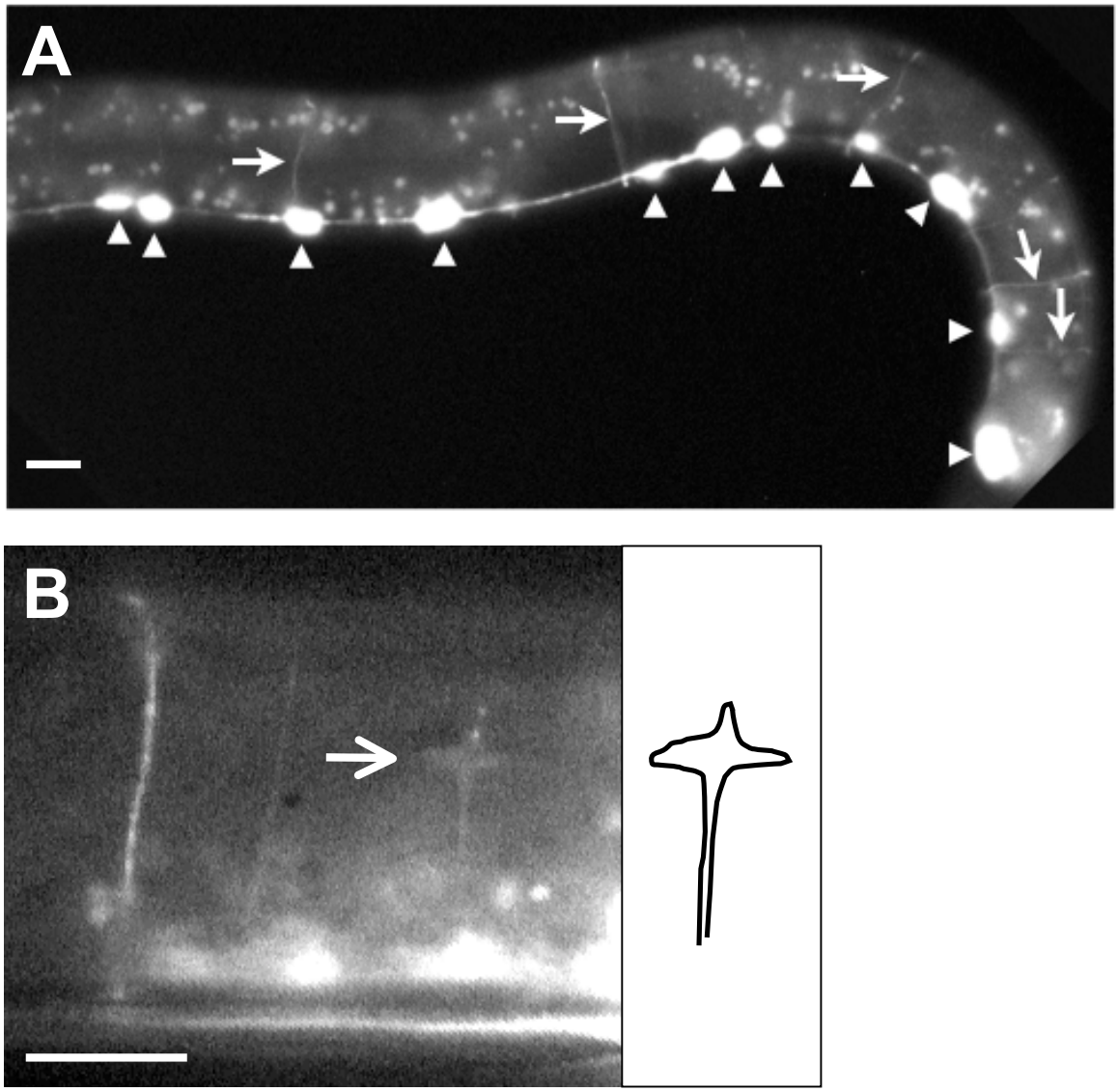

Figure 2.5. RACK-1::GFP expression in GABAergic motor neurons.

Micrographs are of animals harboring an *unc-25::rack-1::gfp* transgene that expresses a full-length RACK-1::GFP fusion protein specifically in the VD/DD GABAergic motor neurons. A) RACK-1::GFP expression is specific to the VD/DD motor neurons. Arrowheads indicate cell bodies in the ventral nerve cord, and arrows indicate commissural axons. The punctate fluorescence throughout the animal is autofluorescence of the gut. B) RACK-1::GFP accumulated in a VD growth cone in an early L2 animal (arrow). The diagram at the right traces the outline of the growth cone and axon. The scale bars represent 5μm.

Figure 2.6

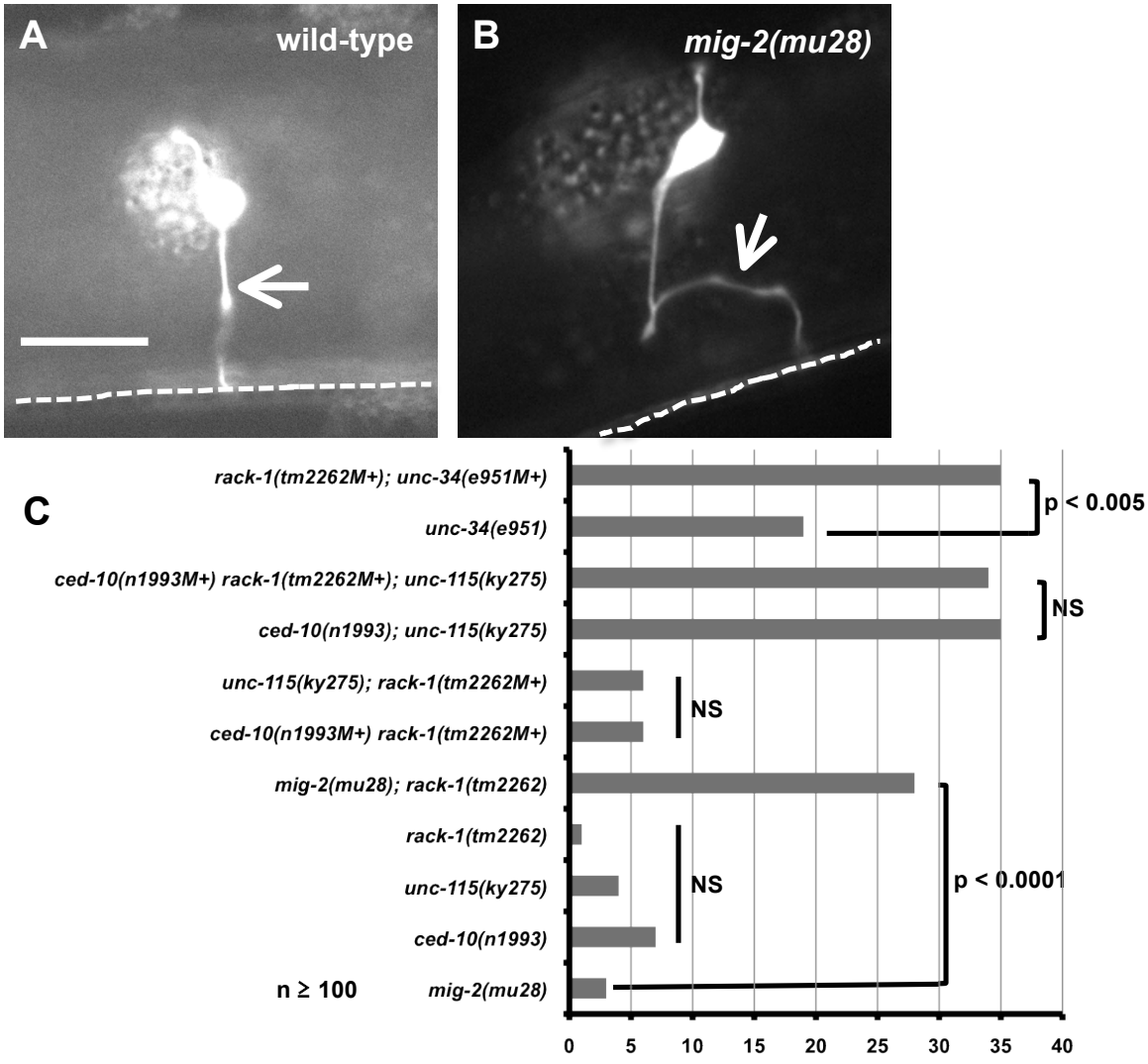
A
wild-type
B
mig-2(mu28)
C
rack-1(tm2262M+); unc-34(e951M+)
unc-34(e951)
ced-10(n1993M+) rack-1(tm2262M+); unc-115(ky275)
ced-10(n1993); unc-115(ky275)
unc-115(ky275); rack-1(tm2262M+)
ced-10(n1993M+) rack-1(tm2262M+)
mig-2(mu28); rack-1(tm2262)
rack-1(tm2262)
unc-115(ky275)
ced-10(n1993)
mig-2(mu28)
n ≥ 100
p < 0.005
NS
NS
NS
p < 0.0001
0
5
10
15
20
25
30
35
40

Figure 2.6. RACK-1 acts genetically in the CED-10/Rac and UNC-115/abLIM pathway. (A and B) Micrographs of animals with *osm-6::gfp* expression in the PDE neurons. The arrow in A indicates a wild-type axon, and the arrow in B indicates a misguided axon in a *mig-2(mu28)* mutant. The scale bar represents 5μm for A and B. C) The graph represents percent of PDE axon pathfinding defects in different genotypes. At least 100 neurons were scored for each genotype, and p-value significance was determined by Fisher Exact Analysis. The genotypes indicated with an NS are not significantly different in any pairwise combination.

Figure 2.7

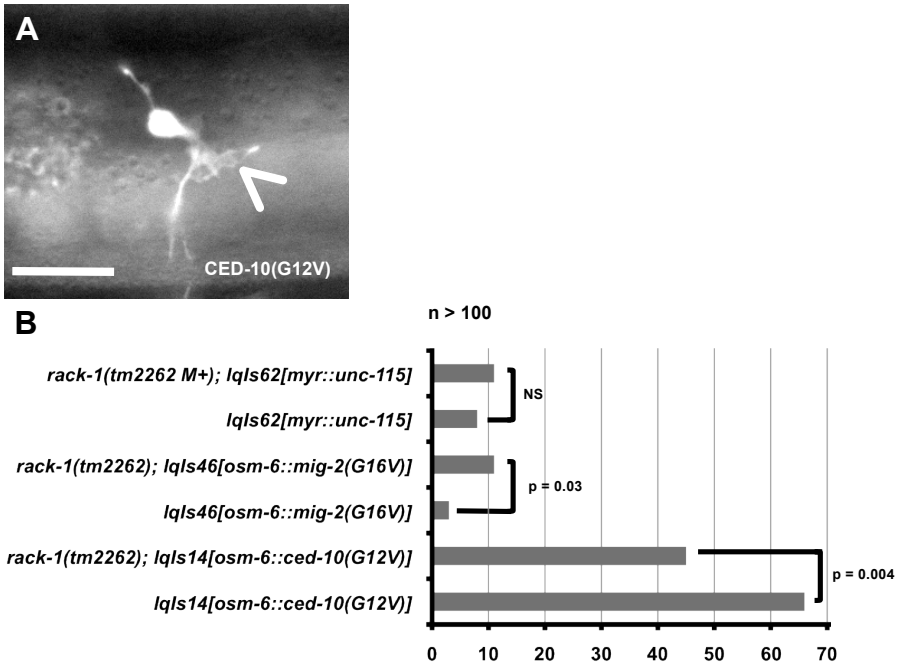
A
CED-10(G12V)
B
n > 100
rack-1(tm2262 M+); lqls62[myr::unc-115]
lqls62[myr::unc-115]
rack-1(tm2262); lqls46[osm-6::mig-2(G16V)]
lqls46[osm-6::mig-2(G16V)]
rack-1(tm2262); lqls14[osm-6::ced-10(G12V)]
lqls14[osm-6::ced-10(G12V)]
NS
p = 0.03
p = 0.004
0
10
20
30
40
50
60
70

Figure 2.7. *rack-1(tm2262)* partially suppresses activated CED-10(G12V), but not MIG-2(G16V) or activated MYR::UNC-115. A) A micrograph of the PDE neuron of an adult animal expressing activated CED-10(G12V). An ectopic lamellipodial protrusion is indicated by an arrow. The scale bar represents 5μm. B) Quantitation of PDE defects. *lqIs14* is the *osm-6::ced-10(G12V)* transgene; *lqIs46* is the *osm-6::mig-2(G16V)* transgene; and *lqIs62* is the *unc-115::myr::unc-115* transgene. At least 100 neurons were scored for each genotype, and p-value significance was determined by Fisher Exact Analysis.

Figure 2.8

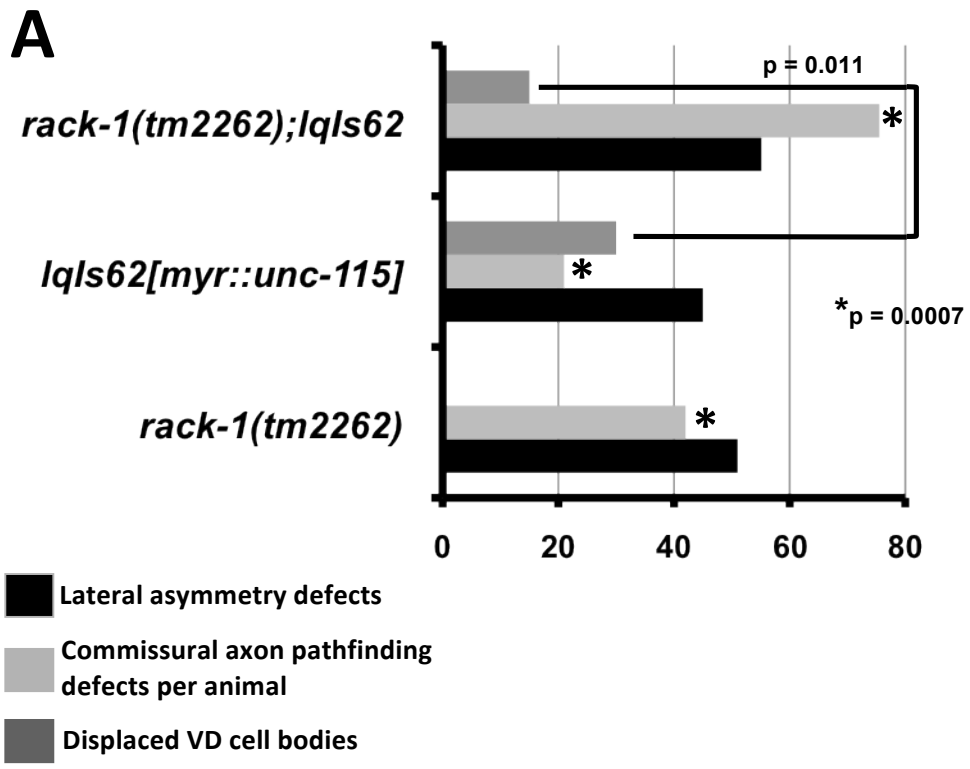
A
rack-1(tm2262);lqls62
lqls62[myr::unc-115]
rack-1(tm2262)
p = 0.011
*p = 0.0007
*
*
*
0
20
40
60
80
Lateral asymmetry defects
Commissural axon pathfinding defects per animal
Displaced VD cell bodies

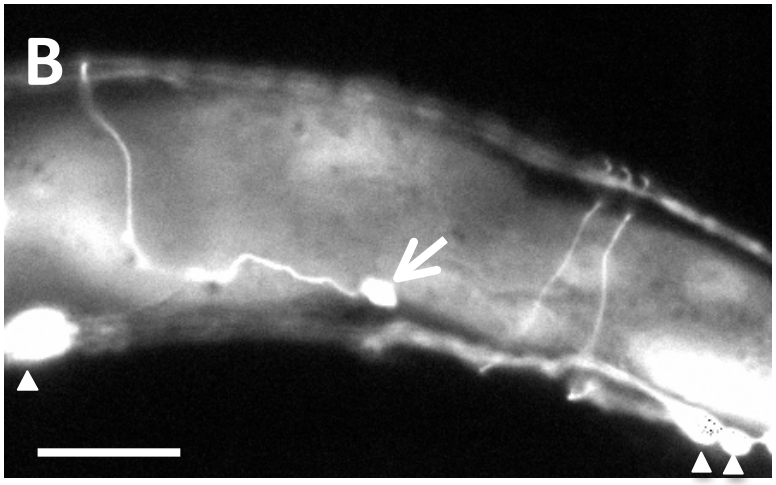
B

Figure 2.8. Activated MYR::UNC-115 in VD/DD motor neurons is not suppressed by *rack-1(tm2262)*. A) Quantitation of VD/DD defects caused by expression of MYR::UNC-115 from the *unc-115* promoter, which is expressed in the VD/DD neurons. The asterisks represent a test of additivity of the represented genotypes. The double mutant is significantly different from each single, and the double mutant had defects that were significantly stronger than the additive effects of each single. The following formula was used to predict the additive effect of the double mutant based on the single mutant phenotypes: *rack-1(tm2262)* + *lqIs62* – (*rack-1(tm2262)* * *lqIs62*); or 0.42 + 0.21 – (0.42 * 0.21) = 0.54. At least 100 animals were scored, and p-value significance was determined by Fisher Exact Analysis. B) A VD neuron cell body was laterally displaced (arrow) in a *rack-1(tm2262M+); lqIs62[myr::unc-115]* animal. *rack-1(tm2262)* partially suppressed this phenotype compared to *lqIs62* alone. Arrowheads indicate VD/DD cell bodies in their normal positions in the ventral nerve cord.

Figure 2.9

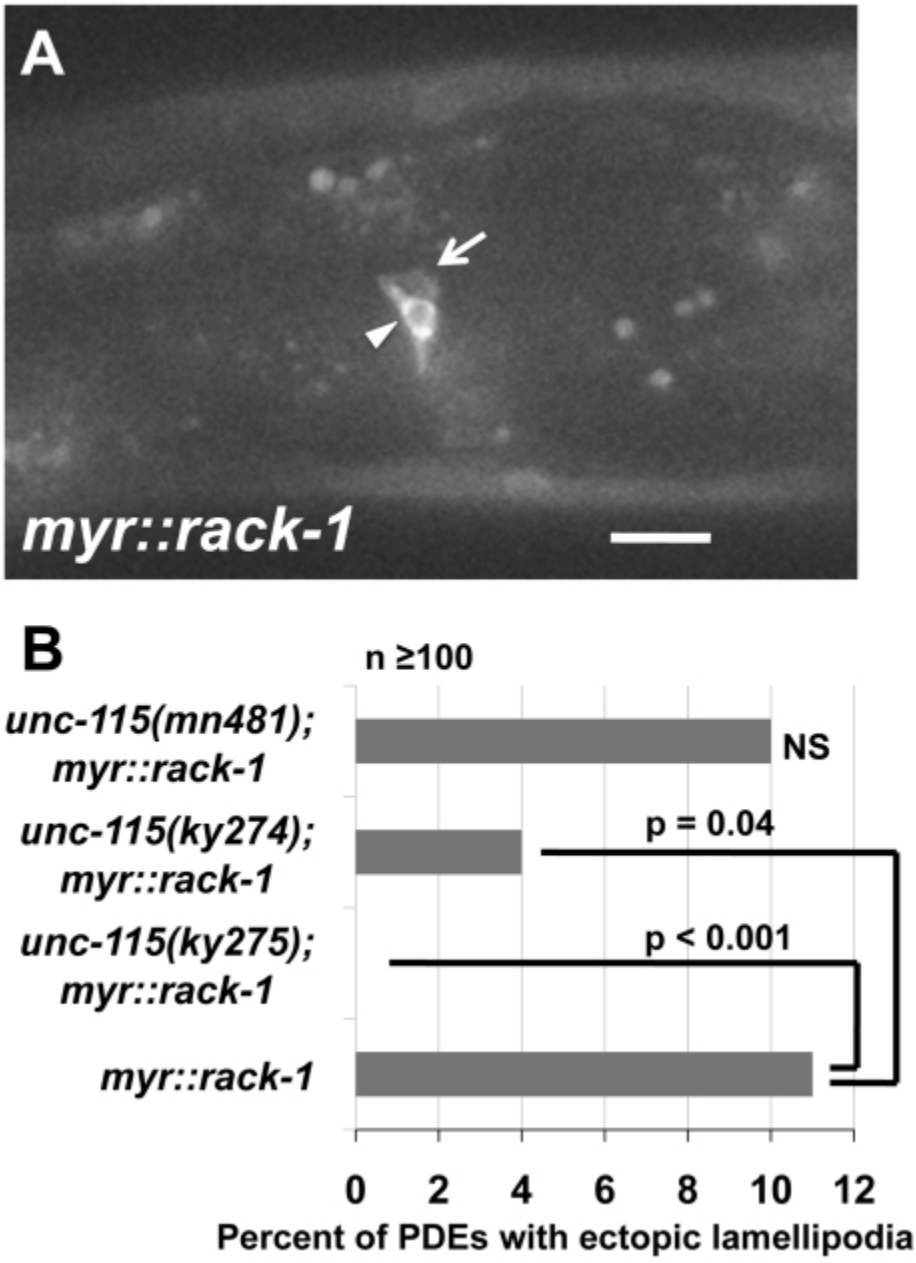
A
myr::rack-1
B
n ≥100
unc-115(mn481); myr::rack-1
NS
unc-115(ky274); myr::rack-1
p = 0.04
unc-115(ky275); myr::rack-1
p < 0.001
myr::rack-1
0
2
4
6
8
10
12
Percent of PDEs with ectopic lamellipodia

Figure 2.9. UNC-115 is required for the effects of MYR::RACK-1. A) A micrograph of MYR::RACK-1::GFP expression in the PDE neuron driven by the *osm-6* promoter. The arrowhead points to the cell surface accumulation of MYR::RACK-1::GFP, and the arrow points to an ectopic lamellipodium. The scale bar represents 5 μm. B) Quantitation of ectopic lamellipodial defects in PDEs expressing MYR::RACK-1::GFP. At least 100 animals were scored for each genotype, and p-value significance was determined by Fisher Exact Analysis.

Figure 2.10

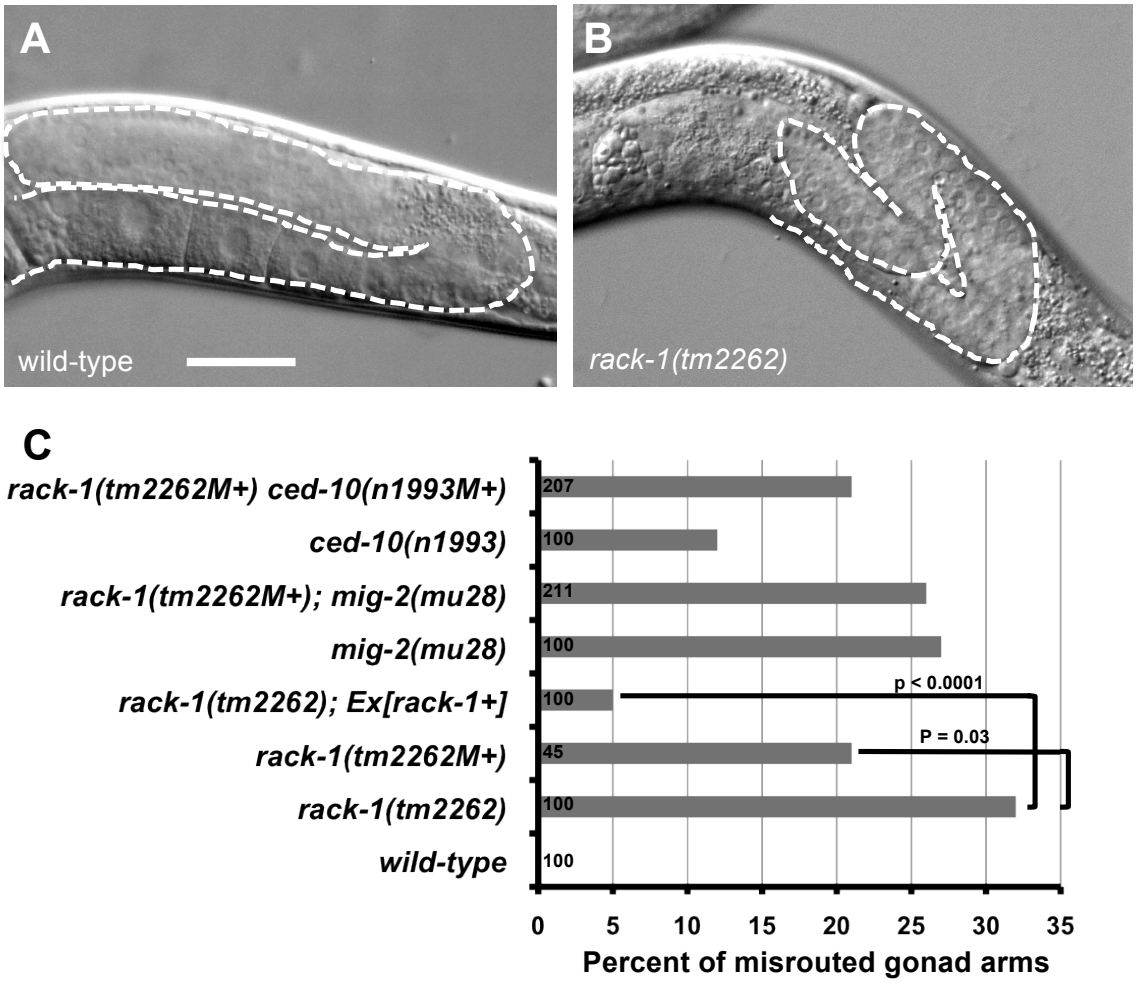
A
wild-type
B
rack-1(tm2262)
C
rack-1(tm2262M+) ced-10(n1993M+)
ced-10(n1993)
rack-1(tm2262M+); mig-2(mu28)
mig-2(mu28)
rack-1(tm2262); Ex[rack-1+]
rack-1(tm2262M+)
rack-1(tm2262)
wild-type
207
100
211
100
100
45
100
100
p < 0.0001
P = 0.03
0
5
10
15
20
25
30
35
Percent of misrouted gonad arms

Figure 2.10. RACK-1 is required for gonadal distal tip cell migration. (A and B) Differential Interference Contrast micrographs of wild-type and *rack-1(tm2262)* gonads. Dashed lines trace the outline of the gonad arm. The scale bar in A represents 10μm. C) Quantitation of gonad arm migration defects. Number of gonad arms scored is indicated in the bars (>100). P-value significance was determined by Fisher Exact Analysis. The predicted additive effect of the *rack-1(tm2262M+) ced-10(n1993M+)* double if they did not interact was calculated by the formula *rack-1(tm2262)* + *ced-10(n1993)* – (*rack-1(tm2262)* * *ced-10(n1993*); or 0.32 + 0.14 – (0.32 * 0.14) = 0.42. This number was also significantly different that the observed *rack-1(tm2262M+) ced-10(n1993M+)* double mutant.

Figure 2.11

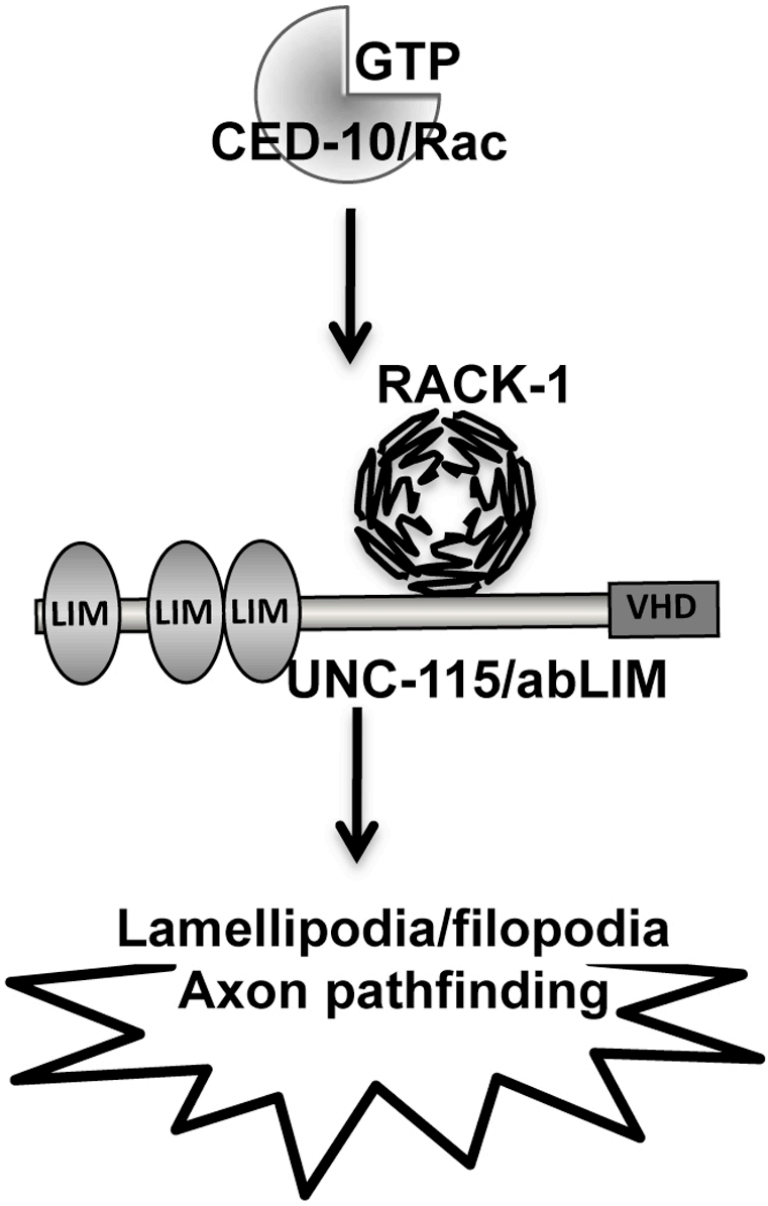
GTP
CED-10/Rac
RACK-1
LIM
LIM
LIM
VHD
UNC-115/abLIM
Lamellipodia/filopodia
Axon pathfinding

Figure 2.11. RACK-1 might regulate UNC-115/abLIM downstream of CED-10/Rac in lamellipodia and filopodia formation. A linear pathway representing the genetic interactions between *ced-10/Rac, rack-1,* and *unc-115*. RACK-1 acts downstream of CED-10/Rac and controls UNC-115/abLIM. LIM = LIM domain; VHD = villin headpiece domain.

Chapter III

The actin-binding protein UNC-115/abLIM interacts with the protein kinase C orthologs PKC-1 and TPA-1, and with the Nck-Interacting Kinase MIG-15/NIK, via the receptor for activated C kinase 1 (RACK-1) during *C. elegans* axon pathfinding

3.1. Abstract

Three of the main pathways involved in the reshaping of the peripheral actin cytoskeleton to promote cell migration and axon guidance are the Rac GTPases, PKCs and Src kinases. In *C. elegans* axon pathfinding, the actin-binding protein UNC-115/abLIM acts with the Rac pathway. UNC-115/abLIM is believed to be activated in a step-wise manner: when at the leading edge of the growth cone, the Rac GTPase CED-10 signals to the scaffolding protein RACK-1 to recruit UNC-115/abLIM. UNC-115/abLIM can possibly be modulated via phosphorylation of its villin headpiece domain. Because RACK-1 is a scaffolding protein that does not have any catalytic domains on itself, but has putative sites of interaction with other molecules such as PKC and Src, we wondered if these kinases could be acting with UNC-115/abLIM and RACK-1 downstream of Rac GTPases in axon pathfinding.

Our data reveal a novel interaction between PKC and UNC-115/abLIM via RACK-1, possibly integrating the PKC and Rac GTPase signaling pathways. We also show that the Nck-interacting Kinase MIG-15 is another putative modulator of the activity of UNC-115 in this process.

3.2. Introduction

During the long journey on which an axon goes to find its proper path, complex extra- and intra-cellular mechanisms act in the receiving, processing and modulation of the guidance signals presented to the growth cone (Chan, Zheng et al. 1996; Hao, Yu et al. 2001; Adler, Fetter et al. 2006; Quinn, Pfeil et al. 2008). As described in the previous chapter, one set of molecules that regulates intra-cellularly filopodia and lamellipodia morphology and dynamics during growth cone migration is the Rac GTPases. MIG-2/RhoG and CED-10/Rac, the two redundant *Caenorhabditis elegans* Rac GTPases, act in parallel to control the actin nucleator Arp2/3 complex (Shakir, Jiang et al. 2008). The Arp2/3 complex has been involved in many aspects of cell and growth cone migration, including the modulation of filopodial and lamellipodial protrusions (Borisy and Svitkina 2000; Pollard and Borisy 2003). MIG-2/RhoG acts in a pathway that activates the GEX-2/Sra-1, GEX-3/Kette and WSP-1/Wasp complex, while CED-10/Rac acts in the GEX-2/Sra-1, GEX-3/Kette and WVE-1/Wave activation pathway. Both WSP-1/Wasp and WVE-1/Wave pathways yield in the Arp2/3 complex activation (Shakir, Jiang et al. 2008).

While much is known about the pathways that lead to the activation of the Arp2/3 complex, less is known about the activation of other actin-binding proteins that also contribute to growth cone dynamics. The actin-binding UNC-115/abLIM acts downstream of CED-10/Rac in axon pathfinding (Struckhoff and Lundquist 2003). In vivo growth cone studies have shown that, like the Arp2/3 complex, UNC-115/abLIM has a role in filopodia and lamellipodia dynamics as well (Norris,

Dyer et al. 2009). UNC-115/abLIM has a C-terminal villin headpiece domain (VHD) that binds to f-actin, and three N-terminal LIM domains that physically interact with the negative Rac regulator SWAN-1 (Yang, Lu et al. 2006). A conserved region of unknown function in the middle of the protein was found to interact with the Receptor for Activated C Kinase (RACK-1), a molecule that also works downstream of CED-10/Rac (Demarco and Lundquist 2010). Epistasis analyses revealed that the activation of UNC-115/abLIM seems to be in a step-wise manner: once activated at the plasma membrane, CED-10/Rac recruits RACK-1, which in turn will recruit UNC-115/abLIM for its actin modulatory activity (Figure 3.1). Because RACK-1 is a seven-WD repeat scaffolding protein, the UNC-115=RACK-1 interaction is hypothesized to be required for the proper spatial regulation of UNC-115/abLIM. Both UNC-115/abLIM and RACK-1 have putative phosphorylation sites that could be regulatory targets for kinases and phosphatases in the appropriate control of axon pathfinding.

In addition, Rack1-like molecules have been suggested to interact with many different proteins involved in cell migration and adhesion, including Integrins, Src, Protein Kinase C (PKC) and Rho GTPase regulators (Chang, Conroy et al. 1998; Liliental and Chang 1998; Buensuceso, Woodside et al. 2001; Sklan, Podoly et al. 2006). In fact, mammalian Rack1 was first identified as the intracellular receptor of PKC (Ron, Chen et al. 1994; Schechtman and Mochly-Rosen 2001). Because *C. elegans* RACK-1 has two conserved predicted PKC-binding sites, and is also a predicted substrate for Src phosphorylation, these two classes of molecules seemed like good candidates for putative

regulators of UNC-115/abLIM. PKCs are master regulators of the cell machinery, and have been implicated in many aspects of cell migration and neuronal development (Kikkawa, Kitano et al. 1986; Besson, Wilson et al. 2002; Wolf, Lyuksyutova et al. 2008). Like UNC-115/abLIM, PKC activity is required for growth cone behavior and filopodia modulation (Cheng, Mao et al. 2000). One PKC effector , the myristoylated, alanine rich C-kinase substrate (MARKS), has a role in growth cone pathfinding (Gatlin, Estrada-Bernal et al. 2006). *C. elegans* has four PKC ortholog genes, and they are all putatively expressed in the nervous system (Tabuse 2002). The *tpa-1* gene encodes two orthologs of the novel PKCs (nPKC) δ and θ, the only phorbol-ester induced PKC isoforms in the nematode (hence its particular name, tetradecanoyl phorbol acetate resistant). The *pkc-1* gene encodes two isoforms, PKC-1A and B, which are neuron-specific and highly homologous to the mammalian nPKCε. PKC-1 displays Ca^{2+}-independent kinase activity, which is typical of nPKCs. The *pkc-2* gene encodes six predicted PKC isoforms, mostly related to the conventional PKCα and β (cPKC). cPKCs require diacylglycerol (DAG), Ca^{2+} and a phospholipid for their activation. Finally, the *pkc-3* gene encodes an atypical PKC (aPKC) isoform that is most similar to mammalian aPKCζ and λ/ι. PKC-3 is involved in establishing the early embryo polarity and interacts with the PAR complex and CDC-42, and has Ca^{2+}- and DAG/phorbol ester-independent kinase activity. Depictions of the longest PKC isoforms from each gene product can be seen in Figure 3.2. Besides *pkc*-3, all other *pkc* genes encode multiple isoforms with differential regulatory elements and/or expression patterns. Therefore, a multitude of

functions could be performed by products from each *pkc* gene depending on how and when they are being expressed.

Srcs are non-receptor tyrosine kinases that, like the PKCs, also control many aspects of cell biology, including axon pathfinding and growth cone morphology (Li, Lee et al. 2004; Robles, Woo et al. 2005; Li, Aurandt et al. 2006). *C. elegans* has two SRC-like proteins (Figure 3.2). SRC-1 has been reported to be expressed in the nervous system, and to work with Wnts for endodermal cell fate specification and the Netrin receptor UNC-5 for cell and growth cone migration independently of Rac GTPases (Bei, Hogan et al. 2002; Itoh, Hirose et al. 2005). Though not as much is known about the function of SRC-2, in a yeast-expression system, SRC-2 overexpression caused an overall increase of tyrosine phosphorylation. In this same system, SRC-2 is suppressed by CSK-1, a predicted negative-regulator of Src activity (Bizat, Peyrin et al. 2010).

Not surprisingly, interactions between the Rho GTPase, Src and PKC signaling pathways have been reported in diverse systems, including the cell extension of vascular smooth muscle and ruffling of MDCK cell plasmalemma (Chianale, Rainero et al. ; Brandt, Gimona et al. 2002). Not all cross-talk between these systems is positive though. Interestingly, after PKC activation, Rack1 inhibits Src signaling in cell migration (Chang, Harte et al. 2002). That we identified RACK-1 as a modulator of UNC-115/abLIM, a downstream component of the CED-10/Rac pathway, suggests we might have uncovered a site of action where PKCs and Srcs cross-talk with Rac GTPases for the proper control of growth cone migration.

Another kinase that could putatively control the activity of UNC-115/abLIM via RACK-1 is the serine-threonine NIK kinase MIG-15. Like the components of the CED-10/Rac pathway, mutations in *mig-15* disrupt wild-type axon pathfinding (Shakir, Gill et al. 2006). *C. elegans* MIG-15 is the counterpart of the mammalian Nck-interacting kinase (NIK) and the Drosophila Misshapen proteins. N-terminally, MIG-15/NIK has a STE20-like serine/threonine kinase domain followed by a proline-rich domain (PRD), while C-terminally it has a putative Rho regulatory CNH domain (Figure 3.2). Besides the genetic evidence linking MIG-15/NIK to Rac GTPases in *C. elegans*, a yeast-two-hybrid screen suggested MIG-15/NIK putatively interacts with RACK-1 (Zhong and Sternberg 2006). Therefore, we also wondered if MIG-15 would be part of the activation complex needed to modulate UNC-115/abLIM.

Here we present evidence that the two novel PKCs TPA-1 and PKC-1, and possibly MIG-15/NIK, interact with RACK-1 and UNC-115/abLIM during axon pathfinding.

3.3 Results

A genetic strategy to screen possible genes that interact with *rack-1* and *unc-115*. In PDE axon pathfinding, CED-10/Rac1 works in parallel to MIG-2/RhoG to solely activate the RACK-1=UNC-115 pathway (Struckhoff and Lundquist 2003). Using the principles of genetic redundancy, in which mutations in genes that act in one pathway synergize with mutations in genes that act in a redundant, parallel pathway, we devised a hypothesis for the screen of candidate genes that could interact with *rack-1* and *unc-115/abLIM*. If a gene acts with *unc-115/abLIM* via *rack-1*, loss-of-function mutations in it should not worsen the defects of loss-of-function alleles of *ced-10/Rac*, *rack-1*, *unc-115/abLIM,* or the gene itself (if it happens to have a higher defect incidence than the established *unc-115* pathway). At the same time, this mutant allele should synergize with *mig-2/RhoG*. However, if a gene acts in both pathways, in a third parallel pathway, or in a hierarchical level different than the *rack-1=unc-115* level, then loss-of-function mutations in it should not follow these predictions.

PKC-1/nPKC acts in the CED-10/Rac=RACK-1=UNC-115/abLIM pathway. We generated double-mutant combinations of all four pkc genes with the genes listed above. *ok563* is a 310bp insertion and 1637bp deletion loss-of-function allele that removes the two first and part of the third exons of both *pkc-1* isoforms. *ok328* is a 7bp insertion and 2310bp deletion that removes part of nine exons of all *pkc-2* isoforms. *ok544* is a G insertion and a 1551bp deletion that removes the four last exons of the *pkc-3* gene. *k501* is a C to T point mutation that affects both

isoforms of the *tpa-1* gene and that causes a missense mutation in the protein (Pro-544-Ser, position based on the B0545.1a cDNA). Finally, *k530* is a Tc1 transposon insertion that also disrupts the function of TPA-1 (wild-type animals are sensitive to PMA, while both *k501* and *k530* mutant animals are resistant to the effects of TPA-1 overactivation with PMA). All chosen alleles are putative null alleles for the corresponding *pkc* genes.

In PDE axon pathfinding, loss-of-function mutations in the genes coding for Rac GTPases and the actin-modulators RACK-1 and UNC-115/abLIM do not have a significant high incidence compared to wild type (Figure 3.3A). In *ced-10(n1993)*, 0% of animals display mutant PDEs. In *mig-2(mu28)*, only 1% displayed mutant PDEs. In *rack-1(tm2262)* and *unc-115(ky275)*, 1% and 4% of animals displayed non-wild type PDEs, respectively.

pkc-1(ok563) animals displayed a mere 2% penetrance of PDE axon pathfinding defects. However, in a double mutant combination with *mig-2(mu28)*, *pkc-1(ok563)* synergized the axon pathfinding defects observed (13% - $p<0.003$)). At the same time, *pkc-1(ok563)* did not significantly increase the defects seen in the other mutant combinations (with *ced-10(n1993)*, 9% ($p<0.025$); with *rack-1(tm2262)*, 8% ($p<0.05$); with *unc-115(ky275)*, 3% ($p<0.72$)) (Figure 3.3C).

PKC-1 acts cell-autonomously downstream of CED-10/Rac, RACK-1 and possibly UNC-115/abLIM in PDE neurons. Because the results above were consistent with *pkc-1* working in the *ced-10=rack-1=unc-115* pathway, we wanted

to investigate when during the activation process of UNC-115 would PKC-1 be required. The GTPase CED-10 can be constitutively activated by the introduction of a point mutation (Gly-12-Val) in the GTPase binding pocket of the protein. Such mutation favors the GTP-bound state of the GTPase, constitutively activating it. When expressed in the PDE neurons, this construct causes ectopic lamellipodia to emanate from the neurons (Figure 3.4B). UNC-115/abLIM and RACK-1 are thought to be active when recruited to the plasma membrane, possibly regulating the actin cytoskeleton in the growth cone during axon extension. When an N-terminal myristoylation sequence is added to these proteins, the resulting covalently-bound myristyl group inserts itself into the plasma membrane. Such membrane localization has been shown to result in ectopic lamellipodia resulting from a putative overactivation of these proteins. We asked if the loss of *pkc-1* activity would suppress the overactivation phenotype resulting from the introduction of of these three constructs.

In animals harboring a *ced-10(G12V)* construct expressed in PDE neurons, 91% of their neurons showed an ectopic lamellipodia. In a *pkc-1(ok563)* background, this number dropped to 67% ($p<0.001$), suggesting PKC-1 is needed for the activity of CED-10(G12V) during ectopic lamellipodia formation. When specifically expressing *myr::rack-1*, 15% of the PDE neurons analyzed displayed ectopic lamellipodia. Consistent with the idea that PKC-1 is needed downstream of its receptor for its activity, *pkc-1(ok563);myr::rack-1* animals displayed only 4% of ectopic lamellipodial projections ($p<0.008$). Finally, when expressed specifically in the PDE neurons, *myr::unc-115* displayed a 5%

penetrance of ectopic lamellipodia. In a *pkc-1(ok563)* background, only 1% of PDEs displayed such phenotype ($p<0.001$) (Figure 3.4A). Therefore, we concluded that PKC-1 is genetically required downstream of CED-10/Rac, RACK-1 and UNC-115/abLIM for their overactivation, and that it most-likely acts cell-autonomously in this process, since all overactive constructs that were suppressed by *pkc-1(ok563)* were expressed by the PDE promoter *osm-6p*. It is possible that PKC-1 is acting at the same level as UNC-115/abLIM, since MYR::UNC-115 only displayed a small percentage of lamellipodial protrusions to start with (i.e., the suppression from 5% to 1% could not be so significant) and UNC-115/abLIM is a possible direct or indirect target of PKC-1 (PKC-1 could be either phosphorylating UNC-115/abLIM directly, or regulating the activity of another kinase that would, in turn, phosphorylate UNC-115/abLIM). Future studies will address that hypothesis, by creating an overactive form of PKC-1 and addressing if the loss of *unc-115* would suppress its overactivation.

TPA-1/nPKC also acts with CED-10/Rac=RACK-1=UNC-115/abLIM in PDE axon pathfinding. Both *tpa-1* loss-of-function alleles *k501* and *k530* displayed similar levels of defects on their own (1% and 0%, respectively). With *mig-2(mu28)*, *k501* increased the defects observed to 13%, and *k530* to 9% (both p values<0.001). Because *k530* is a Tc1 insertion (such transposons have been reported to often excise from their insertion places and promote gene conversion in neurons) and *k501* animals seem to have a similar level of effects on axon pathfinding, we decided to continue our genetic analysis with the *k501* allele only.

tpa-1(k501) rack-1(tm2262) animals displayed only 1% PDE mutant axons, which would be consistent with both molecules acting in a linear pathway. In addition, *tpa-1(k501); unc-115(ky275)* animals displayed 10% of mutant axons ($p<0.1$), a non-significant increase (Figure 3.3D).

PKC-2/cPKC and PKC-3/aPKC do not act at the UNC-115=RACK-1 level with the Rac GTPases in axon pathfinding. *pkc-2(ok328)* displayed 7% of PDE axon pathfinding defects alone. Although there was a slight increase in defects with *mig-2(mu28)* (to 18%, $p<0.02$), that was not significant. Neither were the interactions with *ced-10(n1993)* (12%, $p<0.23$), *rack-1(tm2262)* (3%, $p<0.20$) and *unc-115(ky275)* (14%, $p<0.1$) (Figure 3.3E).

pkc-3(ok544M+) animals had to be maintained in a balancer heterozygous background (*mIn1*) because of its early arresting stages (around the larval stages 2 and 3 – L2/3). Therefore, a maternal contribution might still be present in the PDE neurons analyzed. Even with a maternal effect, double-mutant combinations of *pkc-3(ok544M+)* animals with *unc-115(ky275)* and *rack-1(tm2262)* were lethal probably by embryogenesis, and therefore we were not able to score them. Alone, *pkc-3(ok544M+)* displayed 25% of animals with a misguided PDE axon. Different from other *pkc* mutants, in which the axon misguidance would not be too severe (for example, they would still come out of the ventral side of the cell body and just fail to reach the ventral nerve cord in a wild-type manner – see materials and methods), *pkc-3(ok544M+)* mutant PDE axons would often have polarity defects as well (i.e., axons would come out of the lateral or dorsal side of

the cell body), and wander around in a much more severe way (often not making it all the way to the ventral nerve cord) (Figure 3.3B). This suggests PKC-3 is needed also for neuritogenesis and axon decision, polarity and pathfinding. When in combination with *mig-2(mu28)*, *pkc-3(ok544M+)* mutants increased the PDE pathfinding defects seen to 38% ($p<0.02$); with *ced-10(n1993)*, *pkc-3(ok544M+)* mutants increased the defects observed to 32% ($p<0.8$), both of which were not statistically significant (Figure 3.3F).

SRC-1 and SRC-2 possibly act in a different pathway that does not involve the Rac GTPases in PDE axon pathfinding. SRC-1 has Src-Homology (SH) SH3 and SH2 domains N-terminally, and a kinase domain C-terminally. *src-1(cj293)* is a deletion that removes the SH2 domain and part of the kinase domain of the protein, causing a frame shift. This allele alone caused 8% of PDE neurons to fail in the proper extension of their axons. In a *ced-10(n1993)* background, 21% of PDE neurons were affected ($p<0.01$). Because this increase was significant, we did not pursue the interaction with the other components of this pathway, since we were targeting the most obvious candidates, and many intricate pathways could be envisioned to explain non-trivial genetic results obtained. Similarly, *src-2(ok819)* is a 2426bp deletion that removes portions of the four first exons of the *src-2* gene. *src-2* has not been reported to be expressed throughout the nervous system, so it was not surprising when we observed that src-2(ok819) displayed only 2% axon pathfinding defects, and in a

combination with either *mig-2(mu28)* or *ced-10(n1993)*, *src-2* did not enhance the defects observed (respectively, 6% - p>0.1 , and 5% - p>0.2) (Figure 3.5).

The MIG-15/NIK possibly interacts with RACK-1 to modulate the activity of UNC-115/abLIM in PDE axon pathfinding downstream of CDC-42. An incomplete loss-of-function mutant allele of *mig-15*, called *rh148*, is a Val-168-Glu missense mutation in the ATP-binding pocket of the kinase domain that likely disrupts its kinase activity. The putative null *rh80* allele of *mig-15* is a Trp-898-stop mutation that yields in a premature stop codon that likely results in no protein expression or, if any, a non-functional truncated protein. *mig-15(rh148)* enhances the PDE axon pathfinding defects seen in both *mig-2(mu28)* and *ced-10(n1993)* to levels similar to the null *mig-15(rh80)* allele. In addition, *mig-2(mu28)* and *ced-10(n1993)* do not enhance the *mig-15(rh80)* allele, suggesting MIG-15/NIK acts with both MIG-2/RhoG and CED-10/Rac in this process. We wondered if MIG-15/NIK would be interacting at the UNC-115=RACK-1 level, since MIG-15/NIK has been reported in a yeast-two-hybrid to interact with RACK-1. *mig-15(rh148)* animals had 35% of PDE axon pathfinding defects. A double-mutant of *mig-15(rh148)* and *rack-1(tm2262M+)* displayed 49% defects (p<0.05). *mig-15(rh80)* displayed 47% defects on its own, which are very similar to the double mutant of *mig-15(rh148);rack-1(tm2262)* (p=0.78) (Figure 3.6A). Unfortunately, up-to-date experiments trying to recombine alleles of *mig-15* and *unc-115(ky275)* have proven very difficult, therefore we do not have concrete

evidence of their genetic interaction yet. Nevertheless, other evidence suggests these molecules could be acting together.

The Rho GTPase CDC-42 acts in parallel and upstream of Rac GTPases in the control of axon pathfinding in *C. elegans*. A constitutively activated form of CDC-42, in which the Glycine in position 12 is changed to a Valine (Gly-12-Val), favors the GTP-bound state of this GTPase, and therefore constitutively activates it. *cdc-42(G12V)* animals displayed 55% of PDE neurons with ectopic lamellipodia (Figure 3.6B and C). Loss-of-function mutations in *mig-15* and *unc-115* suppressed ectopic lamellipodial protrusions caused by overactive CDC-42(G12V) (personal communication, data not shown). Therefore, we sought to determine if mutations in *rack-1* would also suppress such defects. *rack-1(tm2262); cdc-42(G12V)* animals displayed some robust suppression of such defects (37%, $p<0.011$) (Figure 3.6B). A double-mutant combination of the null allele of *cdc-42(gk388)* and *rack-1(tm2262)* was lethal even when balanced, and therefore we could not score these animals for defects.

Because RACK-1 is a scaffolding protein that is probably required for the localization of the proteins involved in this process (i.e., UNC-115/abLIM), it is not too surprising that *rack-1(tm2262)* would only partially suppress the effects of CDC-42(G12V). Taken all together, we speculate RACK-1, UNC-115/abLIM and MIG-15/NIK could possibly be interacting together downstream of CDC-42, as well as CED-10/Rac, in PDE axon pathfinding (Figure 3.7).

3.4 Discussion

We previously characterized a step-wise modulation pathway for the actin-binding protein UNC-115/abLIM involving CED-10/Rac activation at the plasma membrane, followed by RACK-1 recruitment to the plasma membrane, and finally UNC-115/abLIM possible activation and localization via RACK-1. Because RACK-1 is a seven-bladed-WD scaffolding protein, it lacks any predicted activation domains and is possibly acting as a molecular assembler, recruiting different molecules together. Rack1-like molecules have been reported to interact with different classes of proteins involved in cell adhesion and migration, including the PKCs, Srcs, Integrins and Rho GTPase regulators. Since UNC-115/abLIM could be putatively modulated by phosphorylation at the C-terminal VHD, where it binds to f-actin, we sought to determine if any of the most well known RACK-1 binding-partners would be modulating the activity of UNC-115/abLIM.

The novel PKCs TPA-1 and PKC-1 interact with the RACK-1=UNC-115 complex downstream of CED-10/Rac. In our genetic screen of all four known *pkc* genes in the *C. elegans* genome, both *pkc-1* and *tpa-1* displayed a genetic interaction consistent with the hypothesis they act with the RACK-1=UNC-115 complex downstream of CED-10/Rac. That all *pkc* genes showed a trend of synergy with *mig-2/RhoG* suggests a possible role of all *pkc* orthologs at this complex level, and that a possible redundancy or pleiotropy of PKC function might hide more clear effects. For example, PKC-3 might act with both CED-

10/Rac and MIG-2/RhoG in particularly different pathways all leading to cell polarity and axon pathfinding. Nevertheless, it is clear to us that at least two PKC classes, PKC-1 and TPA-1, act with RACK-1 and UNC-115/abLIM in this pathway, and that PKC-1 is required cell-autonomously for this process.

SRC kinases affect axon pathfinding possibly in a Rac-independent manner. Neither of the *scr* genes in *C. elegans* displayed a genetic interaction with *mig-2/rhoG* or *ced-10/Rac* consistent with them acting in linear pathways. In the case of SRC-2, where no significant increase was observed in axon pathfinding defects, one could argue SRC-2 and the RacGTPases could possibly interact in parallel but non-redundant pathways (since an additive effect could be hidden due to the fact either gene alone has a very low incidence of defects). However, the *src-2* gene has not been reported to be expressed in the nervous system (at least not in the post-deirid where the PDE neurons are situated). Therefore, it was not too surprising to us that SRC-2 has no direct role in axon pathfinding. Mutations in *src-1*, however, display some minor but significant axon pathfinding defects. This shows SRC-1 has a role in axon pathfinding, and that it may act redundantly with the Rac GTPases.

The NIK kinase MIG-15 possibly acts with RACK-1 and UNC-115/abLIM downstream of CDC-42 and the Rac GTPases in axon pathfinding. The serine-threonine kinase MIG-15/NIK has previously been implicated in acting with the Rac GTPases in PDE axon pathfinding. Moreover, a yeast-two-hybrid screen

has implicated RACK-1 as a binding partner of MIG-15/NIK. Because both UNC-115/abLIM and MIG-15/NIK, and to some extend RACK-1, are needed for the ectopic lamellipodia caused by the overactivation of CDC-42, we speculate these molecules might be acting together during growth cone migration, and that MIG-15/NIK could be controlling the activity of UNC-115/abLIM via RACK-1.

In this work we have dissected another layer of activation needed for the actin-binding UNC-115/abLIM during axonal development. Moreover, we have provided evidence that PKC signaling is involved in axon pathfinding and that it may cross-talk with the Rac GTPase signaling pathway at the level of the RACK-1=UNC-115 complex. Other kinases, such as MIG-15/NIK, could also play a role in the proper control of UNC-115/abLIM during growth cone migration. The different proteins that could interact with UNC-115/abLIM for its proper modulation during axon pathfinding could reveal the different functions UNC-115/abLIM might perform in order for an axon to reach its final target.

3.5. Materials and Methods

Please refer to section 2.4 in Chapter II for PDE axon pathfinding scoring, molecular biology techniques and *C. elegans* culture.

The following mutations and genetic constructs were used: *LGI: src-1(cj293), src-2(ok819), lqIs37[osm-6p::cdc-42(G12V)], hT1 I:V; LGII: cdc-42(gk388), pkc-3(ok544), mIn1[dpy-10(e128) mIs14]; LGIV: ced-10(n1993), rack-1(tm2262), tpa-1(k501 and k530), nT1 IV:V, lqIs3[osm-6::gfp]; LGV: pkc-1(ok563); LGX: unc-115(ky275), mig-2(mu28), pkc-2(ok328), lqIs2[osm-6::gfp]; LG?: lqIs14[osm-6p::ced-10(G12V)], lqIs62[osm-6p::myr::unc-115], lqEx626 [osm-6p::myr::rack-1].*

Figure 3.1

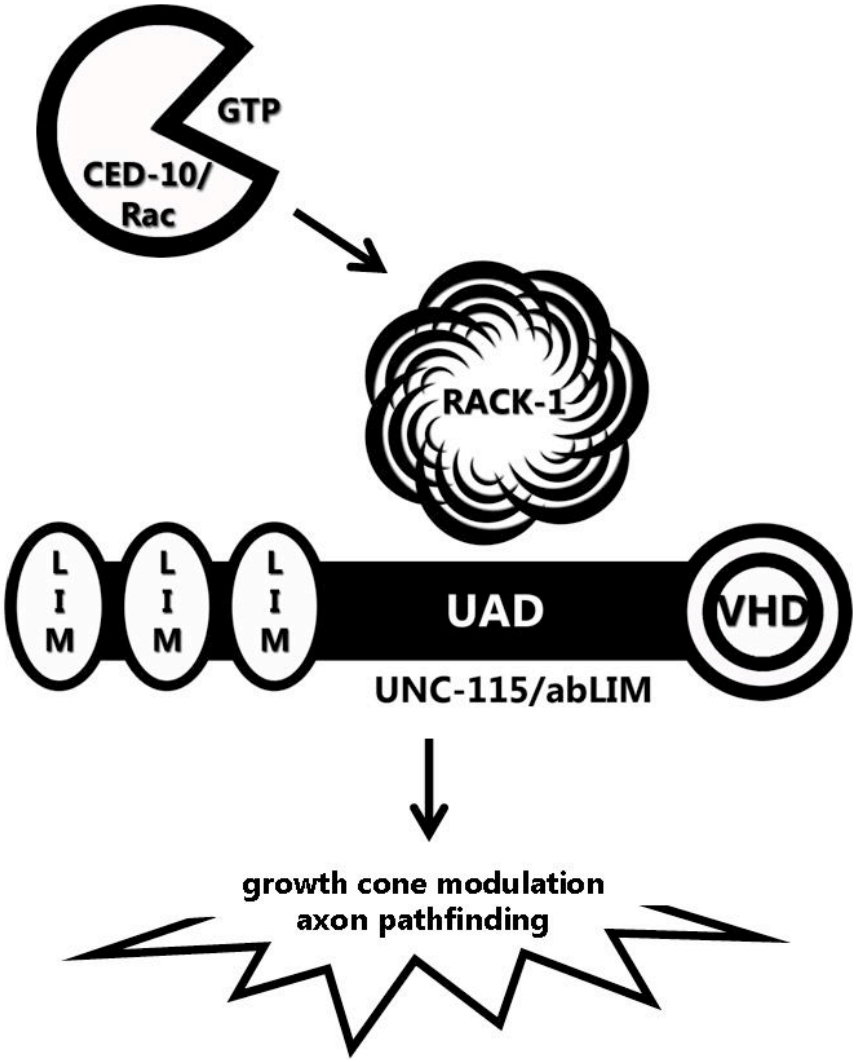
GTP
CED-10/
Rac
RACK-1
L
I
M
L
I
M
L
I
M
UAD
VHD
UNC-115/abLIM
growth cone modulation
axon pathfinding

Figure 3.1. A model for the activation of UNC-115/abLIM. Previous work has established that UNC-115/abLIM is activated in a step-wise manner. When at the plasma membrane, CED-10/Rac is at its GTP-bound form and therefore is active. It then recruits the scaffolding protein RACK-1, which will bind UNC-115/abLIM and possibly activate it with the help of other binding partners.

Figure 3.2

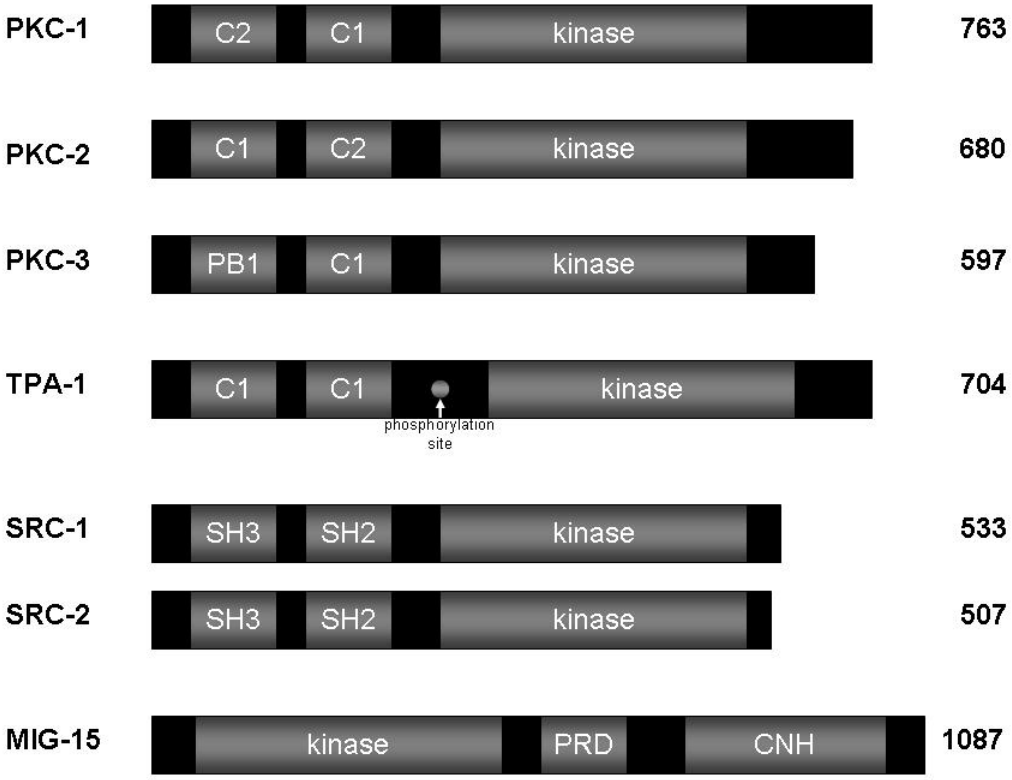
PKC-1
C2
C1
kinase
763
PKC-2
C1
C2
kinase
680
PKC-3
PB1
C1
kinase
597
TPA-1
C1
C1
kinase
phosphorylation site
704
SRC-1
SH3
SH2
kinase
533
SRC-2
SH3
SH2
kinase
507
MIG-15
kinase
PRD
CNH
1087

Figure 3.2. Schematic representations of the C. elegans PKCs, SRCs and MIG-15/NIK kinases. For PKC-1, PKC-2 and TPA-1, the longest isoforms were chosen for representation purposes. Diagrams based of BLAST domain predictions represented on Wormbase. All protein diagrams are followed by their amino-acid lengths (right-most number). C1= PKC conserved region 1; phorbol ester/DAG binding domain. C2= PKC conserved region 2; typically Ca^{2+}-binding domain that targets protein to plasma membrane. PB1= Phox and Bem1 domain. SH3= Src Homology domain 3. SH3= Src Homology domain 2. PRD= Proline-rich domain. CNH= Citron Homology domain. Kinase= kinase domain of the protein.

Figure 3.3

A

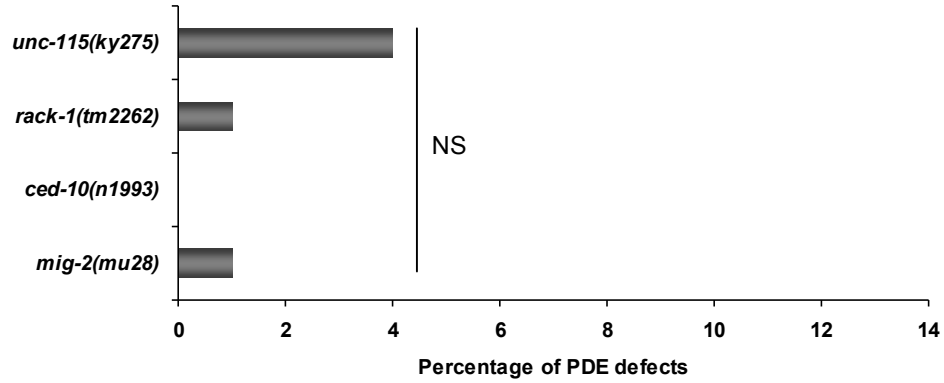
unc-115(ky275)
rack-1(tm2262)
ced-10(n1993)
mig-2(mu28)
NS
0
2
4
6
8
10
12
14
Percentage of PDE defects

B

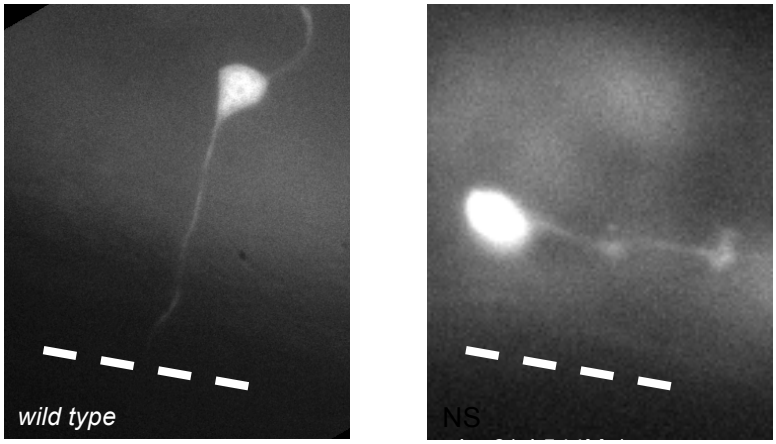
wild type
NS

C

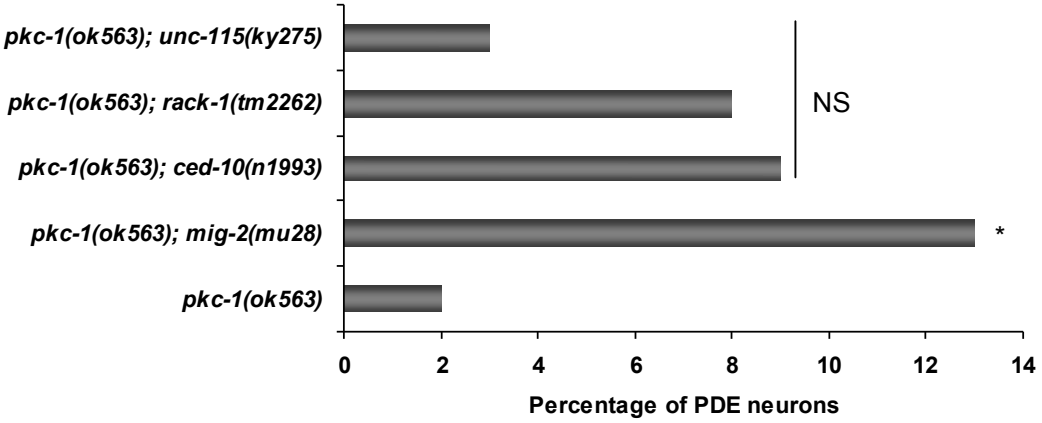
pkc-1(ok563); unc-115(ky275)
pkc-1(ok563); rack-1(tm2262)
pkc-1(ok563); ced-10(n1993)
pkc-1(ok563); mig-2(mu28)
pkc-1(ok563)
NS
*
0
2
4
6
8
10
12
14
Percentage of PDE neurons

D

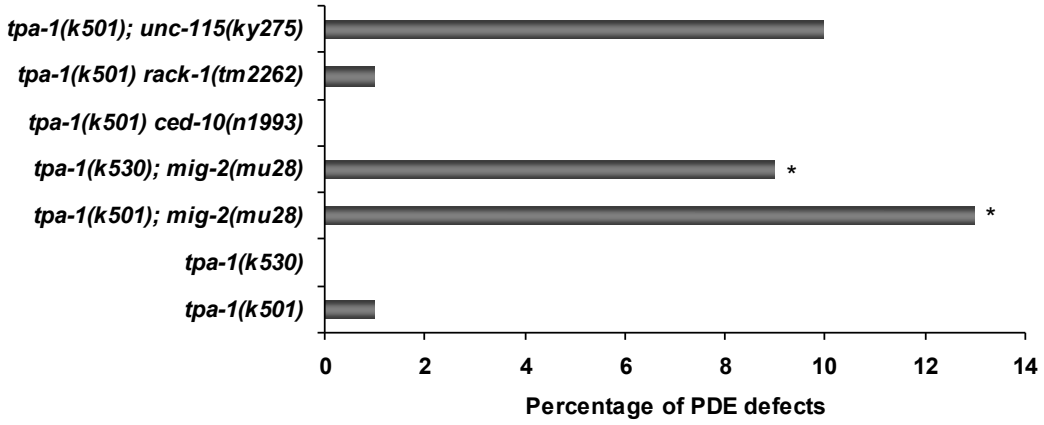
tpa-1(k501); unc-115(ky275)
tpa-1(k501) rack-1(tm2262)
tpa-1(k501) ced-10(n1993)
tpa-1(k530); mig-2(mu28)
tpa-1(k501); mig-2(mu28)
tpa-1(k530)
tpa-1(k501)
*
*
0
2
4
6
8
10
12
14
Percentage of PDE defects

E

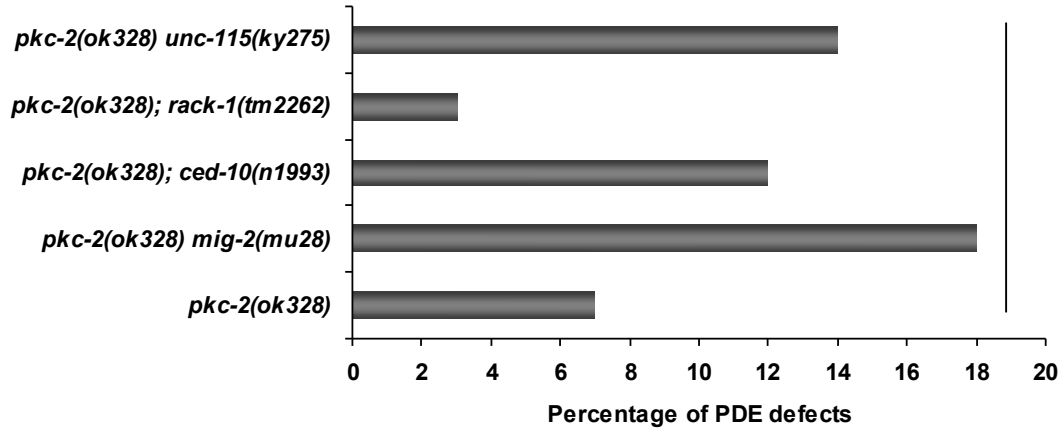
pkc-2(ok328) unc-115(ky275)
pkc-2(ok328); rack-1(tm2262)
pkc-2(ok328); ced-10(n1993)
pkc-2(ok328) mig-2(mu28)
pkc-2(ok328)
0 2 4 6 8 10 12 14 16 18 20
Percentage of PDE defects

F

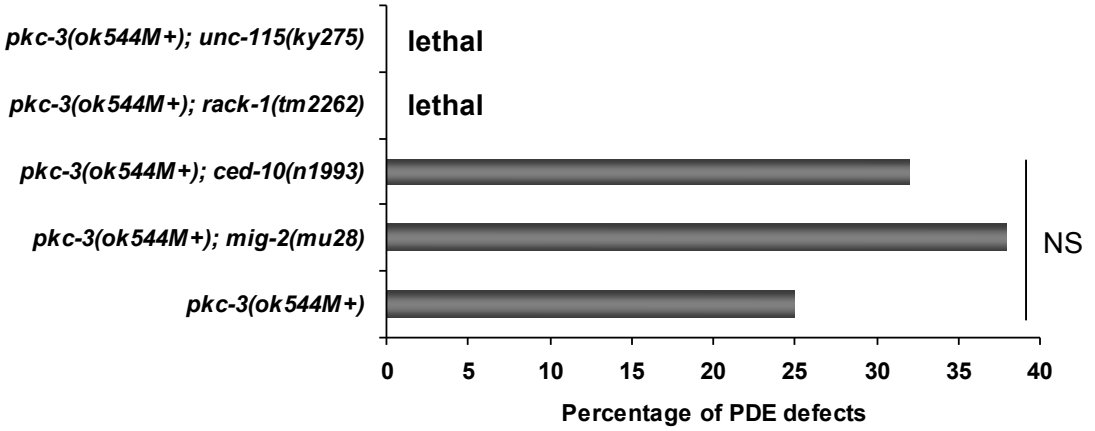
pkc-3(ok544M+); unc-115(ky275)
lethal
pkc-3(ok544M+); rack-1(tm2262)
lethal
pkc-3(ok544M+); ced-10(n1993)
pkc-3(ok544M+); mig-2(mu28)
NS
pkc-3(ok544M+)
0 5 10 15 20 25 30 35 40
Percentage of PDE defects

Figure 3.3. The four *pkc* genes interact differently with the Rac GTPases, *unc-115/abLIM* and *rack-1* in PDE axon pathfinding. A Loss-of-function mutations in the Rac GTPases *mig-2* and *ced-10*, in *rack-1* and in *unc-115/abLIM* do not have a significant effect in PDE axon pathfinding. **B** Fluorescent micrographs of a wild-type and mutant PDE neuron. Dotted line indicates where the ventral nerve cord is situated. **C** Bar graph representing the PDE pathfinding defects in *pkc-1(ok563)* and double-mutant combinations with loss-of-function alleles of *ced-10/Rac*, *mig-2/RhoG*, *rack-1* and *unc-115/abLIM*. **D** Same as C, but with *tpa-1(k501)* and *tpa-1(k530)*. **E** Same as C, but with *pkc-2(ok328)*. **F** Same as C, but with *pkc-3(ok544)*. In all graphs, n=100 (unless otherwise noted); * = statistically significant (for p values, see results section); NS= not significant.

Figure 3.4

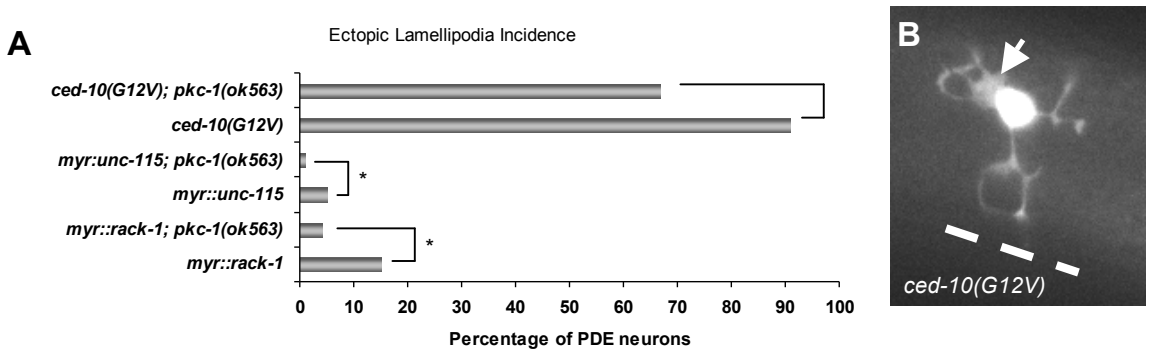
A
Ectopic Lamellipodia Incidence
ced-10(G12V); pkc-1(ok563)
ced-10(G12V)
myr:unc-115; pkc-1(ok563)
myr::unc-115
myr::rack-1; pkc-1(ok563)
myr::rack-1
*
*
0
10
20
30
40
50
60
70
80
90
100
Percentage of PDE neurons
B
ced-10(G12V)

Figure 3.4. PKC-1 is needed for the ectopic lamellipodia caused by overactivation of CED-10/Rac, UNC-115/abLIM and RACK-1. A Bar graph representing the ectopic lamellipodia emanating from PDE neurons in different genotypes. *= statistically significant (for p values, see results section). **B** Fluorescent micrograph of a PDE neuron harboring the *ced-10(G12V)* transgene. An ectopic lamellipodium is depicted by the arrow.

Figure 3.5

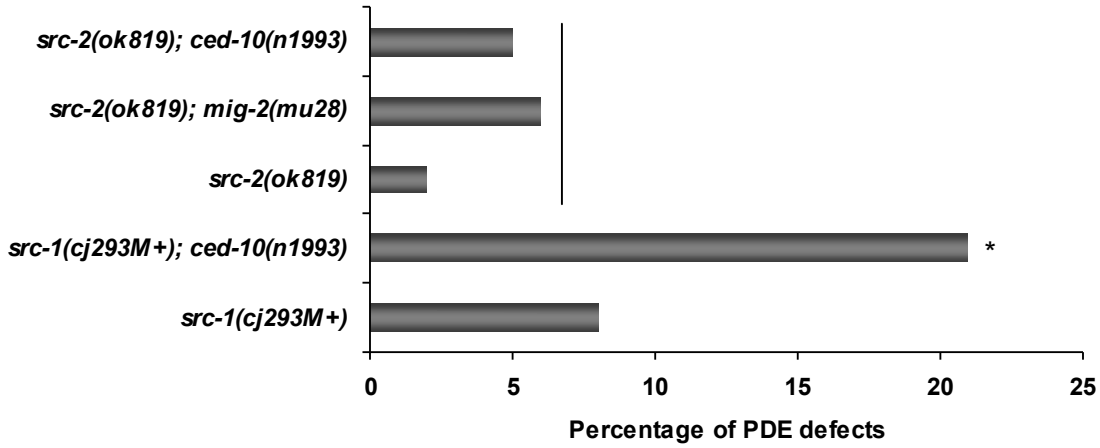
src-2(ok819); ced-10(n1993)
src-2(ok819); mig-2(mu28)
src-2(ok819)
src-1(cj293M+); ced-10(n1993)
src-1(cj293M+)
*
0
5
10
15
20
25
Percentage of PDE defects

Figure 3.5. The *src* genes do not act in a linear pathway with the Rac GTPases in axon pathfinding. Bar graph representing the PDE pathfinding defects in *src-1(cj293)*, *src-2(ok819)* and double-mutant combinations with loss-of-function alleles of *ced-10/Rac* and *mig-2/RhoG*

Figure 3.6

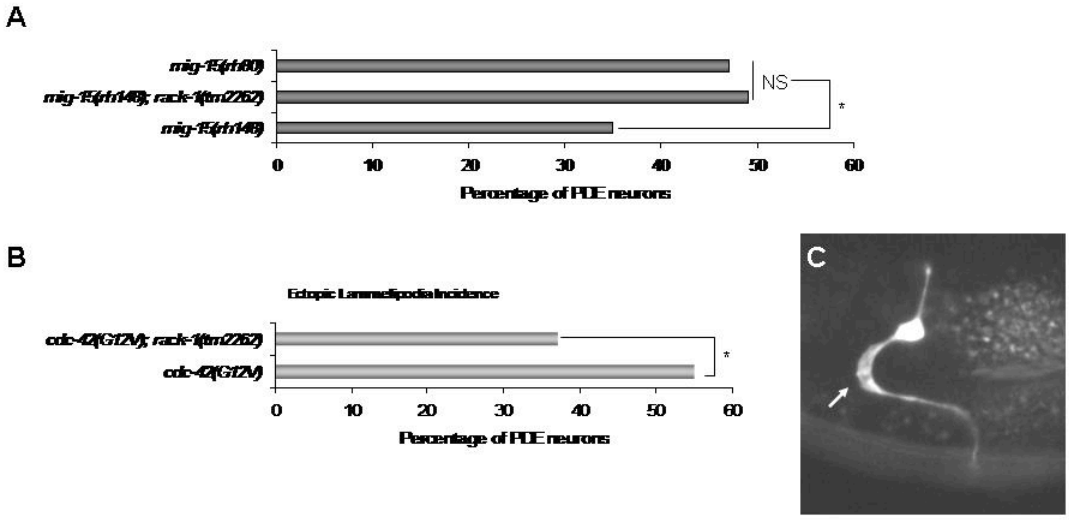
A
mig-15(rh80)
mig-15(rh148); rack-1(tm2262)
mig-15(rh148)
NS
*
0
10
20
30
40
50
60
Percentage of PDE neurons
B
Ectopic Lamellipodia Incidence
cdc-42(G12V); rack-1(tm2262)
cdc-42(G12V)
*
0
10
20
30
40
50
60
Percentage of PDE neurons
C

Figure 3.6. MIG-15/NIK and RACK-1 possibly act in a linear pathway downstream of CDC-42. A Bar graph representing the PDE pathfinding defects in *mig-15 loss-of-function alleles and rack-1(tm2262).* **B** Bar graph representing the ectopic lamellipodial protrusions emanating from the PDE neurons harboring an overactive *cdc-42* transgene. **C** A fluorescent micrograph of a PDE neuron harboring the *cdc-42(G12V)* transgene. The arrow depicts the ectopic lamellipodia.

Figure 3.7

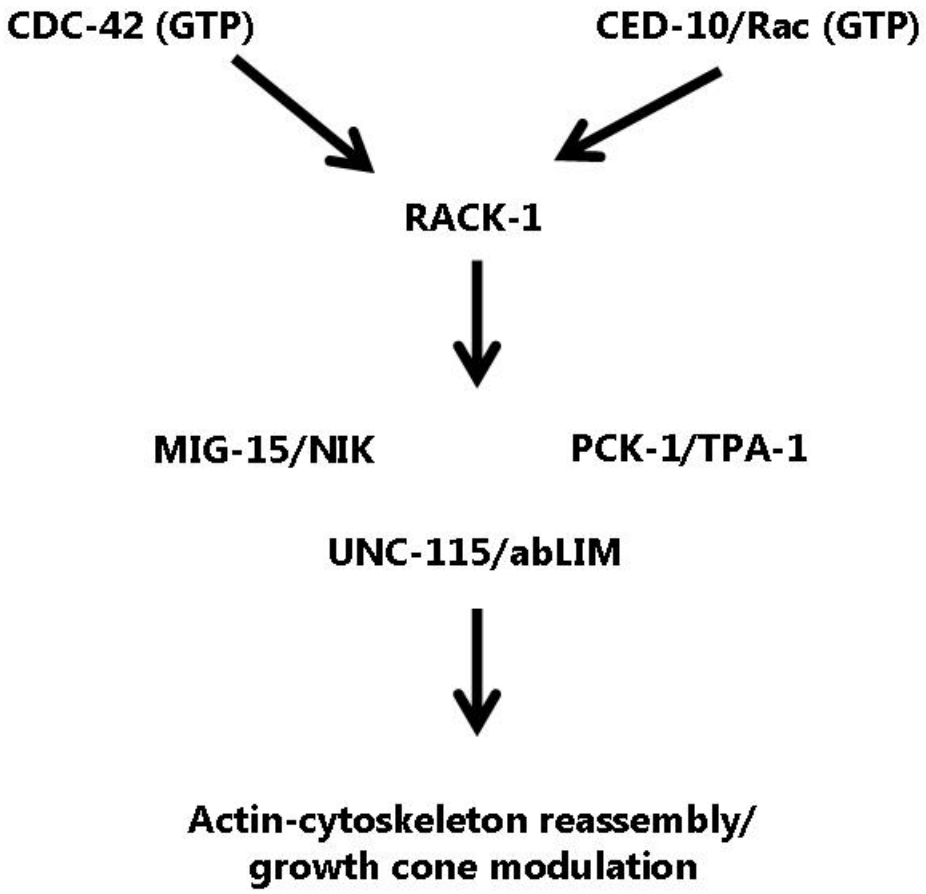
CDC-42 (GTP)
CED-10/Rac (GTP)
RACK-1
MIG-15/NIK
PCK-1/TPA-1
UNC-115/abLIM
Actin-cytoskeleton reassembly/
growth cone modulation

Figure 3.7. A genetic model of the stepwise activation of UNC-115/abLIM.

Chapter IV

The Rac GEF TIAM-1 acts cell autonomously downstream of CDC-42 in the UNC-6/Netrin attractive pathway in *in vivo* axon pathfinding

4.1. Abstract

In the developing nervous system, neurons extend axonal processes in order to communicate with other cells. When extending its axons, a neuron forms a dynamic, actin-rich growth cone that senses the surrounding environment for the proper migration cues through lamellipodial and filopodial structures. Racs are small GTPases from the Rho sub-family that are involved in the regulation of actin-binding proteins that can modulate the actin cytoskeleton. Racs are active when bound to GTP, and inactive when bound to GDP. GEFs - guanosine exchange factors - are molecules that aid Racs in the exchange of GDP for GTP, hence activating them.

UNC-73/Trio is a well characterized GEF for the two redundant Racs CED-10/Rac1 and MIG-2/RhoG in *C. elegans*. However, a loss-of-function (lof) double mutant of *mig-2* and *ced-10* had more severe pathfinding defects than a lof of *unc-73*. While screening the other 18 DH-containing GEFs in the genome, a lof of *tiam-1* displayed axon pathfinding defects when in combination with *mig-2* or *ced-10*. TIAM-1 is a GEF for Rac1 in mammals, and has been implicated *in vitro* in working downstream of Cdc-42.

Our data suggest that in axon pathfinding *in vivo*, the previously uncharacterized GEF TIAM-1 acts upstream of the Rac GTPases. Moreover, we have evidence TIAM-1 could be the link between the CDC-42 and Rac pathways. Our data also suggest that TIAM-1 works downstream of the UNC-6/Netrin and UNC-40/DCC attractive signaling pathway. Future studies with other guidance receptors will further dissect the role of TIAM-1 in axon pathfinding.

4.2 Introduction

In a developing nervous system, axonal growth happens via extension and migration of the growth cone, an actin-rich neuronal structure from which filopodial and lamellipodial structures emanate in order to sense the surrounding environment for appropriate guidance cues (Welch and Mullins 2002; Svitkina, Bulanova et al. 2003; Gallo and Letourneau 2004; Korobova and Svitkina 2008; Pak, Flynn et al. 2008). Guidance receptors such as Deleted in Colorectal Carcinoma (DCC) and Roundabout (ROBO) are present in the leading edge of the growth cone and are activated upon ligand binding (such as Netrin and Slit, respectively) (Zallen, Yi et al. 1998; Brose, Bland et al. 1999; Shekarabi and Kennedy 2002; Gitai, Yu et al. 2003; Killeen and Sybingco 2008). Attractive and repellent guidance systems guide the growth cone towards its final target, presumably by affecting the protrusiveness of filopodial structures in the growth cone (Adler, Fetter et al. 2006; Killeen and Sybingco 2008) . The proper control of the actin cytoskeleton is crucial for the development, maintenance and dynamics of these filopodia and lamellipodia. Failure in the proper extension of axons during development is associated with several neurological disorders, including autism spectrum disorders and dyslexia (Hannula-Jouppi, Kaminen-Ahola et al. 2005; Anitha, Nakamura et al. 2008).

Rac GTPases, members of the Rho subfamily of small GTPases (which also includes Rho and Cdc-42), have been well established as modulators of the actin cytoskeleton (Bishop and Hall 2000). Rac GTPases and their downstream effectors modulate filopodia and lamellipodia morphology and dynamics during

axon pathfinding in vitro in mammalian cell culture, as well as in vivo in the fruit fly *Drosophila melanogaster* and the nematode *Caenorhabditis elegans* (Nobes 1995; Azuma, Witke et al. 1998; Lundquist 2003; Biyasheva, Svitkina et al. 2004). Rac GTPases act on the actin cytoskeleton via diverse downstream effectors such as the actin-filament nucleator Arp2/3 complex, the severing protein Cofilin, the Pak and LIM kinases, and the actin binding protein UNC-115/abLIM (Symons 2000; Aizawa, Wakatsuki et al. 2001; Dan, Kelly et al. 2001; Pollard and Borisy 2003; Norris, Dyer et al. 2009). In *C. elegans* growth cone development and axon pathfinding, the two redundant Rac GTPases CED-10/Rac and MIG-2/RhoG act via two distinct pathways to activate the Arp2/3 complex: CED-10/Rac activates WVE-1/Wave, while MIG-2/RhoG activates WSP-1/Wasp (Shakir, Jiang et al. 2008). CED-10/Rac is also known to activate the actin-binding protein UNC-115/abLIM via recruitment of the Receptor for Activated C Kinase (RACK-1) (Demarco and Lundquist 2010).

Although much is known about the downstream effectors of the Rac GTPases in axon development, not much is known about what controls their activity in vivo. Rac GTPases switch between an inactive, GDP-bound state, and an active, GTP-bound state. Rac GTPase activation can be reached with the aid of a Guanine-nucleotide Exchange Factor (GEF), which catalyzes the exchange of GTP for GDP (Hall 1992). GEFs have a greater affinity for GDP then Rac GTPases. When in contact with the GDP-bound Rac, GEFs facilitate the exit of GDP from the GTPase. Because the intra-cellular concentration of GTP is much higher than that of GDP (it is estimated to be about 10x greater), a GTP molecule

can then enter the GTP-binding pocket of the Rac GTPase for its activation (Schmidt and Hall 2002).

UNC-73/Trio is a well characterized GEF for MIG-2/RhoG and CED-10/Rac in *C. elegans* axon pathfinding (Steven, Kubiseski et al. 1998; Lundquist, Reddien et al. 2001; Wu, Cheng et al. 2002; Kubiseski, Culotti et al. 2003). In its longest isoform (F55C7.7a, see Wormbase), UNC-73/Trio has eight spectrin repeats N-terminally, followed by a RacGEF-specific Double Homology (DH)/Pleckstrin Homology (PH) domain, an SH3 domain, a RhoGEF-specific DH/PH domain, an Immunoglobulin domain and a Fibronectin Type-III domain (Figure 4.1D). A mutation that disrupts specifically the RacGEF activity of UNC-73/Trio (*rh40*, see Figure 1D) disrupts axon pathfinding. Nevertheless, total abolishment of Rac GTPase activity in *C. elegans* has more severe defects in axon pathfinding (Lundquist, Reddien et al. 2001).

Here we show that another GEF, the previously uncharacterized *C. elegans* counterpart of human Tiam1 (henceforth called TIAM-1), is involved in the upstream modulation of Rac GTPases for axon pathfinding.

4.3 Results

T21E12.2 and C11D9.1 are one single gene and code for a GEF similar to mammalian Tiam1. The *C. elegans* Rac GTPases MIG-2/RhoG and CED-10/Rac1 act redundantly in PDE axon pathfinding (Lundquist, Reddien et al. 2001). Loss-of-function mutations in either *mig-2* or *ced-10* alone did not disturb

significantly the pathfinding of the PDE axons (1% and 0%, respectively), but when in a double mutant combination (*mig-2(mu28); ced-10(n1993M+)*), most PDE neurons were affected (84%, Figure 4.2 and (Lundquist, Reddien et al. 2001)). UNC-73/Trio is a well characterized GEF for MIG-2/RhoG and CED-10/Rac1 in axon pathfinding (Steven, Kubiseski et al. 1998). A mutation that specifically abolishes the Rac GEF activity of UNC-73 (*rh40*, a Ser-1216-Phe substitution in the Rac-specific DH1 domain) displayed severe axon pathfinding defects (42%, Figure 4.2), but not as strong as the double mutant of *mig-2(mu28); ced-10(n1993M+)* ($p<0.0001$). When in combination with either *mig-2(mu28)* or *ced-10(n1993)*, *unc-73(rh40)* synergizes to similar levels as *mig-2(mu28); ced-10(n1993M+)* in axon pathfinding (Lundquist, Reddien et al. 2001). These results suggest there might be other GEF(s) acting in parallel to UNC-73 in axon pathfinding.

The *C. elegans* genome encodes a total of 19 predicted DH-containing GEFs. From a screen we performed of the other 18 DH-containing GEFs (with either deletion alleles or RNAi), we found two alleles of *C11D9.1* (*ok772* and *tm1556*) that showed synthetic synergy with *mig-2(mu28)* and *ced-10(n1993)* in PDE axon pathfinding (Figure 4.2). *ok772* had only 1% of affected PDEs, but when in combination with *mig-2(mu28)*, it had 6% of PDEs misrouted ($p<0.001$), and with *ced-10(n1993)*, 14% ($p<0.001$). *tm1556* displayed 2% of PDE pathfinding defects on its own, but increased defects in *mig-2(mu28)* to 15% ($p<0.001$), and in *ced-10(n1993)* to 12% ($p<0.005$).

We then obtained three isolated cDNAs containing sequence complimentary to *C11D9.1* (courtesy of Yuji Kohara). To our surprise, the cDNAs contained sequences complimentary not only to *C11D9.1*, but also to the predicted gene *T21E12.2*, in one single message (Figure 4.1A,B,C). After searching for the cDNA sequences within the genome of other organisms using BLAST, we found the combined message codes for a putative Rac GEF domain composed of a Double Homology (DH) followed by a Pleckstrin Homology (PH) domain, similar to mammalian Tumor Invasive and Metastasis Factor-1 (Tiam1). In other nematodes, insects and mammals, Tiam1-like proteins have other domains than just the DH/PH, which direct protein localization and function (Hoshino, Sone et al. 1999; Matsuo, Hoshino et al. 2002). In order to test if *C. elegans* TIAM-1 would have other putative functional domains as well, we performed a targeted BLAST search of small regions of the TIAM-1 amino-acid sequence against Still Life/Tiam1 from *Ascaris suum*, an evolutionarily diverse nematode. If recognized, this region would then be searched for in *Drosophila melanogaster* Still Life/Tiam1 for further comparison (Figure 4.S1). Using the longest cDNA (H9) as a model, *C. elegans* TIAM-1 putatively has an N-terminal EVH1/PH domain (amino-acids 1-100), followed by a PDZ domain (amino-acids 398-486) (Figure 4.1A,B,C). Although we do not claim these are *bona fide* EVH1 and PDZ domains, it is possible that these domains are still functioning in a way similar to their counterparts in other organisms. Future work will dissect the roles, if any, of these putative functional domains.

In other organisms, the DH-PH domain of Tiam1 is Rac specific (Worthylake, Rossman et al. 2000; Matsuo, Terao et al. 2003). Both alleles used in the screen (*ok772* and *tm1556*) remove at least part of the DH domain of TIAM-1. *ok772* is a 18bp insertion (CTGTAACTTAACTGTAAC) and an out-of-frame 838bp deletion that removes exon 15 of the gene (region coding part of the DH and PH domains), and *tm1556* is an out-of-frame 851bp deletion that removes exons 11, 12 and 13 of the gene (region coding part of the DH domain) (Figure 4.1A,B,C). In both cases, even if any protein were to be made, it would not contain the DH-PH domains, which are responsible for its GEF activity.

***tiam-1* is expressed primarily in the nervous system and controls different aspects of neuronal development.** We next sought to determine where *tiam-1* is expressed. We amplified the region upstream of T21E12.2 until reaching the next open reading frame (a region of 4793bp), and placed it upstream of the *cyan fluorescent protein* (*cfp*) gene. When nematodes were made transgenic, this reporter construct was expressed primarily in the nervous system (Figure 4.3A). Many neurons in the head and tail, as well as throughout the body of the animal expressed CFP, including the GABAergic and cholinergic neurons (V and D-types) in the ventral nerve cord, ALM, CAN, PDE, PVD, AVM and PVM (Figure 4.3A). *tiam-1 expression began* in embryos and lasted throughout adulthood.

Because of its broad expression in the nervous system, we decided to test whether if *tiam-1* controls development in neurons other than the PDEs (utilized in our screen). *tiam-1(ok772)* was crossed to *zdIs4(mec-4p::gfp)*, which is a

marker for touch-sensory neurons including AVM (Figure 4.3B), and *juIs76(unc-25p::gfp)*, which illuminates the GABAergic motorneurons VDs and DDs (Figure 4.3C). In both cases, *tiam-1(ok772)* displayed some minor neuronal developmental defects. The AVM neuron is located in the anterior part of the nematode, and its cell body resides in the middle right side of the animal. It extends an axon until reaching the ventral nerve cord, where it turns anteriorly and extends its axon till close to the nerve ring. In these neurons, *tiam-1(ok772)* showed 1% axon pathfinding defects, 6% ectopic neurite occurrence and 10% ectopic lamellipodia occurrence. None of these phenotypes were ever seen in wild type animals (data not shown).

The VD and DD motorneuron nuclei are situated in the ventral nerve cord. They each first extend an axon anteriorly, then a branch turns dorsally and extends in a right angle until reaching the dorsal nerve cord, where it extends anterior and posteriorly. Usually more than one motorneuron axon will follow the same commissure in the animal. In these neurons, *tiam-1(ok772)* did not show defects on its own, but synergized significantly to the defects caused by *unc-73(rh40)*. *unc-73(rh40)* showed many defects in the VD and DD neurons, including axon pathfinding (26.15% of axons), ectopic branching of the commissures (20.76% of commissures) and failure of P-cell migration (the precursor cells of the VDs) to locate to the ventral nerve cord (20% of animals). *unc-73(rh40) tiam-1(ok772)* animals had 51.45% of axon pathfinding defects, 50.43% ectopic branches coming out of the axonal commissures, and 60% of animals with P-cell migration defects. These results are consistent with the idea

TIAM-1 is needed in the nervous system for different aspects of development, and that it acts in a different pathway than UNC-73/Trio.

Loss-of-function mutations in *tiam-1* showed additive effect when in combination with *unc-73(rh40)* in the pathfinding of PDE axons. As mentioned previously, both *ok772* and *tm1556* alleles of *tiam-1* synergized to significant levels with *ced-10(n1993)* and *mig-2(mu28)* in PDE axon pathfinding (Figure 4.2). In order to determine if TIAM-1 and UNC-73 act in a linear or parallel pathway, we created double mutant combinations of *unc-73(rh40)* with either allele of *tiam-1*. *unc-73(rh40)* alone displayed 42% of PDEs affected. Interestingly to us, neither *ok772* nor *tm1556* alleles of *tiam-1* seemed to synergize with *unc-73(rh40)* (51% and 57%, respectively. p=0.2 when compared to *unc-73(rh40)* only). Because neither *ok772* not *tm1556* display significant defects on their own, they could have a rather additive increase when combined with *unc-73(rh40)* (Figure 4.2). One explanation would be that although these two GEFs work in parallel pathways in the control of axon pathfinding, they are not totally redundant and may have specific functions in the activation of the Rac GTPases (e.g., TIAM-1 might be acting in the filopodia-protrusive activation of Rac GTPases, while UNC-73 might be acting in the filopodia-retractive activation of Rac GTPases). Another explanation would be that TIAM-1 works independently of the UNC-73/MIG-2/CED-10 pathway, and therefore would increase the number of defects in both GTPases and UNC-73 because it does not work in the same pathway as they.

TIAM-1 acts upstream of MIG-2/RhoG and CED-10/Rac1 in PDE axon pathfinding. In order to test the hypothesis that TIAM-1 acts in a linear pathway upstream of CED-10/Rac1 and MIG-2/RhoG, we created a constitutively activated form of this molecule. Because the DH/PH domains are essential and sufficient to facilitate the exchange of GTP for GDP in the GTPases, and because there is evidence for different intramolecular inhibition mechanisms in different GEFs, we decided to amplify the DH/PH region and overexpress it in the PDE neurons. In *Drosophila* Trio, a similar construct has been made and it acted as if constitutively active (Seipel, Medley et al. 1999).

We cloned the DH/PH region of TIAM-1 (amino-acids 488 - 856), added an N-terminal myristoylation sequence (to ensure this construct would go to the plasma membrane), and fused it C-terminally with GFP. We placed this construct under the control of the PDE promoter *osm-6*. As controls, we also amplified and cloned the DH/PH regions of UNC-73 (DH1/PH1 is Rac specific – amino-acids 1193 - 1527, DH2/PH2 is Rho specific – amino-acids 1795 - 2129; all amino-acid positioning is based on the longest isoform of UNC-73 – F55C7.7a) as described for TIAM-1.

When expressed in transgenic animals, the DH1/PH1 of UNC-73/Trio and DH/PH of TIAM-1 promoted ectopic lamellipodial and filopodial protrusions that emanated from the cell body and axons of PDEs (51% and 34% respectively). Axon branching and defects in pathfinding also occurred in a lesser scale. The DH2/PH2 of UNC-73, which is Rho specific, did not cause any significant defects

(1%). This is consistent with the hypothesis these GEFs are recruited to the plasma membrane for the activation of Rac GTPases. Hence the ectopic lamellipodial and filopodial projections seen could be equivalent to the lamellipodial and filopodial structures present in the developing growth cones of these axons, which are primarily controlled by Rac GTPases. In addition to our controls, we mimicked the *rh40* mutation (that changed Ser-1216-Phe) in our DH1/PH1 construct of UNC-73/Trio (Ser-11-Phe in the construct), and made an equivalent substitution (Thr-516-Phe) in the DH/PH of TIAM-1 (Thr-08-Phe in the construct). Both constructs were expressed (as seen by the expression of the tagged GFP), but neither promoted significant ectopic lamellipodial protrusions (1% for UNC-73[DH1(Ser-11-Phe)/PH1] and 6% for TIAM-1[DH(Thr-08-Phe)/PH]).

Next, we crossed loss-of-function *mig-2* and *ced-10* with these overactive constructs to test for suppression of the ectopic lamellipodia/filopodia phenotype. When using overexpression transgenes, we were careful to outcross the transgene away from the loss-of-function and re-score the transgene to ensure it had not broken down and lost the effect. Therefore, for each experiment (i.e., for each loss-of-function *rac* gene), we outcrossed the transgene and re-scored it as control. Both *mig-2(mu28)* and *ced-10(n1993)* were able to significantly suppress the ectopic lamellipodial/filopodial projections caused by constitutively activated UNC-73/Trio and TIAM-1 (Fig4). *mig-2(mu28)* suppressed the ectopic lamellipodia and filopodia caused by UNC-73[DH1/PH1] (96% to 44%, $p<0.0001$) and TIAM-1[DH/PH] (74.51% to 23%, $p<0.0001$). Likewise, *ced-10(n1993)* also

significantly suppressed this phenotype in both UNC-73[DH1/PH1] (93% to 79%, $p<0.003$) and TIAM-1[DH/PH] (48% to 13%, $p<0.0001$). Together with the loss-of-function data, these results suggest TIAM-1 acts upstream and in a linear pathway with both MIG-2/RhoG and CED-10/Rac1 in axon pathfinding, and that TIAM-1 acts in a parallel pathway to UNC-73/Trio.

TIAM-1, but not UNC-73/Trio, acts downstream of CDC-42. Evidence from cell culture studies (Nishimura, Yamaguchi et al. 2005) suggests mammalian Tiam1 acts downstream of Cdc-42 in the activation of Rac1. In order to investigate if TIAM-1 acts downstream of CDC-42 in axon pathfinding in vivo, we first built loss-of-function double mutants of *tiam-1* and *cdc-42*. *tiam-1(ok772);cdc-42(gk388M+)* did not increase in the amount of defective PDE axon pathfinding. This result is consistent with the hypothesis that CDC-42 and TIAM-1 work in the same pathway. A Gly-12-Val substitution in the GTPase binding pocket of small GTPases has been shown to favor the GTP-bound state of these molecules, constitutively activating them (Struckhoff and Lundquist 2003) . Transgenic animals harboring an integrated array of *cdc-42(G12V)* under the control of the *osm-6* promoter display ectopic lamellipodial and filopodial protrusions (44%), as well as disruption of proper axon pathfinding (50%) in the PDE neurons. When crossed to *tiam-1(ok772)* or *tiam-1(tm1556)*, both phenotypes were significantly suppressed (12% and 8% for *ok772*, 8% and 10% for *tm1556,* in all cases $p<0.000001$). As a control, we re-introduced *tiam-1* in these animals by crossing an extra-chromosomal fosmid containing *tiam-1* under its endogenous promoter,

and most strongly the ectopic lamellipodia and filopodia phenotype seen in *cdc-42(G12V)* came back (56% and 15% for *ok772*, 61% and 15% for tm1556) (respectively, $p<0.001$, $p<0.06$, $p<0.001$ and $p<0.1$). Together, these data suggest TIAM-1 acts downstream of CDC-42 for proper axon guidance.
We also analyzed double mutants of *unc-73(rh40);cdc-42(gk388M+)*. Animals carrying both mutations displayed a synergistic increase in the number of PDE pathfinding defects (90%, $p<0.001$). In addition, when crossed into *cdc-42(G12V)* animals, *unc-73(rh40)* did not suppress the ectopic defects caused (47% for lamellipodia/filopodia, 71% for pathfinding). Hence UNC-73/Trio does not seem to act with CDC-42 in PDE axon pathfinding.

TIAM-1 localizes to the plasma membrane of neurons and NIH3T3 fibroblasts. To determine the localization of TIAM-1 in neurons, we amplified the coding region of *tiam-1* based on its longest cDNA (H9), fused it C-terminally with *mcherry*, and placed this construct under the control of either the *unc-25* (VD/DD-specific) or *osm-6* (PDE-specific) promoter. In the PDE and VD/DD motorneurons, TIAM-1::mCherry localized primarily to the periphery of the cell bodies, consistent with a plasma membrane localization. When active, Rac GTPases localize to the plasma membrane. The fact that TIAM-1::mCherry also localized to the plasma membrane suggests a possible interaction between these molecules. To verify if that is the case, animals containing *unc-25p::gfp::ced-10* or *unc-25p::gfp::mig-2* were generated and observed for Rac localization in the VD/DD motorneurons. In these cells, GFP::CED-10 and GFP::MIG-2 were

enriched at plasma membrane (Figure 4.6). TIAM-1::mCherry, GFP::CED-10 and MIG-2 were also found in the growth cone of the developing VD neurons. Such localization supports the idea these molecules are required for proper re-shaping of the growth cone during axon pathfinding. We also tested the possibility that CDC-42 controls the localization of TIAM-1 in the neuron (Figure 4.6). We analyzed the localization pattern of TIAM-1::mCherry in PDE and VD/DD neurons in a *cdc-42(gk388M+)* background, but we did not notice any significant change of protein accumulation in these mutants (data not shown).

C. elegans neurons are very small in scale. Although TIAM-1 and the Racs seem to be present at the plasma membrane, we could not rule out the possibility these molecules were just being excluded from the nucleus (they could have a cytoplasmic localization pattern instead). In addition, due to the poor signal, we were not able to obtain convincing co-localization data between TIAM-1 and the Racs at the plasma membrane. Therefore, we analyzed the localization pattern of TIAM-1 and CED-10 in NIH-3T3 fibroblasts. Full –length TIAM-1 and CED-10 molecules were amplified from their respective cDNAs using PCR and fused in frame N-terminally with either mCherry or GFP, respectively. The overexpression of GFP::CED-10 in fibroblasts caused them to ruffle, a phenotype previously observed by the overexpression of Rac (Nobes 1995). GFP::CED-10 localized to some intracellular membraneous organelles (presumably the endoplasmic reticulum) and plasma membrane (Figure 4.7A). The overexpression of mCherry::TIAM-1 did not affect cell shape, and mCherry::TIAM-1 also localized to the plasma membrane and intracellular

membraneous organelles (Figure 4.7A). These localization patterns were different than those observed by the expression of the empty vectors (Figure 4.7A). When expressed together, mCherry::TIAM-1 and GFP::CED-10 co-localized strongly to membraneous organelles, and to certain domains of the plasma membrane (Figure 4.7B). These data support the idea TIAM-1 and RacGTPases co-localize at the plasma membrane for Rac activation, and that this interaction is transient (since only a few domains of co-localization were observed).

TIAM-1 acts cell-autonomously in PDE axon pathfinding. As previously mentioned, *cdc-42(G12V)* causes ectopic lamellipodial protrusions and axon pathfinding defects that are dependent on *tiam-1* in the PDE neurons (since the loss-of-function alleles of *tiam-1* suppressed the phenotypes). When crossed to *cdc-42(G12V) tiam-1(ok772)*, two lines of *osm6p::tiam-1::mcherry* (at 10 and 100ng/μL) were able to restore the defects caused by *cdc-42(G12V)* (70% and 76% respectively). A similar trend happened when *cdc-42(G12V) tiam-1(tm1556)* was used (57% and 64% for the 10 and 100ng/μL lines, respectively). These results suggest TIAM-1 acts cell-autonomously within the PDE neurons in axon pathfinding and that TIAM-1 is needed for the ectopic protrusions caused by overactive CDC-42.

TIAM-1 acts as a GEF for Rac, but not Cdc-42 nor Rho in an in vitro mant-GTP exchange assay. Genetic data implicated TIAM-1 acting in a linear

pathway with CDC-42 and CED-10/Rac1 and MIG-2/RhoG. Although TIAM-1 has a predicted Rac-specific DH domain, there is a possibility TIAM-1 could be working indirectly in the activation of CED-10/Rac1 and MIG-2/RhoG (i.e., TIAM-1 could recruit other molecules that would then activate the Racs, or could only act as a scaffold for Rac recruitment). In order to investigate mechanistically the role of TIAM-1 in the activation of Rac GTPases, we measured the exchange rates of mant-GTP incorporation by the GTPases in the presence or absence of TIAM-1 *in vitro*, using the RhoGEF exchange assay Biochem Kit from Cytoskeleton.

N- methylanthraniloyl-GTP (mant-GTP) is a fluorescently labeled nucleotide analog that can be incorporated by small GTPases. We measured the amount of mant-GTP incorporated by the GTPase due to the spectroscopic difference between bound and free mant-GTP (when in the GTPase binding pocket, mant-GTP increases its fluorescence).

We amplified from the TIAM-1 cDNA a region containing the DH and PH domains, and cloned it in frame with a 6 Histidine tag into a pET-28b vector (EMD Biosciences). We then expressed and purified the protein (TIAM-1[DH/PH]) and purified using a Ni^{+}-column based affinity chromatography.

After five minutes of incubation with mant-GTP and buffer, the GTPase (human Rac1, Cdc-42 or RhoA) was exposed to either solvent (control) or GEF (TIAM-1[DH/PH]).

In the absence of GEF, none of the GTPases seems to incorporate mant-GTP (the fluorescence does not change over the time of 30min). In the presence

of TIAM-1[DH/PH], the fluorescence readings from Rac1, but not Cdc-42 nor RhoA, dramatically increased, suggesting mant-GTP is being incorporated by Rac1 in the presence of TIAM-1[DH/PH]. We then introduced the Thr-08-Phe mutation that putatively abolishes the GEF activity of this molecule into this construct. When performing the mant-GTP exchange assay with TIAM-1[DH(Thr-08-Phe)/PH], the fluorescence readings of Rac1 did not increase significantly, suggesting this point mutation indeed disrupts the guanosine exchange activity of TIAM-1[DH/PH].

Because human Rac1 and Cdc-42 are similar to their *C. elegans* counterparts (90-95% amino-acid similarity to CED-10 and CDC-42), we believe *C. elegans* TIAM-1 is a Rac-specific GEF and works with CED-10/Rac and MIG-2/RhoG, but not CDC-42, in axon pathfinding.

TIAM-1 acts in the UNC-6/Netrin-UNC-40/DCC attractive signaling pathway in parallel to SLT-1/Slit-SAX-3/Robo and VAB-1/EphR pathways. In order to identify under which guidance pathway TIAM-1 would be acting, we crossed *tiam-1(ok772)* into loss-of-function alleles of the different parallel ventral guidance pathways present in *C. elegans*. UNC-6/Netrin is a secreted ligand expressed in the ventral side of the animal that attracts axons that express its receptor UNC-40/DCC (Hedgecock, Culotti et al. 1990). SLT-1/Slit is expressed primarily in the dorsal side and is thought to act as a repellent for ventrally-guided axons that express its receptor SAX-3/Robo (Hao, Yu et al. 2001). Besides these two major pathways, Ephrins have also been involved in directing proper axon

pathfinding (Flanagan and Vanderhaeghen 1998). VAB-1/EphR is the only *C. elegans* Ephrin receptor and has been shown to work in parallel with UNC-6/Netrin and SLT-1/Slit in axon ventral guidance (Zallen, Kirch et al. 1999).

tiam-1(ok772) did not increase the amount of PDE pathfinding defects of *unc-6(ev400)* (from 59% to 56%), but did significantly increase the defects of *vab-1(dx31)* (from 4% to 46%, $p<0.001$) and *slt-1(eh15)* (11% to 22%, $p=0.037$). In addition, we can constitutively activate the UNC-40/DCC Netrin receptor by fusing its cytoplasmic domain N-terminally to a myristoylation sequence. (Gitai, Yu et al. 2003) have previously shown that in the AVM neurons (also ventrally guided and responsive to UNC-6/Netrin), ectopic lamellipodial-like protrusions emanate from the cell body when activated UNC-40 (myr::cytoUNC-40) is expressed, and that UNC-73 was not required for such effects. In our hands, myr::cytoUNC-40 displayed 53% of AVMs with ectopic lamellipodial-like structures. *unc-73(rh40)* indeed did not suppress such defects (58%), confirming the results previously described by Gitai et al. (2003). Nevertheless, *tiam-1(ok772)* significantly suppressed the ectopic lamellipodia incidence in these neurons (down to 22%, $p<0.001$). Adding together the loss- and gain-of-function data, we believe TIAM-1 works in the UNC-6/UNC-40 attractive pathway, in parallel to SLT-1/SAX-3 and VAB-1, for the axon ventral guidance.

4.4 Discussion

In this report we identified the C. elegans protein TIAM-1 and presented evidence that IAM-1 acts specifically as a GEF for Rac GTPases in axon pathfinding. We

presented evidence that TIAM-1 might act upstream of the two redundant Rac GTPases MIG-2/RhoG and CED-10/Rac, and downstream of CDC-42 and the UNC-6/Netrin attractive signaling pathway.

Previous studies have demonstrated that the guanine exchange factor UNC-73/Trio acts with CED-10/Rac and MIG-2/RhoG in axon pathfinding. Nevertheless, mutations that disrupted the Rac GEF specific domain of UNC-73/Trio did not display axon pathfinding defects as penetrant as those seen in the complete abolishment of Rac activity (i.e., in the *mig-2;ced-10* double mutant). In addition, despite the fact CED-10/Rac and the actin-binding protein UNC-115/abLIM have been suggested to act downstream of the UNC-6/Netrin-UNC-40/DCC attractive signaling pathway, UNC-73/Trio did not seem to be part of this signaling cascade. Together, this evidence led us to conclude there must be other factors, possibly GEFs, acting upstream of MIG-2/RhoG and CED-10/Rac for their proper activation in axon pathfinding. After performing a genetic screen for the other 18 DH-containing GEF genes in the *C. elegans* genome, we observed a genetic interaction between *tiam-1* and the Rac GTPases.

TIAM-1 acts cell-autonomously in axon pathfinding. The *tiam-1* gene is expressed primarily, if not exclusively, in the nervous system. *tiam-1(ok772)* and *(tm1556)* mutant animals displayed defects alone and in combination with Rac GTPase mutants in axon guidance in different types of neurons, including the commissural VD and DD GABAergic motorneurons and the ciliated serotonergic PDE neurons. The fact that the VD and DD axons are dorsally attracted and the

PDE axons are guided ventrally suggest TIAM-1 is required for not just one type of neuronal guidance. In PDE neurons, overactivation of CDC-42 cause ectopic ectopic lamellipodial and filopodial structures that resemble those seen in axonal growth cones. TIAM-1 molecules expressed specifically in the PDEs are required for such a phenotype, since TIAM-1 removal suppressed the ectopic lamellipodia and filopodia seen in CDC-42-overactive PDEs. In sum, we presented strong evidence that TIAM-1 acts cell-autonomously in axon guidance.

TIAM-1 acts upstream of MIG-2/RhoG and CED-10/Rac and downstream of CDC-42 in axon pathfinding. A proposed model for the role of TIAM-1 in axon pathfinding is seen in Figure 4.10. Epistasis analysis with loss- and gain-of-function mutants have shown a genetic interaction between TIAM-1 and the GTPases MIG-2 and CED-10. Because a loss of activity of either GTPase suppressed overactivated TIAM-1, we concluded TIAM-1 acts upstream of MIG-2/RhoG and CED-10/Rac. In addition, biochemical (mant-GTP based exchange assay) and cell biological (co-localization studies) data supports the model in which TIAM-1 acts as a GEF for the activation of Rac GTPases in *C. elegans*.

In vitro studies of human Cdc-42 and Tiam1 have suggested these molecules act in the same pathway. Moreover, hTiam1 has been implicated as a downstream effector of hCdc-42. In order to test this hypothesis in vivo, we analyzed both loss- and gain-of-function CDC-42 combinations with both loss-of-function alleles of TIAM-1. It seems that also in vivo *C. elegans* TIAM-1 acts in a linear pathway downstream of CDC-42 for axon guidance.

The UNC-6/Netrin-UNC-40/DCC signaling machinery recruits TIAM-1 for its effect on attraction of axon guidance. UNC-6/Netrin is the ventrally-expressed ligand for the UNC-40/DCC receptor present in ventrally-attracted axons. Several reports have elucidaded some of the intracellular machinery required downstream of the UNC-40/DCC attractive response. The Rac GTPase CED-10 and the actin-binding protein UNC-115/abLIM act downstream of UNC-40/DCC, but not the Rac GEF UNC-73/Trio. We then tested whether or not TIAM-1 would be the GEF recruited in this pathway. TIAM-1 suppressed the ectopic lamellipodial structures caused by an overactive construct of UNC-40 in AVM neurons, which are also attracted to UNC-6/Netrin. In addition, *tiam-1* and *unc-6/Netrin* seem to act in a linear pathway, in parallel to other guidance systems such as SLT-1/Slit and VAB-1/Eph.

In summary, we have presented evidence that TIAM-1 acts cell-autonomously in the control of axon pathfinding, and that it does so by facilitating the exchange of GTP for GDP in the Rac GTPases CED-10/Rac and MIG-2/RhoG. We have also shown that TIAM-1 acts downstream of CDC-42, linking both CDC-42 and Rac GTPase signaling together. Moreover, we demonstrated that TIAM-1 is the GEF used in the protrusive, attractive signaling pathway mediated by UNC-6/Netrin and UNC-40/DCC in ventrally guided neurons. Future work will focus on the detailed growth cone observations of the mechanisms by which TIAM-1 controls filopodial and lamellipodial dynamics.

4.5 Materials and Methods

***C. elegans* genetics and culture**: *C. elegans* handling and culture were performed using standard techniques (Brenner 1974; Sulston and Hodgkin 1988). All experiments were performed at 20^{o}C. The *tiam-1(tm1556)* allele was provided to us by the National Bioresource Project for the Experimental Animal "Nematode *C. elegans*" (S. Mitani), and the *tiam-1(ok772)* allele was provided to us by the *C. elegans* Gene Knockout Consortium via the *C. elegans* Genetic Center (CGC). Polymerase chain reaction (PCR) was used to verify the homozygosity in the *tiam-1(ok772)* and *(tm1556)* in strains. The following mutations and genetic constructs were used: *LGI: unc-73(rh40), tiam-1(ok772) and (tm1556), lqIs37[osm-6::cdc-42(G12V)]; LGII: cdc-42(gk388), mIn1,vab-1(dx31), juIs76[unc-25::gfp]; LGIV: ced-10(n1993), zdIs4[mec-4::gfp], lqIs3[osm-6::gfp]; LGV: lqIs123[osm-6::myr::unc-73(DH1/PH1)]; LGX: mig-2(mu28), unc-6(ev400), slt-1(eh15), lqIs2[osm-6::gfp]; LG?: lqIs125[osm-6::myr::unc-73(DH2/PH2)], lqIs131[mec-7::myr::unc-40(cyto)::gfp], lqIs134[osm-6::myr::unc-73(DH1-S11F-/PH1)], lqIs165[osm-6::myr::tiam-1(DH/PH)], lqIs193[osm-6::myr::tiam-1(DH-T08F-/PH)]. C. elegans* transformation was performed with standard methods by microinjection of DNA into the hermaphroditic syncytial germline (Epstein and Shakes 1995). Transgenes were integrated into the genome using trimethylpsoralen and standard techniques (Mello, Kramer et al. 1991; Anderson 1995).

All micrographs were obtained on a Leica DMRE microscope with a Qimaging Rolera MGi EMCCD camera or a Qimaging Retiga CCD camera. Openlab and IPlab software were used to obtain images.

Molecular biology: Coding region sequencing was performed after PCR amplification to verify for any possible undesirable mutations. Molecular biology techniques were performed as previously described (Sambrook 1989). Primer and plasmid sequences are available upon request.

Scoring of PDE, VD/DD and AVM axon defects: Fluorescence microscopy was used to score axon pathfinding defects of fourth larval stage (L4) or young adult hermaphrodite animals expressing a green fluorescent protein transgene for specific cells. To score and visualize PDE axons, the integrated transgenes *lqIs2 X* and *lqIs3 IV [osm-6 promoter::gfp]* were used (Collet, Spike et al. 1998; Struckhoff and Lundquist 2003). To score and visualize VDs and DDs axons, the integrated transgene *juIs76 II [unc-25 promoter::gfp]* was used (Jin, Jorgensen et al. 1999). To score and visualize AVM axons, the integrated transgene *zdIs4 IV [mec-7 promoter::gfp]* was used. PDE axon pathfinding: The cell bodies of the PDE neurons (PDEL and PDER) are situated in the posterior lateral post-deirid ganglion. PDEs extend an axon ventrally to the ventral nerve cord, which then bifurcates and extends anteriorly and posteriorly in the ventral nerve cord. If the axon failed to reach the ventral nerve cord or wandered beyond a 45^{o} angle from a straight line ventrally from the cell body, it was

considered mutant. VD/DD axon pathfinding: A VD/DD commissural axon that failed to reach the dorsal nerve cord or that wandered laterally before reaching the dorsal nerve cord was considered mutant. The percent of animals with pathfinding defects was noted, and the percentage of defective axons was noted. VD cell body displacement: The VD neurons are descendants of the P cells. If the P nuclei fail to migrate ventrally, the resulting VD cell bodies can be laterally displaced out of the ventral nerve cord. The percentage of animals with laterally displaced VD cell bodies was scored. AVM axon pathfinding: The AVM cell body is situated laterally on the right side, in the anterior half of the body of the animal. The axon extends ventrally towards the ventral nerve cord, which then extends anteriorly until the first pharyngeal bulb. Similarly to PDE axons, if the axon failed to reach the ventral nerve cord or wandered beyond a 45^{o} angle from a straight line ventrally, it was considered mutant. Significance was determined using Fisher Exact Analysis.

Activated *cdc-42(G12V)*, *myr::unc-40(cyto)*, *myr::unc-73(DH/PH)* and *myr::tiam-1(DH/PH)* transgenes. The *cdc-42(G12V)* transgene under the control of the *osm-6* promoter was used similarly to as described previously for *ced-10(G12V)* (Struckhoff and Lundquist 2003). A *myr::unc-40(cyto)* transgene under the control of the *mec-7* promoter was used as described in Gitai *et al.*,2003. The myr::GEF(DH/PH) transgenes under the control of the osm-6 promoter was used as means of overactivating the GEF. The catalytic DH/PH domains can potentially be inhibited intra- or inter-molecularly. By cloning out the

DH/PH domains, we are potentially relieving any sort of intra-molecular inhibition, and any other inter-molecular inhibitory mechanisms that would include other portions of the molecule (eg., if an inhibitor binds another domain of the GEF to inhibit the DH/PH domains). The myristoylation sequence was added N-terminally to ensure the construct would reach the plasma membrane.

TIAM-1 and CED-10 transgenes. The WRM0633ch01 fosmid (Geneservice) containing the full-length *tiam-1* transgene, with its entire upstream and downstream regions (past the poly-A addition site), was used for the first rescue experiment. The *cmv::mCherry*::*tiam-1* fusion construct were generated by PCR amplifying the entire *tiam-1* coding region based on the H9 cDNA (courtesy of Yuji Kohara). The *tiam-1* construct was placed under the CMV promoter and fused N-terminally with *mCherry* by cloning the *tiam-1* coding gene into the pTriEx-mCherry (kindly provided by the Hahn lab). A similar *tiam-1* coding region construct was also amplified without the stop codon. This construct was fused C-terminally in frame to the worm *mCherry* gene, and placed under the *osm-6* or *unc-25* promoters. The *gfp::ced-10* transgene was built by PCR amplification of the *ced-10* cDNA and cloned into the pEGFP-C1 vector (Clonetech), which fused the *ced-10* coding region N-terminally to *gfp*.

Cell culture, transfections and co-localization assays in NIH3T3 fibroblasts. NIH 3T3 mouse fibroblasts were grown in DMEM (Cellgro) supplemented with 10% Cosmic Calf serum (HyClone) and 1% penicillin-streptomycin (P/S) and

maintained in 5% CO_2 at 37°C. Cells were plated onto coverslips the day before transfection at a density of 200,000 cells per well in a 6-well plate. For co-localization assays, pEGFP-C1 (vector only, “GFP”), pEGFP-C1 expressing CED-10 (“GFP::CED-10”), pTriEx-mCherry (vector only, “mCherry”) and pTriEx-mCherry expressing TIAM-1 (“mCherry::TIAM-1”) were transiently transfected into NIH3T3 cells using GeneExpresso Transfection reagent (Lab Supply Mall) according to the manufacturer's specifications. To visualize subcellular protein localizations at high magnification, the NIH 3T3 cells grown on coverslips and transiently transfected were fixed in 3.7% formaldehyde for 1 h at room temperature. Coverslips were then washed three times in 1× Phosphate Buffered Saline (PBS), one time in ddH_2O, and then mounted onto a glass slide using ProLong Gold antifade (Invitrogen/Molecular Probes) mounting medium. The cells were then visualized using compound fluorescence microscopy (a Leica DMRE microscope with a Qimaging Rolera MGi EMCCD camera was used along with the IPLab and ImageJ softwares).

Mant-GTP based exchange assay. We amplified the DH-PH domains of TIAM-1 (based on the H9 cDNA) (aminoacids 488 till 856), placed it into the pET-28b vector (Novagen), which has a T7 IPTG-inducible promoter and a C-terminal 6HIS-tag, and transformed this construct into BL21(DE3) Gold competent cells (Agilent Technologies). For the TIAM-1[DH(Thr-08-Phe)/PH] construct, we designed primers to make a point mutation in the wild-type construct using the QuickChange kit (Stratagene). We purified TIAM-1[DH/PH]::6HIS using Ni-

column based chromatography. For the mant-GTP assay, we used the RhoGEF Exchange Assay Biochem Kit (Cytoskeleton). Experiments were performed as described in the Cytoskeleton manual. We used 12.5μM of TIAM-1[DH/PH] in our experiments.

Figure 4.1

A

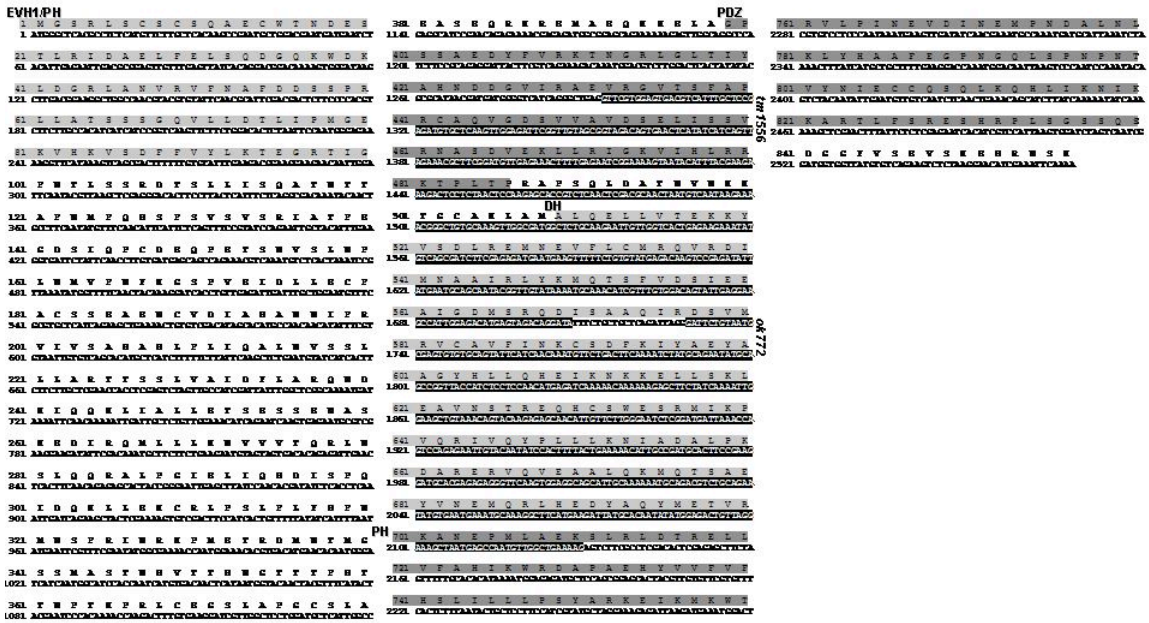

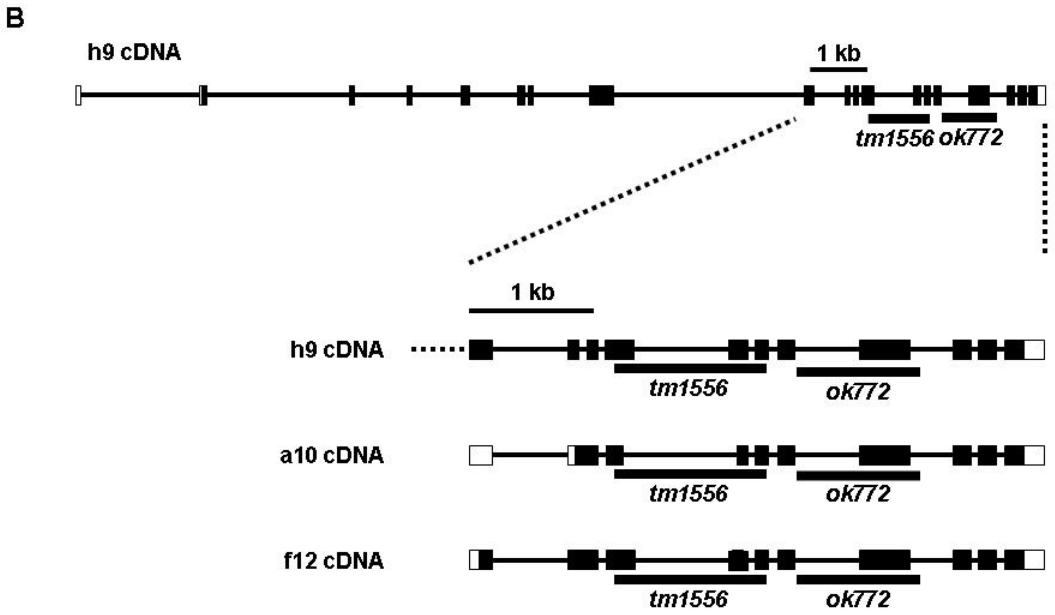
B
h9 cDNA
1 kb
tm1556 ok772
1 kb
h9 cDNA
tm1556
ok772
a10 cDNA
tm1556
ok772
f12 cDNA
tm1556
ok772

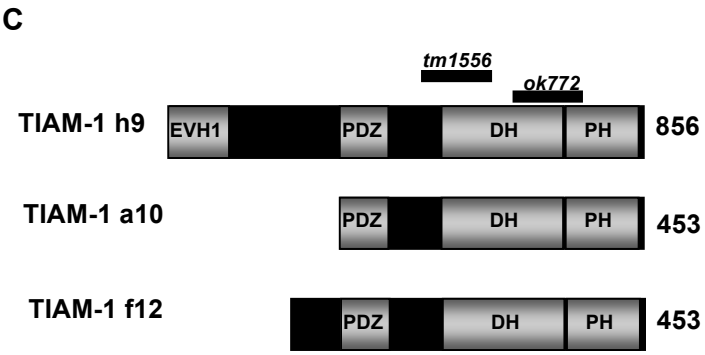
C
tm1556
ok772
TIAM-1 h9
EVH1
PDZ
DH
PH
856
TIAM-1 a10
PDZ
DH
PH
453
TIAM-1 f12
PDZ
DH
PH
453

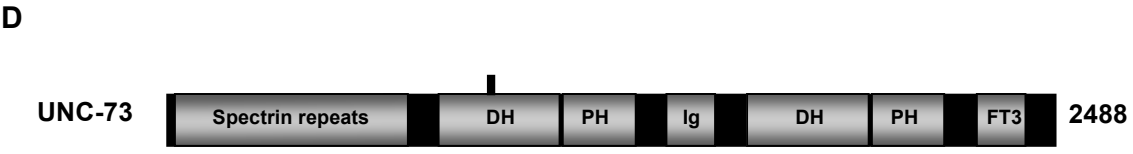
D
UNC-73
Spectrin repeats
DH
PH
Ig
DH
PH
FT3
2488

Figure 4.1 Gene and protein sequence and structure of TIAM-1. **A** Top lane – protein sequence of the TIAM-1 protein. Bottom lane - coding region of the *tiam-1* gene. Both sequences are based on the longest (h9) cDNA. The putative EVH1/PH and PDZ domains, along with the predicted DH and PH domains, are highlighted in the protein sequence in shades of gray. The two deletion alleles, *tm1556* and *ok772*, are highlighted in the DNA sequence in black. **B** Representative schemes of the *tiam-1* gene. All three cDNAs obtained (h9, a10 and f12) were sequenced and served as models for the three gene structures presented. Black boxes – exons. White boxes – untranslated regions. Both deletion alleles (*tm1556* and *ok772*) are depicted underneath the structures, demonstrating the deletion span in the gene. **C** Representative schemes of the TIAM-1 protein. The h9-cDNA-based protein has a putative EVH1/PH N-terminally, followed by a putative PDZ domain and the RacGEF DH/PH domains. Both a10- and f12-cDNA-based proteins lack the putative EVH1/PH domain. The deletion alleles *tm1556* and *ok772* are depicted above the protein structures. **D** A representative scheme of the UNC-73 protein, based on its longest cDNA (F55C7.7a). UNC-73 has eight spectrin repeats, RacGEF DH/PH domains, an Immunoglobulin domain (Ig), RhoGEF DH/PH domains, and a Fibronectin TypeIII (FT3) domain. The point mutation allele *rh4*0 is depicted above the protein structure. In both C and D, the protein length in amino-acid is shown to the right of the schemes. DH - Double Homology domain. PH - Pleckstrin Homology domain. PDZ – PSD95, DlgA, Zo-1 domain. EVH1 – Enabled/VASP Homology domain.

Figure 4.2

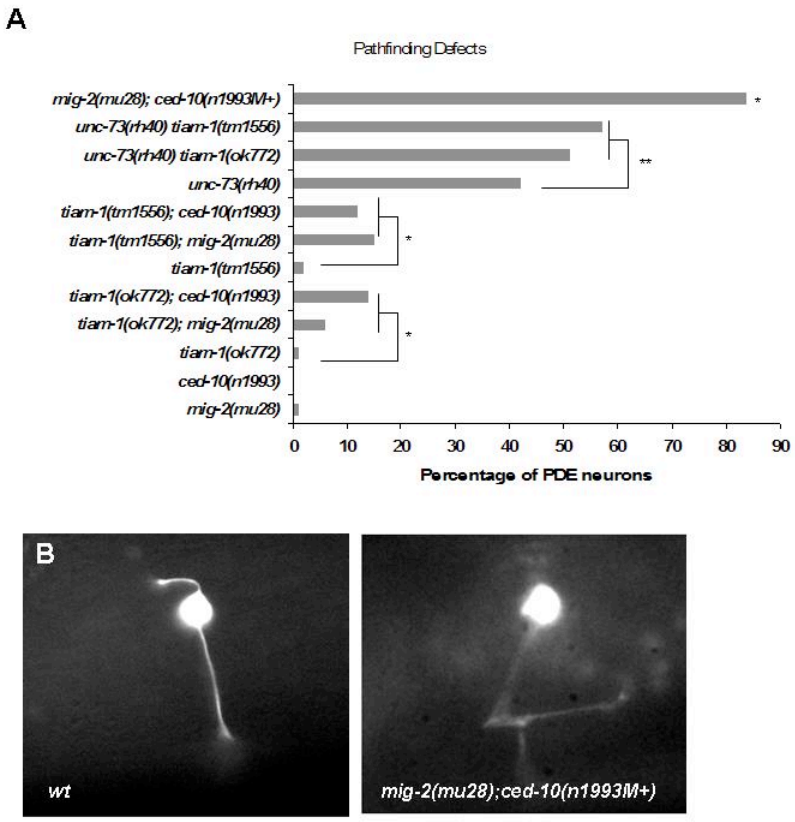
A
Pathfinding Defects
mig-2(mu28); ced-10(n1993M+)
unc-73(rh40) tiam-1(tm1556)
unc-73(rh40) tiam-1(ok772)
unc-73(rh40)
tiam-1(tm1556); ced-10(n1993)
tiam-1(tm1556); mig-2(mu28)
tiam-1(tm1556)
tiam-1(ok772); ced-10(n1993)
tiam-1(ok772); mig-2(mu28)
tiam-1(ok772)
ced-10(n1993)
mig-2(mu28)
*
**
*
*
0
10
20
30
40
50
60
70
80
90
Percentage of PDE neurons
B
wt
mig-2(mu28);ced-10(n1993M+)

Figure 4.2. Rac GTPases and GEFs affect PDE axon pathfinding. **A** Percentage of PDE pathfinding defects in different genotypes shown. Both *tiam-1* alleles synergize with *mig-2(mu28)* and *ced-10(n1993)* to significant levels ($p<0.01$ as shown with *). Both *tiam-1* alleles possibly add to the defects of *unc-73(rh40)*, without synergizing ($p=0.2$ as shown with ** when compared to *unc-73(rh40)* alone). The double mutant *mig-2(mu28); ced-10(n1993M+)* is significantly different than any mutant combination ($p=0.001$ as shown with *). In all graphs, unless otherwise noted, $n>100$. **B** Fluorescent micrographs of wild-type (wt) and mutant PDE neurons.

Figure 4.3

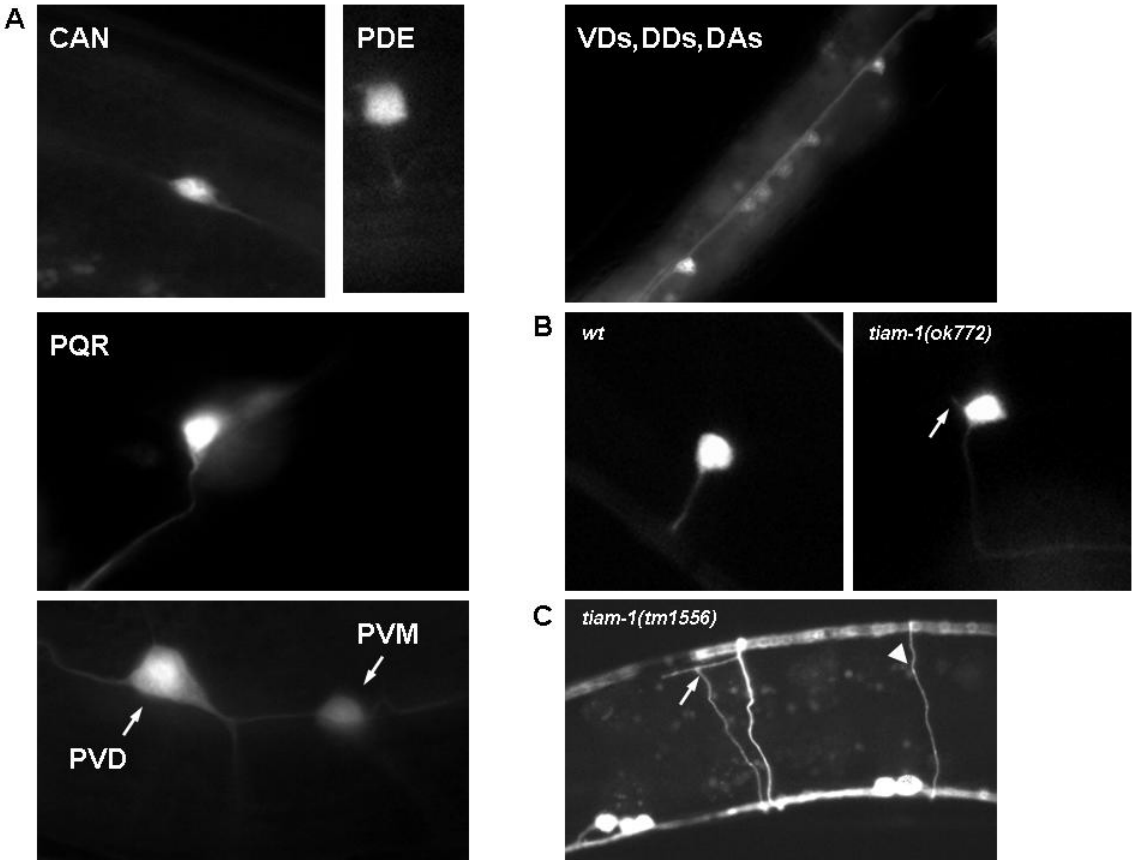
A
CAN
PDE
VDs, DDs, DAs
PQR
PVM
PVD
B
wt
tiam-1(ok772)
C
tiam-1(tm1556)

Figure 4.3. *tiam-1* was expressed in and required for nervous system development. A Fluorescent micrographs of animals harboring a *tiam-1p::cfp* transgene. *tiam-1* was expressed through the nervous system, including the depicted neurons. **B** Micrographs of animals harboring the *zdIs4[mec-7p::gfp]* transgene. A wild-type and *tiam-1(ok772)* mutant neuron (with an ectopic neurite) are shown. **C** Micrograph of an animal harboring the *juIs76[unc-25p::gfp]* transgene. The arrowhead points to a normal VD neuron, and the arrow points to a neuron that failed to extend properly until the ventral nerve cord in *tiam-1(tm1556)*.

Figure 4.4

A

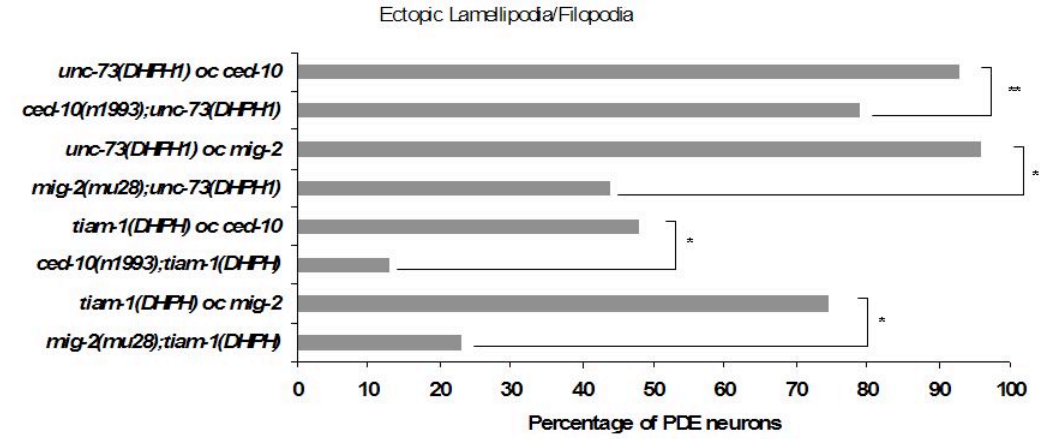
Ectopic Lamellipodia/Filopodia
unc-73(DHPH1) oc ced-10
ced-10(n1993);unc-73(DHPH1)
unc-73(DHPH1) oc mig-2
mig-2(mu28);unc-73(DHPH1)
tiam-1(DHPH) oc ced-10
ced-10(n1993);tiam-1(DHPH)
tiam-1(DHPH) oc mig-2
mig-2(mu28);tiam-1(DHPH)
**
*
*
*
0
10
20
30
40
50
60
70
80
90
100
Percentage of PDE neurons

B

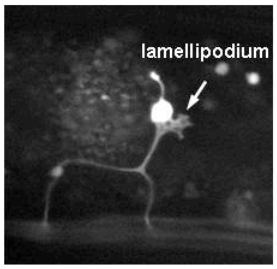
lamellipodium

Figure 4.4. Ectopic lamellipodia caused by overactive TIAM-1 and UNC-73 was suppressed by loss-of-function of Rac GTPases. **A** Percentage of PDE neurons displaying ectopic lamellipodial and filopodial protrusions caused by overactive UNC-73 (MYR::UNC-73[DH1/PH1]) and TIAM-1 (MYR::TIAM-1[DH/PH]). Both *mig-2(mu28)* and *ced-10(n1993)* suppressed these ectopic protrusions. * - $p<0.001$, ** - $p<0.003$. **B** Fluorescent micrograph of an animal harboring the integrated array *lqIs123[osm-6p::myr::unc-73[DH1/PH1]*. The arrow depicts an ectopic lamellipodial protrusion caused by this array.

Figure 4.5

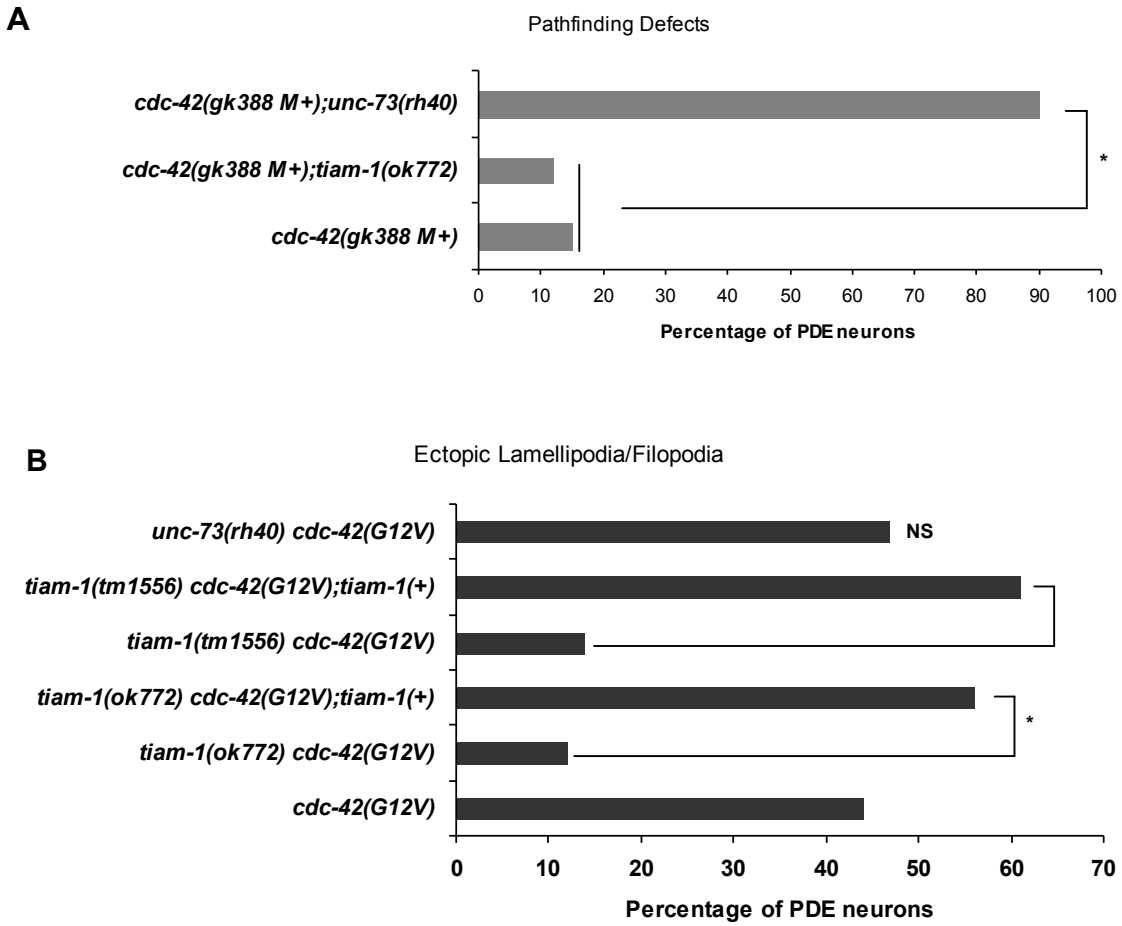
A
Pathfinding Defects
cdc-42(gk388 M+);unc-73(rh40)
cdc-42(gk388 M+);tiam-1(ok772)
cdc-42(gk388 M+)
*
0 10 20 30 40 50 60 70 80 90 100
Percentage of PDE neurons
B
Ectopic Lamellipodia/Filopodia
unc-73(rh40) cdc-42(G12V)
NS
tiam-1(tm1556) cdc-42(G12V);tiam-1(+)
tiam-1(tm1556) cdc-42(G12V)
tiam-1(ok772) cdc-42(G12V);tiam-1(+)
*
tiam-1(ok772) cdc-42(G12V)
cdc-42(G12V)
0 10 20 30 40 50 60 70
Percentage of PDE neurons
C
cdc-

D

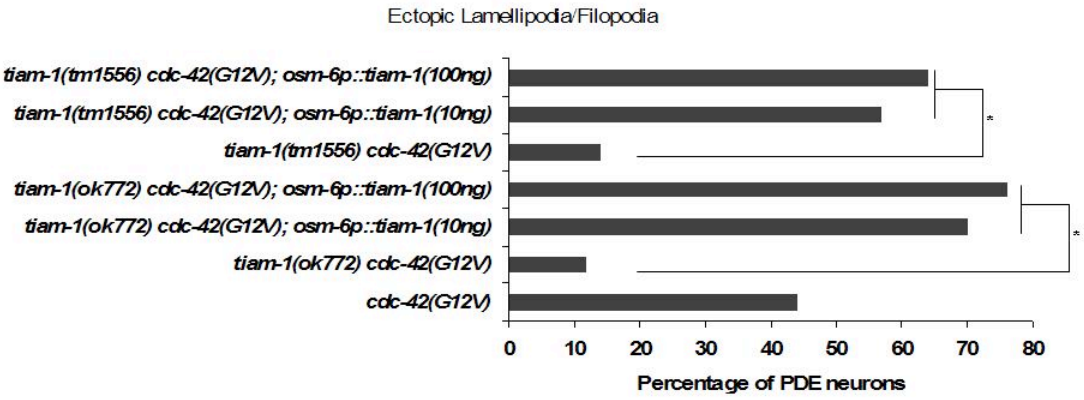
Ectopic Lamellipodia/Filopodia
tiam-1(tm1556) cdc-42(G12V); osm-6p::tiam-1(100ng)
tiam-1(tm1556) cdc-42(G12V); osm-6p::tiam-1(10ng)
tiam-1(tm1556) cdc-42(G12V)
tiam-1(ok772) cdc-42(G12V); osm-6p::tiam-1(100ng)
tiam-1(ok772) cdc-42(G12V); osm-6p::tiam-1(10ng)
tiam-1(ok772) cdc-42(G12V)
cdc-42(G12V)
*
*
0
10
20
30
40
50
60
70
80
Percentage of PDE neurons

Figure 4.5. TIAM-1 and CDC-42 act cell-autonomously in a linear pathway. **A** Percentage of PDE axon pathfinding defects. *tiam-1(ok772)* and *cdc-42(gk388M+)* have similar penetrance of defects as *cdc-42(gk388M+)* alone. *unc-73(rh40)* and *cdc-42(gk388M+)* synergize in axon pathfinding defects. **B** Constitutively activated CDC-42(G12V) expressed in PDE neurons displays ectopic lamellipodial protrusions that are suppressed by the lack of *tiam-1*. As a control, we introduced a fosmid containing the *tiam-1* gene back as an extra-chromosomal array (*tiam-1(+)*), and this array rescued the ectopic lamellipodia in this animals. **C** *tiam-1* acts cell autonomously in the PDE neurons for the ectopic lamellipodial protrusions caused by CDC-42(G12V). Two injected lines of the cDNA amplified coding region of *tiam-1* placed under the *osm*-6 promoter were injected at different concentrations. Both rescued the incidence levels of lamellipodia in the absence of either allele of *tiam-1*. In all graphs, * - $p<0.001$; NS – not significantly different from *cdc-42(gk388M+)* (A) or *cdc-42(G12V)* (B).

Figure 4.6

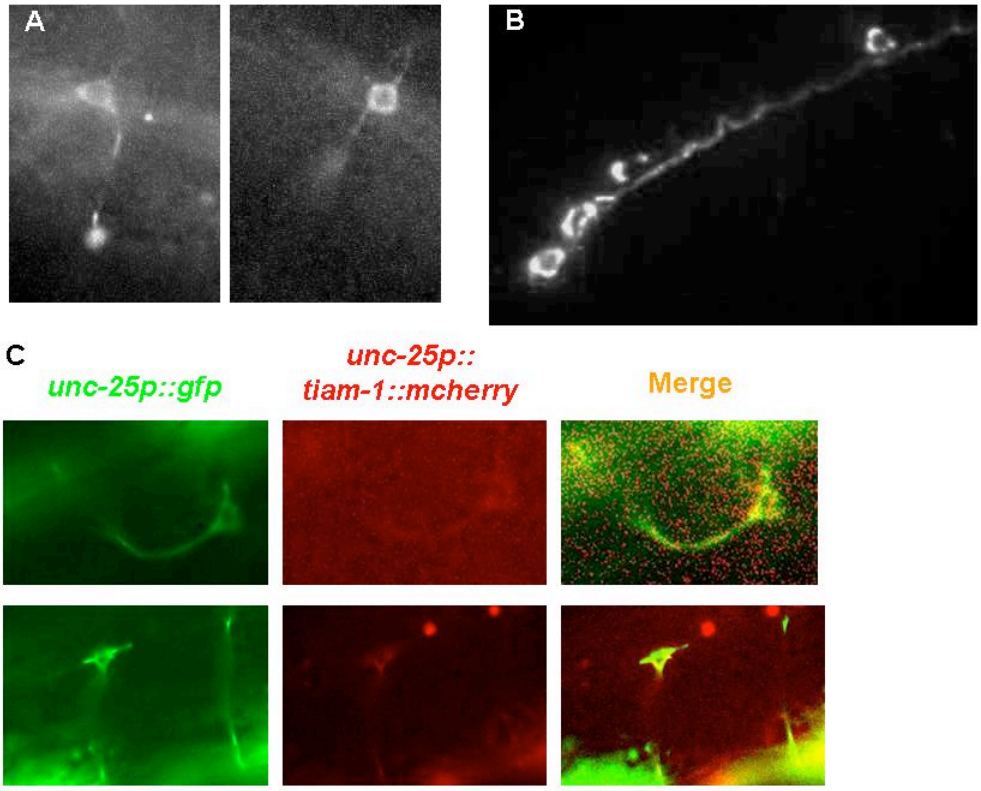

Figure 4.6. TIAM-1 localizes to the cell body periphery, and is present in neurites and in the VD growth cones. **A** Micrographs of animals carrying an *osm-6p::tiam-1::mCherry* array. TIAM-1 is excluded from the nucleus and is possibly associated with the plasma membrane in the cell bodies of the PDE neurons. **B** Micrographs of animals carrying an *unc-25p::tiam-1::mCherry* array. Similarly to the PDE neurons, TIAM-1 seems to be associated with the plasma membrane of the cell body of these neurons. TIAM-1 is also present in the axons and dendrites of both PDEs and VD neurons. **C** TIAM-1 is present in the growth cones of growing VD neurons.

Figure 4.7

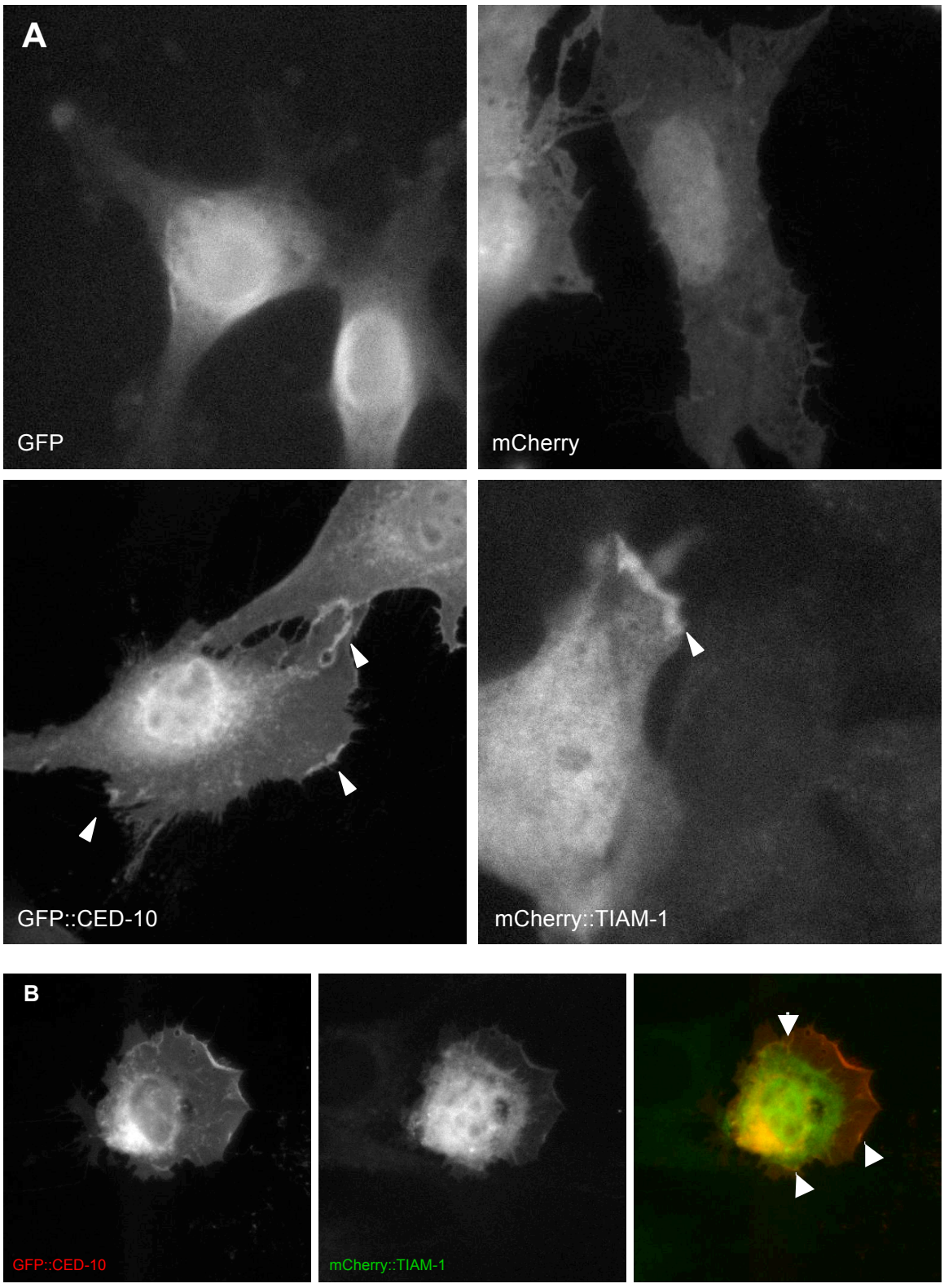
A
GFP
mCherry
GFP::CED-10
mCherry::TIAM-1
B
GFP::CED-10
mCherry::TIAM-1

Figure 4.7. TIAM-1 co-localized with CED-10 in certain domains of NIH 3T3 plasma membrane. **A** Fluorescent micrographs of NIH 3T3 cells expressing GFP (vector only), mCherry (vector only), GFP::CED-10 and mCherry::TIAM-1. Arrowheads depict protein accumulation by the plasma membrane. **B** Co-transfection of GFP::CED-10 (in red) and mCherry::TIAM-1 (in green) show these two proteins co-localize in certain domains of the plasma membrane (depicted by the arrows).

Figure 4.8

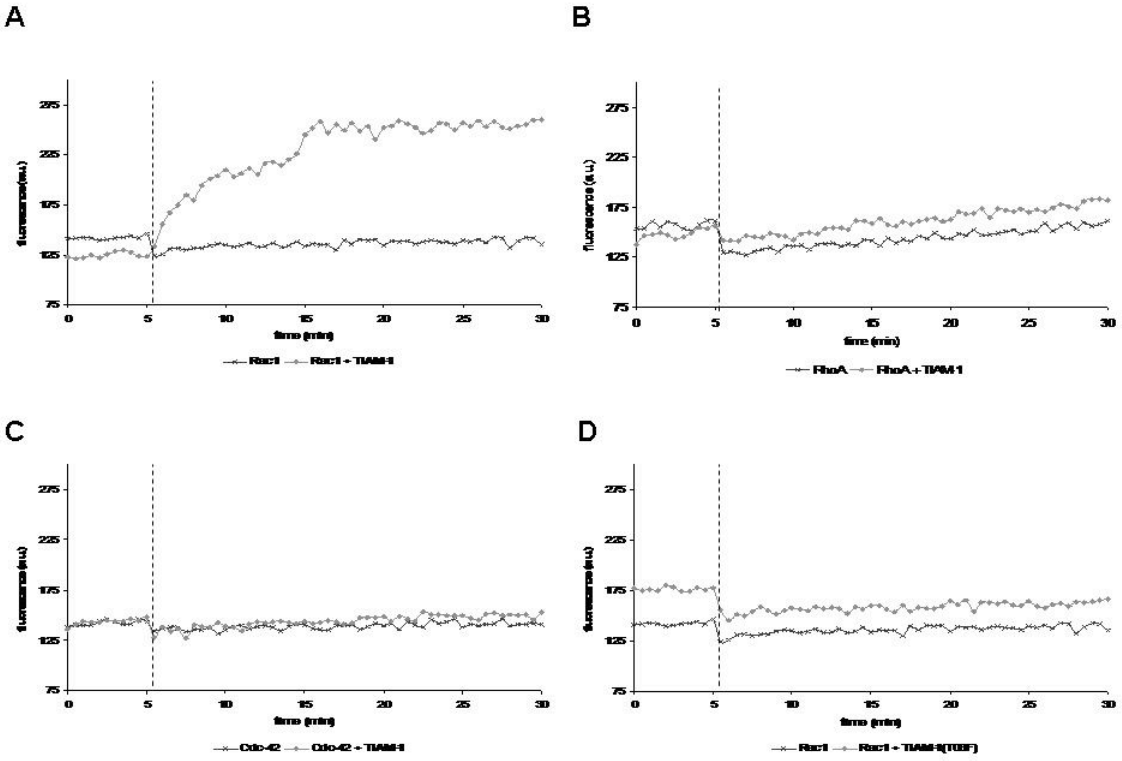
A
B
C
D
time (min)
Rac1
Rac1 + TIAM-1
RhoA
RhoA + TIAM1
Cdc-42
Cdc-42 + TIAM-1
Rac1
Rac1 + TIAM-1(T05F)

Figure 4.8. TIAM-1[DH/PH] catalyzed the incorporation of mant-GTP by Rac1, but not Cdc-42 nor RhoA. A-D Arbitrary fluorescence units representing the amount of fluorescence emitted by mant-GTP over the period of 30 minutes. Light-colored lines represent the assay with the addition of 12.5μM wilt-type TIAM-1[DH/PH] or mutant TIAM-1[DH(Thr-08-Phe)/PH] after five minutes of incubation (dotted vertical line). Dark-colored lines represent addition of vehicle after five minures of incubation (dotted vertical line). All reactions were incubated for five minutes with mant-GTP, reaction buffer and GTPase. **A** Human Rac1 is used as substrate. After the addition of wild-type TIAM-1[DH/PH] to Rac1, mant-GTP-derived fluorescence increases dramatically to around 2-fold. The mere addition of vehicle does not change the overall fluorescence of the reaction. **B and C** Cdc-42 and RhoA were used as substrates, respectively. The addition of wilt-type TIAM-1[DH/PH] did not change the mant-GTP-derived fluorescence of the reaction. **D** The addition of mutant TIAM-1[DH(Thr-08-Phe)] did not affect the fluorescence levels overall in the assay. For all reactions, n=3.

Figure 4.9

A

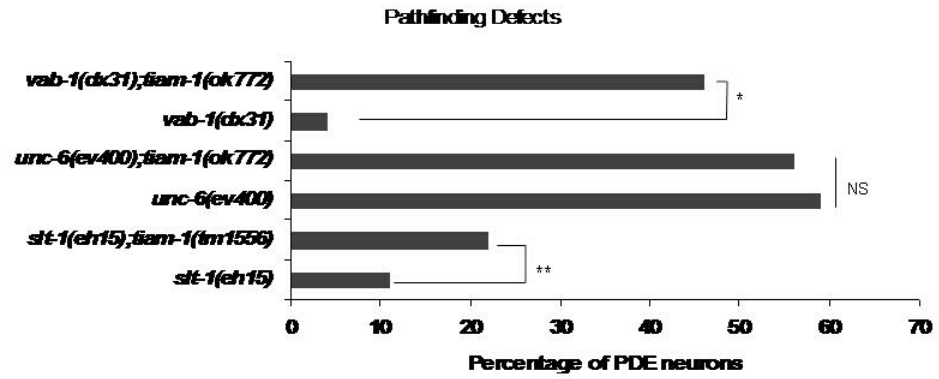
Pathfinding Defects
vab-1(dx31);tiam-1(ok772)
vab-1(dx31)
unc-6(ev400);tiam-1(ok772)
unc-6(ev400)
slt-1(eh15);tiam-1(tm1556)
slt-1(eh15)
*
NS
**
0
10
20
30
40
50
60
70
Percentage of PDE neurons

B

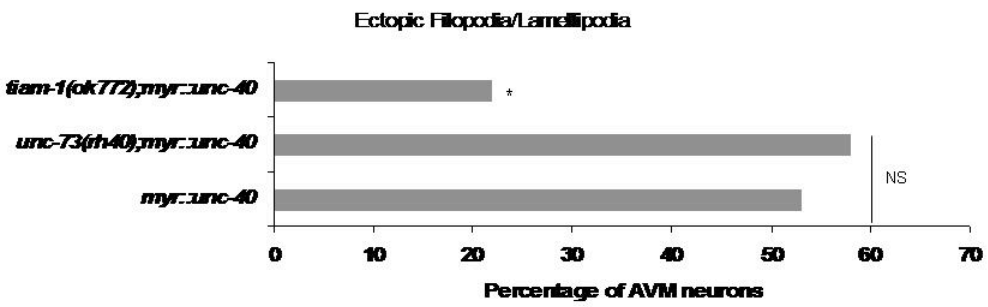
Ectopic Filopodia/Lamellipodia
tiam-1(ok772);myr::unc-40
unc-73(rh40);myr::unc-40
myr::unc-40
*
NS
0
10
20
30
40
50
60
70
Percentage of AVM neurons

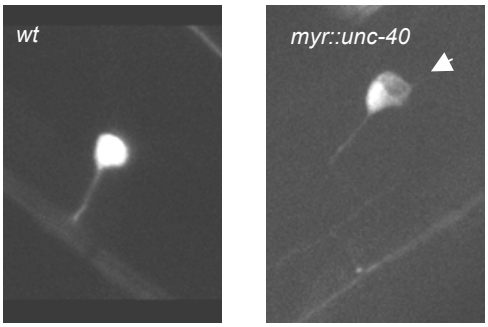
wt
myr::unc-40

Figure 4.9. *tiam-1* acts downstream of *unc-6/Netrin*, in parallel to *slt-1/Slit* and *vab-1/Ephrin*. **A** Percentage of PDE axon pathfinding defects in different guidance mutants. *tiam-1(ok772)* increased the defects seen in axon pathfinding of *vab-1(dx31)* (* p<0.001) and *slt-1(eh15)* (** p<0.1) mutants, but not in *unc-6(ev400)* animals. **B** Percentage of lamellipodial and filopodial protrusions caused by overactivated MYR::UNC-40(cyto) in AVM neurons. *tiam-1(ok772)* significantly suppresses such defects (* - p<0.001), while *unc-73(rh40)* does not have an effect. **C** Fluorescent micrographs of a wild-type and a mutant *myr::unc-40(cyto)* AVM neuron. The arrow depicts an ectopic lamellipodial protrusion coming out of the cell body.

Figure 4.10

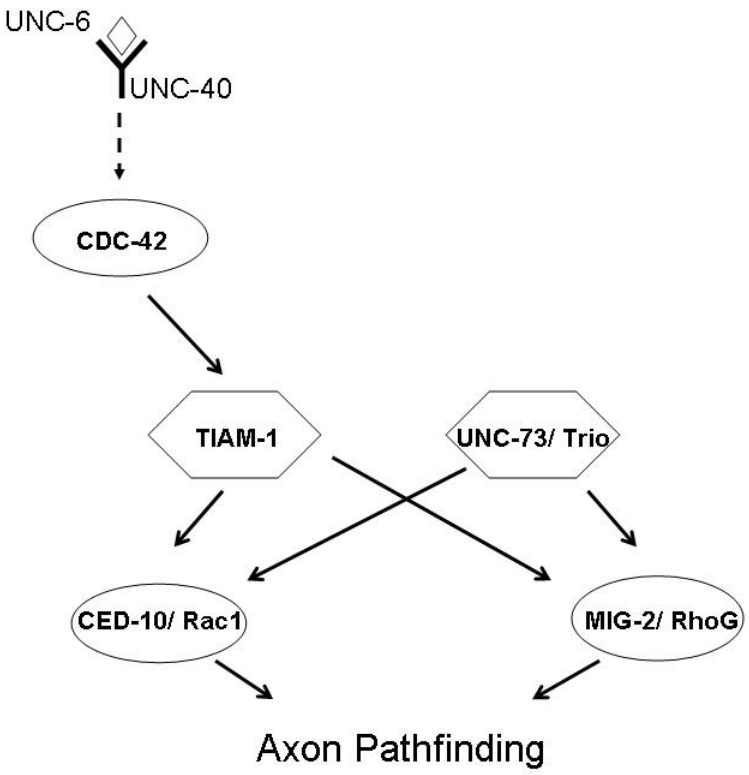
UNC-6
UNC-40
CDC-42
TIAM-1
UNC-73/ Trio
CED-10/ Rac1
MIG-2/ RhoG
Axon Pathfinding

Figure 4.10. A model of the molecules involved in the UNC-6/Netrin attractive signaling pathway. The ligand UNC-6/Netrin binds to its receptor UNC-40/DCC in the plasma membrane of the growth cone. Upon binding to its ligand, UNC-40/DCC activates the CDC-42-TIAM-1 pathway for the activation of the Rac GTPases MIG-2/RhoA and CED-10/Rac, in parallel to the UNC-73/Trio Rac activation pathway, in axon pathfinding.

Figure 4.S1


A
EVH1 domain comparisons
Ce 21 TLRIDAELFELSQDGQKWDKEVHPHLDGRLANVRVFNAFDDSSPRLLATSSSGQVLLDTL 80
R AELF LS D W P L V V S D L
As 3 VVRFWAELFQLSADRSQW-AILYPSL----LSVTVSEISRKRHAVHVTATSASRIIVDQL 57
Ce 81 IPMGEKVHKVSDFFVYLKTEGRTIGFNTLSSRDTSLLISQATNTTAFNMF 130
V VS F Y T G N S D T F F
As 58 LDSSSQVTRVSSCFAYWRHQCQTYGVNFVSAEDCDHFCELSMETSRFIKF 107
As 5 RFWAELFQLSADRS---QWAILYPSLLSVTVSEISRKRHAV-HVTA--TSASRIIVDQLL 58
R WAE F SA W L V I H TA I L
Dm 39 RLWAEVFHVSASGAGTVKWQQVSEDLVPVNITCIQDSPECIFHITAYNSQVDKILDVRLV 98
As 59 -DSSSQVTRVSSCFAYWRHQC—QTYGVNFVSAEDCDHFCELSMETSRFIKFGTTS 111
S CF YW T G NF S D F E F S
Dm 99 QPGTRIGQASECFVYWKDPMTNDTWGLNFTSPIDAKQFRECCSPSFKFSRKASSS 153
Ce 21 TLRIDAELFELSQDGQ---KWDKEVHPHLDGRLANVRVFNAFDDSSPRLLATSSSGQVLL 77
R AE F S G KW V L N A S L
Dm 39 --RLWAEVFHVSASGAGTVKW-QQVSEDLVP--VNITCIQDSPECIFHITAYNSQVDKIL 93
Ce 78 DT-LIPMGEKVHKVSDFFVYLKTE--GRTIGFNTLSSRDTSLLISQATNTTAFNM----F 130
D L G S FVY K T G N S D F
Dm 94 DVRLVQPGTRIGQASECFVYWKDPMTNDTWGLNFTSPIDAKQFRECCSPSFKFSRKASSS 153

B

PDZ domain comparisons

```
Ce          410  DYFVRKTNGRLGLTIYAHNDDGVIRAEVRGVTSFAPRCAQVGDSVVAVDSELISSVPDZR  469
                  Y   KT   LGLTI A   D VI AEVR V        QVGD VV VD   IS
As          410  EYRIEKTDRSLGLTICARQVDDVIKAEVRAVRD-GTTMVQVGDTVVSVDEHPISEL----  464

Ce          470  EMOVEDBYOKRNASDVEKLLRIGKVIHLRRK  500
                        A  VE LLR      LRR+
As          465  ----------QTADQVETLLRSATALVLRRR  485


As          410  -EYRIEKTDRSLGLTICARQVDDVIKAE-----VRAVRDGTTMVQVG----DTVVSVDEH  459
                  E          G    A               V  V D       G    D
Dm         1185  VELQRTTLEQMWGFSVEAELIENAERQDELCCYVSRVEDKSVAMHNGIIKGDEIMVINGA  1244

As          460  PISELQTADQVETLLRSATALVLRRR  485
                   S L      E  L
Dm         1245  IVSDLDMM-YLESVLQ---------E  1260


Ce          410  DYFVRKTNGRL-GLTIYAHNDDGVIRAEVRGVTSFAPRCAQVGDSVVAVDSELISSVPDZ  468
                     R T     G    A       R          R   V D  VA     I    D
Dm         1185  VELQRTTLEQMWGFSVEAELIENAERQDE--LCCYVSR---VEDKSVAMHNGIIKG--DE  1237

Ce          469  REMVEDBYKRNASDVEKLLRIGKVIHLRRK 485
                         SD         V
Dm         1238  IMVINGAI---VSDLD-MMYLESVLQ---E 1260
```

C

```
EVH1 ClustalW
Ce              TLRIDAELFELSQDGQ---KWDKEVHPHLDGRLANVRVFNAFD-DSSPRLLATS—SSGQ
As              VVRFWAELFQLSADRS---QWAILYP-----SLLSVTVSEISR-KRHAVHVTAT—SASR
Dm              --RLWAEVFHVSASGAGTVKWQQVSE-----DLVPVNITCIQDSPECIFHITAYNSQVDK
                  *: **:*.:* .     :*           *  * :            :::   . .:

Ce              VLLDTLIPMGEKVHKVSDFFVYLKTEGR--TIGFNTLSSRDTSLLISQATNTTAFNMF———
As              IIVDQLLDSSSQVTRVSSCFAYWRHQCQ--TYGVNFVSAEDCDHFCELSMETSRFIKF———
Dm              ILDVRLVQPGTRIGQASECFVYWKDPMTNDTWGLNFTSPIDAKQFRECCSPSFKFSRKASSS
                ::   *:  . :: :.*. *.* :      * *.*  *. * . : . .  :  *
```

```
PDZ Clustal W
Ce              -DYFVRKTNGRLGLTIYAHNDDGVIRAEVRGVTSFAPRCAQVGDSVVAVDSELISSVPDZ
As              -EYRIEKTDRSLGLTICARQVDDVIKAEVRAVR-DGTTMVQVGDTVVSVDEHPISELQT-
Dm              VELQRTTLEQMWGFSVEAELIENAERQDELCCYVSRVEDKSVAMHNGIIKGDEIMVING-
                 :    . :   *::: *.  :.. : :            .*.     :. . *  :

Ce              REMVEDBYKRNASDVEKLLRIGKVIHLRRK
As              -----------ADQVETLLRSATALVLRRR
Dm              ------------AIVSDLDMMYLESVLQE-
                             *. *        *:.
```

Figure 4.S1. TIAM-1 has putative EVH1 and PDZ domains. **A and B** BLAST alignments of the predicted EVH1 regions of *C. elegans* TIAM-1 (Ce) (this work), Still life/Tiam1 from *Ascaris suum* (As) (GenBank: ADY42014), and Still Life/Tiam1 isoform E from *Drosophila melanogaster* (Dm) (Genbank NP_001097519). **C** ClustalW alignment of the predicted EVH1 and PDZ domains of the same molecules mentioned above A and B.

Chapter V

A Genetic Screen of DH-Containing Guanine-Nucleotide Exchange Factor Genes Reveals that in addition to UNC-73/Trio and TIAM-1, PIX-1/βPIX, UIG-1/Clg and EXC-5/FGD1 also participate in PDE Axon Pathfinding

5.1. Abstract

In *C. elegans* axon guidance, UNC-73/Trio is a well established GEF for the two redundant Rac GTPases MIG-2 and CED-10. Nevertheless, there is compelling evidence UNC-73/Trio is not the only GEF controlling the Rac GTPases in this process. We performed a candidate-approach genetic screen with the other 18 DH-containing GEF genes in the *C. elegans* genome, and found that besides UNC-73/Trio and TIAM-1 (another GEF known to act in parallel, but not redundantly, to UNC-73), one other Rac-specific GEF (PIX-1/βPIX) and two CDC-42-specific GEFs (UIG-1/Clg and EXC-5/FGD1) also have a role in PDE axon pathfinding.

Genetic data suggests PIX-1/βPIX acts redundantly with UNC-73/Trio, in parallel to CDC-42 and TIAM-1, in the control of the Rac GTPases. Also, UIG-1/Clg possibly acts in the CDC-42 and TIAM-1 upstream of MIG-2/RhoG and CED-10/Rac. Finally, our EXC-5/FGD1 results suggest this molecule acts in parallel to MIG-2/RhoG in axon pathfinding.

5.2. Introduction

Rac GTPases are key regulators of the actin cytoskeleton (Hall 1998; Bishop and Hall 2000). Like other members of the Rho subfamily of small GTPases Cdc-42 and Rho, Racs are active when bound to GTP and inactive when bound to GDP (Bar-Sagi and Hall 2000). Guanine-nucleotide exchange factors (GEFs) aid in the exchange of GTP for GDP. GEFs facilitate the exit of a GDP molecule from the GTP-binding pocket of Rac. Since the concentration of GTP inside the cell is much higher than that of GDP, a GTP molecule can then enter the Rac GTP-binding pocket and activate the molecule (Schmidt and Hall 2002).

Rac GTPases have been implicated in many different aspects of cell migration and neurite extension (Dickson 2001). Both cell and growth cone migration require the constant extension and retraction of cell processes (i.e., filopodia and lamellipodia), and the regulation or adhering molecules (such as cadherins and integrins) (Huber, Kolodkin et al. 2003). Failure in the proper extension or retraction of cell protrusions in axonal development may lead to improper axon extension and guidance (Prasad and Pasterkamp 2009).

The peripheral actin cytoskeleton is the main constituent of lamellipodial and filopodial extensions. In lamellipodia, the actin cytoskeleton is primarily architected in 70^{o} angle branches that spread around the protrusion, yielding in an actin filament meshwork. In filopodia, actin filaments bundle together to yield in the pointy-like structures that are the basis for these finger-like protrusions (Dent and Kalil 2001; Dent and Gertler 2003). The precise control of actin-binding

proteins is of vital importance for the modulation and occurrence of these cellular processes (Machesky and Insall 1998). Actin-modulating proteins such as formins, the Arp2/3 complex, UNC-115/abLIM, capping and anti-capping proteins (such as Enabled), and many others have specific and sometimes overlapping functions during the development of lamellipodia and filopodia (Lundquist, Herman et al. 1998; Dong, Pruyne et al. 2003; Norris, Dyer et al. 2009). Formins, Arp2/3 complex and possibly UNC-115/abLIM are involved in the polymerization of actin-filaments, most likely in different aspects (for example, Arp2/3 could have a greater role in the modulation of the actin meshwork present in lamellipodia, while formins and UNC-115/abLIM could act in the bundling and polymerization of actin in filopodia) (Dong, Pruyne et al. 2003; Yang and Lundquist 2005; Beltzner and Pollard 2007). The capping and anti-capping proteins regulate actin polymerization at the tips of actin filaments, by preventing and allowing, respectively, actin-monomers to be added to these ends (Bashaw, Kidd et al. 2000).

Many of these actin-modulating proteins – the Arp2/3 complex and UNC-115/abLIM for instance – are Rac GTPase effectors (Struckhoff and Lundquist 2003; Shakir, Jiang et al. 2008). While much is known about downstream effectors of Rac GTPases in axon guidance in vivo, not as much is known about their upstream regulators. In *Caenorhabditis elegans* axon pathfinding, loss-of-function mutations in either *ced-10/Rac* or *mig-2/RhoG* alone did not cause significant defects in the PDE ventrally-guided model neurons, nor in the VD and DD dorsally-guided model neurons. However, a double mutant combination of

mig-2;ced-10 resulted in misguided axons in almost every PDE and VD/DD neuron, indicating Rac GTPase activity is crucial for this process (Lundquist 2003).

UNC-73/Trio is a well characterized Rac GEF for the two redundant Rac GTPases CED-10/Rac and MIG-2/RhoG (Lundquist, Reddien et al. 2001). This GEF has two Double Homology (DH) and Pleckstrin Homology (PH) domain sets, which are the domains that have guanine-nucleotide exchange activity. The first DH/PH set of UNC-73/Trio has been biochemically and genetically characterized as Rac-specific, while the second DH/PH set is Rho-specific (Figure 5.1) (Steven, Kubiseski et al. 1998). A point mutation that changes a serine to a phenylalanine in the first, Rac-specific DH/PH set of UNC-73/Trio (*rh40*) disrupted significantly axon pathfinding of both PDE and VD/DD neurons, but not as severe as the double Rac GTPase mutant *mig-2;ced-10 (*Lundquist, Reddien et al. 2001) . Therefore, we hypothesized other upstream activators of Rac GTPases might be needed for the proper control of axon pathfinding in these neurons.

We searched in the *C. elegans* genome for all genes that would encode a DH-containing molecule. Besides UNC-73/Trio, there are 18 other predicted DH-containing molecules in the nematode genome. We then obtained loss-of-function alleles or RNAi constructs to down-regulate the function of these 18 genes alone and in combination with either *mig-2/RhoG* or *ced-10/Rac*, and we analyzed the PDE morphology of these mutants (Table 5.1).

DH domains are not specific for Rac GTPases only, but for all proteins of the family of the Rho subfamily of small monomeric GTPases (Schmidt and Hall 2002). From these 18 genes, seven contained a predicted Rac-specific DH domain, six contained a predicted Rho-specific DH domain, seven with a predicted Cdc-42-specific DH domain, one with a Ras-specific DH domain, and one with a DH domain of predicted specificity (Table 5.1).

In this report, we provide evidence that besides UNC-73/Trio and TIAM-1/Still life (see chapter IV), one other Rac-specific GEF (PIX-1/βPIX) and two other Cdc-42-specific GEFs (UIG-1/Clg and EXC-5/FGD1) interacted genetically with either MIG-2/RhoG or CED-10/Rac in PDE axon pathfinding (Figure 5.1 and 5.2).

5.3 Results

The Rac GEF PIX-1/βPIX acts with MIG-2/RhoG and CED-10/Rac in PDE axon pathfinding. PIX-1 (PAX [p21-activated kinase] interacting exchange factor) if the *C. elegans* counterpart of β-PIX, a Rac-specific GEF implicated in many aspects of cellular and neuronal development, including cell migration and lamellipodial protrusiveness (Ciani and Salinas 2008). In *C. elegans*, PIX-1 signals in a complex with GIT and PAK independently of Rac and CDC-42 in distal tip cell migration (Lucanic and Cheng 2008). Nevertheless, in the migration of Q-neuroblast descendent neurons, PIX-1 has been implicated in acting with CED-10/Rac, in parallel with MIG-2/RhoG and UNC-73/Trio (Dyer, Demarco et

al. 2010). We investigated the role of PIX-1/βPIX in PDE axon pathfinding. The loss-of-function mutation *pix-1(ok982)* is a one base-pair insertion (A) and 1002bp deletion that removes amino-acids 244-450, which include part of the DH domain of the molecule. In the ventrally guided post-deirid sensory set of PDE neurons, *pix-1(ok982)* did not display significant defects in axon pathfinding compared to wild type (1%) (Table 5.2). However, in combination with either *mig-2(mu28)* or *ced-10(n1993)*, *pix-1(ok982)* increased the penetrance of defects significantly to 19% and 19.6% respectively ($p<0.001$ in both cases). The loss-of-function allele *unc-73(rh40)* displayed a similar trend of increased PDE pathfinding defects when in combination with either *mig-2(mu28)* or *ced-10(n1993)*. Therefore, PIX-1/βPIX could act similarly to UNC-73/TRIO with both Rac GTPases.

PIX/βPIX acts redundantly to UNC-73/Trio in PDE pathfinding. Because *pix-1* displayed similar genetic interactions with *mig-2* and *ced-10* to *unc-73*, we investigated if these two GEFs also interact genetically. *unc-73(rh40)* mutants displayed 42% of PDE guidance defects. In a double mutant *pix-1(ok982); unc-73(rh40)* background, 77% of PDE neurons had disrupted axons ($p<0.001$) (Table 5.2). Such results are quite similar to what *mig-2(mu28); ced-10(n1993M+)* mutant animals displayed (84%), suggesting UNC-73/Trio and PIX/βPIX could be acting redundantly to control the activity of MIG-2/RhoG and CED-10/Rac1 in PDE axon pathfinding.

The other Rac GEF known to participate in PDE axon pathfinding, TIAM-1, acts in parallel, but not redundantly, to UNC-73/Trio (Chapter IV). Contrary to the

results with *pix-1*, loss-of-function mutations in both *tiam-1* and *unc-73* increased PDE axon guidance defects observed in an additive rather than synergistic manner, suggesting a non-overlap of functions between these molecules. Similarly to *unc-73(rh40)*, mutations in both *pix-1(ok982); tiam-1(ok772)* displayed a possibly additive increase in PDE axon pathfinding defects (4%) ($p=0.99$ when compared to addition $q=0.0399$; $p=0.17$ when compared to either mutant alone) (Table 5.2).

In addition, TIAM-1, but not UNC-73/Trio, was required for the ectopic lamellipodia caused by the overactivation of CDC-42 in PDE neurons. We then investigated whether PIX-1 was required for such a phenotype.
CDC-42, another member of the Rho subfamily of small GTPases, can be constitutively activated by a Glycine-12-Valine substitution in the GTP-binding pocket of the molecule. This mutation favors the GTP-bound state of the GTPase, hence activating it. Animals harboring the *cdc-42(G12V)* construct displayed 42% of their PDEs with ectopic lamellipodial projections. Like *unc-73(rh40)* animals, *pix-1(ok982)* did not suppress this phenotype (47% for *unc-73*, 82% for *pix-1*) (Table 5.3). In fact, *pix-1(ok982)* mutants significantly increased the lamellipodia observed ($p<0.001$), consistent with the hypothesis these two molecules (CDC-42 and PIX-1) act in different, parallel pathways.

PIX-1/βPIX can act with CED-10/Rac in parallel to MIG-2/RhoG in VD and DD axon pathfinding. In the dorsally attracted GABAergic VD and DD motorneurons, some of the intracellular machinery used for their guidance is

shared with the ventrally guided PDE neurons. *ced-10(n1993)* and *mig-2(mu28)* mutants disturbed pathfinding weakly (2.31% and 3.85%, respectively), but in combination, *mig-2(mu28); ced-10(n1993M+)* affected every VD and DD axon (100%, $p<0.001$) (Table 5.4). *unc-73(rh40)* displayed 26.15% defects alone, and synergistically increased the defects of *mig-2(mu28)* to 55.28% ($p<0.001$). Similarly, *unc-73(rh40); ced-10(n1993M+)* displayed 47.79% of VD/DD axon defects ($p<0.001$). Hence also in the VD and DD motorneurons UNC-73/Trio interacts with both MIG-2/RhoG and CED-10/Rac for proper axon pathfinding.

We decided to investigate the role of PIX-1 in these neurons. Alone, *pix-1(ok982)* displayed 3.08% of VD and DD commissural axon pathfinding defects. *pix-1(ok982)* additively increased the defects seen in a *mig-2(mu28)* background to 16.15% ($p=0.23$ when compared to addition $q=0.0681$; $p<0.001$ when compared to either mutant alone), suggesting these two molecules are acting in a parallel but not redundant pathway. However, *pix-1(ok982); ced-10(n1993M+)* animals displayed 1.54% of pathfinding defects, which was not statistically different from either mutant alone ($p>0.4$). With *unc-73(rh40), pix-1(ok982)* also did not increase significantly the defects observed (26.67%, $p=0.92$) (Table 5.4). These results suggest PIX-1/βPIX could act with CED-10/Rac, in parallel to MIG-2/RhoG, for VD and DD axon pathfinding. Though MIG-2/RhoG and CED-10/Rac act redundantly in this process, they are also known to have different, specific effects during neuronal development. Therefore, it could be that PIX-1/βPIX acts with CED-10/Rac in a specific process of axon pathfinding (for example, a pathway involving PIX-1/CED-10 could act to promote filopodia and lamellipodia

extension during growth cone migration, while another one involving UNC-73/MIG-2/CED-10 could act to promote protrusion retraction). Future studies will aim to identify the cellular basis of these differences by growth cone dynamics analysis.

UIG-1/Clg could act with CDC-42 and TIAM-1 to control Rac GTPases in PDE pathfinding. UIG-1 (UNC-112-Interacting GEF) is a novel CDC-42-specific GEF that in body wall muscle forms a complex with UNC-112/Mitogen inducible gene-2 and PAT-3/β-integrin to regulate PAT-3-mediated adhesive structure (Hikita, Qadota et al. 2005). UIG-1 is similar to human common site lymphoma/leukemia GEF (Clg), a molecule implicated in pancreatic and breast cancers (Himmel, Bi et al. 2002). Both CLG and UIG-1 have been shown to biochemically activate Cdc-42, but not Rac nor RhoA (Himmel, Bi et al. 2002; Hikita, Qadota et al. 2005). In *C. elegans, uig-1(ok884)* is a 1337bp deletion that removes part of the DH domain and virtually the entire PH domain that follows it (*ok884* deletes aminoacids 358-535). *uig-1(ok884)* did not display any PDE pathfinding defects on their own, but increased the defects seen in a *mig-2(mu28)* background to 11% (p=0.003), and in a *ced-10(n1993)* to 7% (p=0.007) (Table 5.5). In addition, *uig-1(ok884); unc-73(rh40)* animals had 66% of their PDEs affected (p=0.001), which suggests UIG-1/Clg1 and UNC-73/Trio act in parallel pathways.

Accordingly with this idea, UIG-1/Clg1 could act with CDC-42 and TIAM-1 act in a linear pathway. *uig-1(ok884); tiam-1(ok772)* mutants had only 3% of PDE

defects (p=0.3), and *uig-1(ok884); cdc-42(gk388M+)* displayed 13% of PDE pathfinding defects, which was not significantly different than *cdc-42(gk388M+)* alone (p=0.7). *uig-1(ok884)* also did not suppress the ectopic lamellipodia caused by the constitutively active *cdc-42(G12V)* (84%) (Table 5.6). These results suggest UIG-1/Clg1 acts upstream of CDC-42 in the control of TIAM-1 and the Rac GTPases. One intriguing result was that *uig-1(ok884)* not only did not suppress the ectopic lamellipodia caused by cdc-42(G12V) but significantly enhanced it. This could mean UIG-1/Clg1 could act in other pathways, possibly acting as a GEF for CDC-42-like proteins. Future studies will address this hypothesis by looking at GTPases that act redundantly with CDC-42.

EXC-5/FGD1 putatively acts with CDC-42 and CED-10/Rac in PDE axon guidance. EXC-5 (Excretory Canal abnormal) is the *C. elegans* counterpart of human FGD1 (Facial Genital Dysplasia). FGD1 is a GEF for hCdc42 that, when mutated, causes Aarskog syndrome, with an impairment of proper skeletal development (Zheng, Fischer et al. 1996; Bedoyan, Friez et al. 2009). In *C. elegans*, EXC-5/FGD1 has been characterized to be involved in the development of the excretory canal (Gao, Estrada et al. 2001). The loss-of-function *rh232* is a 4564bp deletion that putatively abolishes protein translation. It removes the start codon plus the first 651 aminoacids, including its start and the DH and PH domains. In PDE neurons, *exc-5(rh232)* displayed 6% of pathfinding defects on its own, 8% when with *ced-10(n1993)* (p=0.6, a non significant change) and 23% when with *mig-2(mu28)* (p=0.001) (Table 5.5). *exc-5(rh232); unc-73(rh40)* had

54% of pathfinding defects, which did not increase significantly the defects of *unc-73(rh40)* alone or the addition of both mutant defects (p=0.2 when compared to addition q=0.4548). *exc-5(rh232); cdc-42(gk388)* displayed 22% of misguided axons, which is not significantly different then *cdc-42(gk388)* alone (p=0.3). In a combination with *cdc-42(G12V)*, *exc-5(rh232)* failed to suppress the ectopic lamellipodia caused by this construct (37%, p=0.3) (Table 5.6). *With tiam-1(ok772), exc-5(rh232)* displayed 9% of PDE pathfinding defects, a non-significant increase (p>0.4 for both *exc-5* alone or the addition q=0.0694). These results suggest EXC-5/FDG1 possibly acts in a linear pathway with CDC-42 and CED-10/Rac, in parallel to MIG-2/RhoG, during axon guidance. Interestingly, *uig-1(ok884); exc-5(rh232)* double mutants displayed only 3% of PDE pathfinding defects (p=0.3) (Table 5.5). While we expected these two GEFs to act redundantly to modulate CDC-42, one could speculate these two GEFs could have differential effects, or that one (or both) could be acting non cell autonomously. Future work will aim to identify if autonomy is required in the PDE neurons for these molecules.

5.4 Discussion

PIX-1/βPIX is a Rac GEF that acts with MIG-2/RhoG and CED-10/Rac1 redundantly with UNC-73/Trio in axon guidance. In the genetic screen for other GEFs that would act redundantly with UNC-73/Trio for the activation of MIG-2/RhoG and CED-10/Rac, PIX-1/βPIX was the only Rac-specific GEF that

seemed to act redundantly with UNC-73/Trio. The fact that the loss-of-function of *pix-1* behaved similarly to *unc-73* when in combination with *mig-2* and *ced-10*, and that the double *pix-1; unc-73* synergized in defects to very similar levels of the abolishment of Rac activity seen in *mig-2; ced-10* animals suggest UNC-73/Trio and PIX-1/βPIX might share the same role in the control of Rac GTPases during growth cone migration. In addition, the genetic interaction with *tiam-1* suggests PIX-1/βPIX, just like UNC-73/Trio, acts in a parallel but non-redundant pathway with this molecule. The current hypothesis is that TIAM-1 acts as a pro-protrusiveness GEF, activating Rac GTPases to promote filopodia nad lamellipodia formation, while UNC-73/Trio acts in an opposite, anti-protrusiveness pathway, stimulating Rac GTPases to retract filopodia and lamellipodia. PIX-1/βPIX might act with UNC-73/Trio in this retractive pathway. A more careful analysis of growth cone dynamics should enlighten the knowledge of what these molecules are doing during axon guidance.

UIG-1/CIg putatively activates CDC-42 in the TIAM-1-mediated control of Rac GTPases. The role of CDC-42 *in vivo* in *C. elegans* axon pathfinding has not been wellh characterized as of yet. In the previous chapter, we have shown that TIAM-1 is an effector of CDC-42 in this process. In chapter III, we have also shown that the scaffolding protein RACK-1 is possibly acting downstream of CDC-42 with the acting binding protein UNC-115/abLIM and the serine/threonine kinase MIG-15/NIK in PDE guidance. During development, the PAR proteins act with PKC-3/aPKC upstream of CDC-42 to establish early embryo polarity.

In PDE axon pathfinding, we found UIG-1/Clg to interact with the Rac GTPases and possibly act in a linear pathway with CDC-42 and TIAM-1, the Rac GEF involved in the modulation of Rac activity in the UNC-6/Netrin pathway (Chapter IV). Our findings might reveal the path in which CDC-42 is activated in the nervous system. UIG-1/Clg possibly is the GEF utilized by the newborn neuron in order to activate CDC-42 and the TIAM-1/Rac pathway. In the future, we would like to assess if we can overactivate UIG-1/Clg in a similar manner we have activated TIAM-1 and UNC-73/Trio (Chapter IV) and test for suppression of overactivation by the loss of CDC-42 activity.

The putative CDC-42 GEF EXC-5/FGD1 might act exclusively in the CED-10/Rac1 pathway in parallel to MIG-2/RhoG in PDE axon guidance. Our genetic analysis revealed that EXC-5/FGD1 acts in parallel to the Rac GTPase MIG-2/RhoG in PDE axon pathfinding. Because MIG-2/RhoG and CED-10/Rac1 act redundantly in this process, and mutations in *exc-5* and *ced-10* were not worse than *exc-5* alone, we hypothesize these two molecules act in a linear pathway. Similarly, our results suggest EXC-5/FGD1 acts upstream of CDC-42 in the same pathway. Our genetic data in instances proved hard to be analyzed (i.e., mutations in *unc-73* and *exc-5* did not worsen mutations in *unc-73* alone). Such phenomenon indicates that, when far away from each other in a certain pathway, molecules could branch out and have multiple effectors, making a simple genetic conclusion problematic. Nevertheless, we still have good evidence the putative CDC-42 GEF EXC-5/FGD1 acts in PDE axon pathfinding

with CDC-42 and the Rac GTPase CED-10 in parallel to MIG-2/RhoG. Future studies using overactivated EXC-5 (see Chapter IV) could help up better dissect this intricated pathway.

From all the 19 genes screened in the *C. elegans* genome, we found five GEFs to play a role in PDE axon pathfinding. Nevertheless, we cannot exclude the possibility other GEFs are also used in this process. For instance, the Ras- or Rho-specific GEFs screened could have a role in axon pathfinding that is masked by redundancy with other more prominent GEFs. We did not conduct the screen with Ras or Rho, since these molecules do not seem to play a crucial role in PDE axon pathfinding and we were interested in molecules that participate in the Rac-mediated mechanisms of axon guidance.

In sum, in support of the idea that multiple GEFs are implicated in the many different cellular events that involve the activation of Rho GTPases, five different GEFs (UNC-73/Trio, TIAM-1, PIX-1/βPIX, UIG-1/Clg and EXC-5/FGD1) are required for the Rac-mediated mechanisms of axon guidance. Three of them (UNC-73/Trio, TIAM-1 and PIX-1/βPIX) are Rac-specific GEFs that all seem to interact with MIG-2/RhoG and CED-10/Rac, though in different pathways (i.e., only TIAM-1 acts downstream of CDC-42). Two of them are CDC-42-specific and might also act in distinctive pathways (UIG-1/Clg potentially acts linearly with CDC-42 and TIAM-1 to control both CED-10/Rac and MIG-2/RhoG, while EXC-5/FGD1 does not seem to act in the same pathway as MIG-2/RhoG).

The magnificence of the cell biological mechanisms involved in the extension of an axon to its final target can be appreciated by the multitude of

pathways involved during this process. Rac GTPases have been known to act in axon guidance in diverse ways, including the polymerization of actin filaments in order to create filopodia and lamellipodia in the growth cone, and also in the retraction of such protrusions. Most likely, the diverse (and sometimes competitive) effects Rac GTPases accomplish during growth cone migration happen via a differential spatio-temporal recruitment and activation of the diverse GEFs present in the cell. Our results help elucidate some of the molecular combinations involved in this process.

5.5. Materials and Methods

Please refer to section 2.4 in Chapter II for PDE axon pathfinding scoring, molecular biology techniques and *C. elegans* culture.

The following mutations and genetic constructs were used: *LGI: unc-73(rh40), tiam-1(ok772), unc-89(st85), Y95B8a.12(ok1820), lqIs37[osm-6p::cdc-42(G12V)]; LGII: cdc-42(gk388), ect-2(gk-44), tag-218(ok494), rhgf-2(gk216); LGIII: R02F2.2(ok1894); LGIV: ced-10(n1993), exc-5(rh232), tag-77(gk206), gei-18(ok788), lqIs3[osm-6::gfp]; LGV: uig-1(ok884), sos-1(cs41); LGX: mig-2(mu28), tag-52(gk162), rhgf-1(ok880), cgef-1(gk261), vav-1(ok425), pix-1(ok982), lqIs2[osm-6::gfp].*

Table 5.1

GEF	Homology	Specificity	Synergy with *mig-2* or *ced-10*
UNC-73	TRIO	Rac, Rho	Yes
TIAM-1	Tiam1, Still life	Rac	Yes
PIX-1	βPIX, GEF7	Rac	Yes
UIG-1	Clg	CDC-42	Yes
EXC-5	FGD1	CDC-42	Yes
ECT-2	Pebble, Ect2	Rho	No
TAG-218	Ephexin, Ngef	Rho	No
TAG-77	Fgd family (Frabin)	CDC-42	No
TAG-52	Fgd family (Frabin)	CDC-42	No
RHGF-1	Leukemia-associated RhoGEF	Rho	No
CGEF-1	Dbl's Big Sister (Dbs)	CDC-42	No
RHGF-2	Unnamed, conserved	Rho	No
VAV-1	Vav	Rac	No
SOS-1	Son of Sevenless (Sos)	Ras	No
UNC-89	Human Unc-89	Rac	No
GEI-18	Tuba	Rac	No
R02F2.2	RhoGEF17	Rho	No
Y95B8a.12	Unnamed, converved	CDC-42	No
Y105E8A.24	Lymphoid blast crisis-like	Rho, Rac	No

Table 5.1. Summary of the DH-containing GEFs encoded by the C. elegans Genome and their interactions with Rac GTPases. The C. elegans GEF name of the protein (first column) is shown, followed by its homologous proteins in other systems (second column), the predicted specificity of its DH(s) domain(s) (third column), and the genetic results of the synergy experiments with either *mig-2/RhoG* or *ced-10/Rac1* in PDE axon pathfinding (fourth column).

Table 5.2

Genotype	Percentage of PDE axon pathfinding defects
mig-2(mu28)	1
ced-10(n1993)	0
pix-1(ok982)	1
unc-73(rh40)	42
tiam-1(ok772)	1
mig-2(mu28); ced-10(n1993M+)	84
pix-1(ok982) mig-2(mu28)	19
pix-1(ok982); ced-10(n1993)	19.6
pix-1(ok982); unc-73(rh40)	77
pix-1(ok982); tiam-1(ok772)	4

Table 5.2. Percentage of PDE axon pathfinding defects in different genetic backgrounds. *pix-1(ok982)* significantly increased the defects of *mig-2(mu28)*, *ced-10(n1993)*, and *unc-73(rh40)*. n=100 in all cases, unless otherwise noted.

Table 5.3

Genotype	Percentage of PDE ectopic lamellipodia
cdc-42(G12V)	42
unc-73(rh40); cdc-42(G12V)	47
pix-1(ok982); cdc-42(G12V)	82

Table 5.3. Percentage of PDE axon ectopic lamellipodia incidence in different genetic backgrounds. Neither *unc-73(rh40)* nor *pix-1(ok982)* suppressed the ectopic lamellipodia caused by the overactivation of CDC-42.

Table 5.4

Genotype	Percentage of VD/DD pathfinding defects
mig-2(mu28)	3.85
ced-10(n1993)	2.31
mig-2(mu28); ced-10(n1993M+)	100
unc-73(rh40)	26.15
unc-73(rh40); mig-2(mu28)	55.28
unc-73(rh40); ced-10(n1993M+)	47.79
pix-1(ok982)	3.08
pix-1(ok982) mig-2(mu28)	16.15
pix-1(ok982); ced-10(n1993)	1.54
pix-1(ok982); unc-73(rh40)	26.67

Table 5.4. Percentage of VD and DD commissural axon pathfinding defects in different genetic backgrounds. *pix-1(ok982)* synergized with *mig-2(mu28)* but not *ced-10(n1993)* nor *unc-73(rh40)* in motorneuron axon pathfinding. In all cases, n>130.

Table 5.5

Genotype	Percentage of PDE axon pathfinding defects
cdc-42(gk388M+)	15
uig-1(ok884)	0
exc-5(rh232)	6
uig-1(ok884); mig-2(mu28)	11
uig-1(ok884); ced-10(n1993)	7
uig-1(ok884); unc-73(rh40)	66
uig-1(ok884); tiam-1(ok772)	3
uig-1(ok884); cdc-42(gk388M+)	13
exc-5(rh232); mig-2(mu28)	23
exc-5(rh232); ced-10(n1993)	8
exc-5(rh232); unc-73(rh40)	54
exc-5(rh232); tiam-1(ok772)	9
exc-5(rh232); cdc-42(gk388M+)	22
exc-5(rh232); uig-1(ok884)	3

Table 5.5. Percentage of PDE axon pathfinding defects in different genetic backgrounds. *uig-1(ok884)* and *exc-5(rh232)* displayed a role in PDE axon pathfinding when interacting with the Rac GTPases and their regulators.

Table 5.6

Genotype	Percentage of PDE ectopic lamellipodia
cdc-42(G12V)	42
uig-1(ok884); cdc-42(G12V)	84
exc-5(rh232); cdc-42(G12V)	37

Table 5.6. Percentage of PDE axon ectopic lamellipodia incidence in different genetic backgrounds. Neither *uig-1(ok884)* nor *exc-5(rh232)* suppressed the ectopic lamellipodia caused by the overactivation of CDC-42.

Figure 5.1

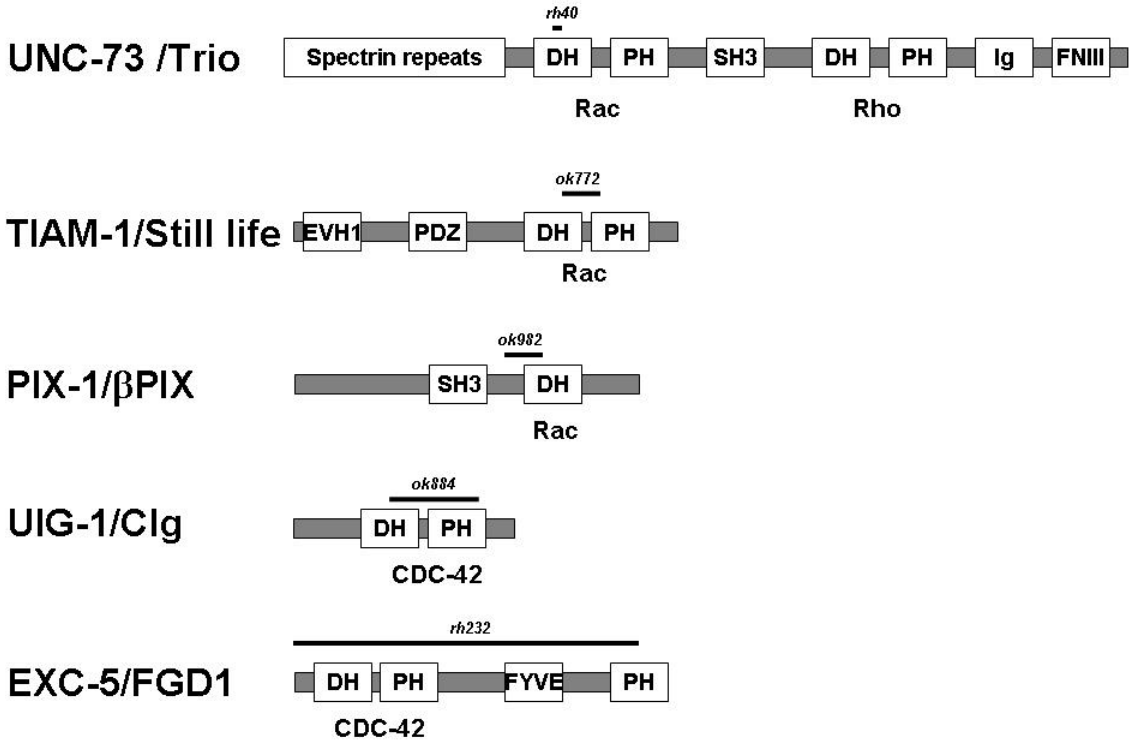
UNC-73 /Trio
rh40
Spectrin repeats
DH
PH
SH3
DH
PH
Ig
FNIII
Rac
Rho
TIAM-1/Still life
ok772
EVH1
PDZ
DH
PH
Rac
PIX-1/βPIX
ok982
SH3
DH
Rac
UIG-1/CIg
ok884
DH
PH
CDC-42
EXC-5/FGD1
rh232
DH
PH
FYVE
PH
CDC-42

Figure 5.1. Protein structure representations of the five GEFs that interacted with the Rac GTPases in PDE axon pathfinding. The loss-of-function alleles of the genes used are represented with a dash, indicating where the point mutation (*rh40*) or deletions would be if a protein is produced. In all five cases, at least the DH domain is affected by the mutation. GEF specificity for either Rac or CDC-42 is depicted underneath the correspondent DH domain.

\

Figure 5.2

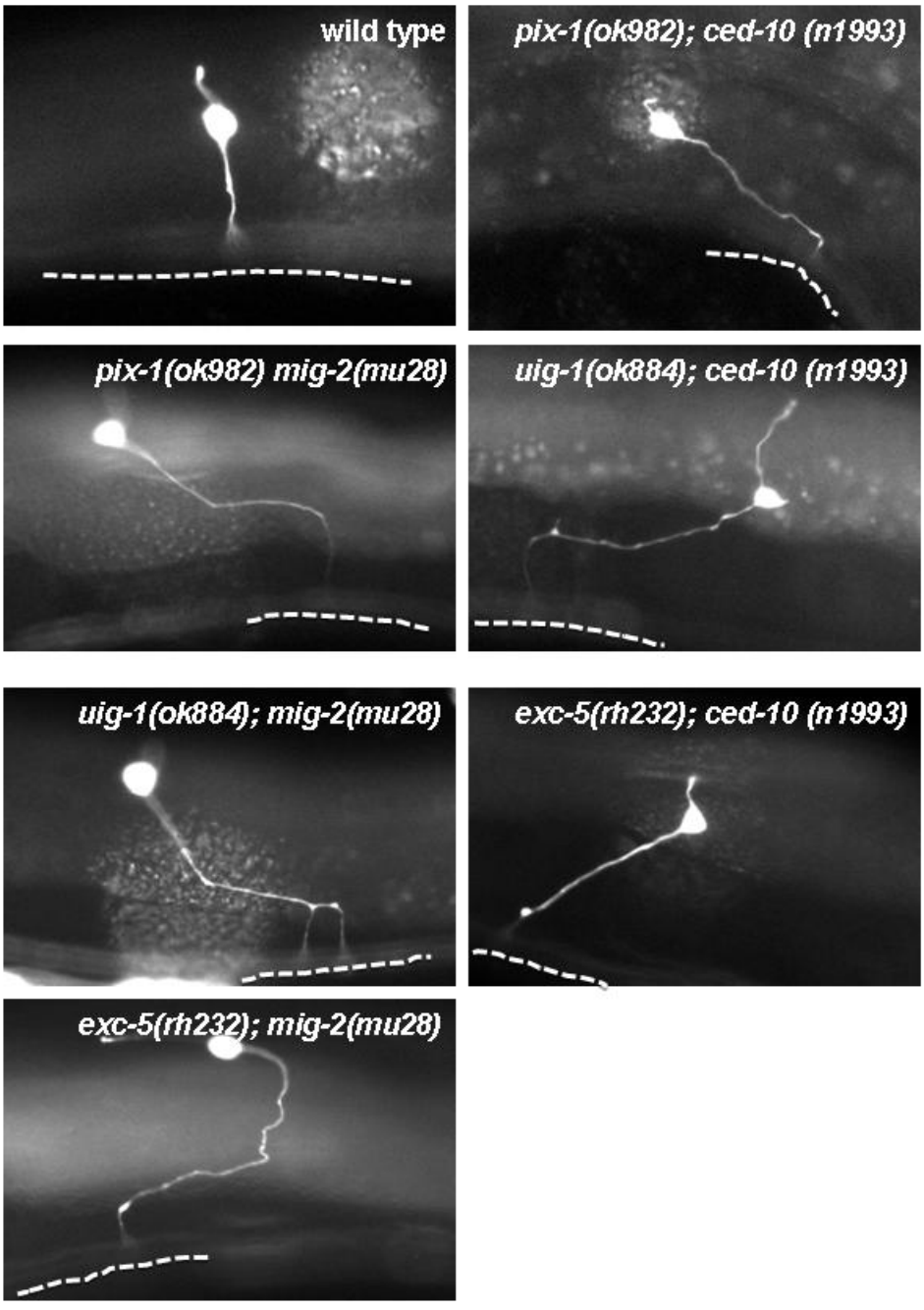
wild type
pix-1(ok982); ced-10 (n1993)
pix-1(ok982) mig-2(mu28)
uig-1(ok884); ced-10 (n1993)
uig-1(ok884); mig-2(mu28)
exc-5(rh232); ced-10 (n1993)
exc-5(rh232); mig-2(mu28)

Figure 5.2. Fluorescent micrographs of PDE neurons in different genetic backgrounds. *pix-1(ok982)*, *uig-1(ok884)* and *exc-5(rh232)* interact genetically with mig-2(mu28) and ced-10(n1993) in axon guidance.

References

Adler, C. E., R. D. Fetter, et al. (2006). "UNC-6/Netrin induces neuronal asymmetry and defines the site of axon formation." Nat Neurosci 9(4): 511-518.

Aguda, A. H., L. D. Burtnick, et al. (2005). "The state of the filament." EMBO reports 6(3): 220-226.

Ai, E., D. S. Poole, et al. (2009). "RACK-1 directs dynactin-dependent RAB-11 endosomal recycling during mitosis in Caenorhabditis elegans." Mol Biol Cell 20(6): 1629-1638.

Aizawa, H., S. Wakatsuki, et al. (2001). "Phosphorylation of cofilin by LIM-kinase is necessary for semaphorin 3A-induced growth cone collapse." Nat Neurosci 4(4): 367-373.

Anderson, P. (1995). "Mutagenesis." Methods Cell Biol 48: 31-58.

Anitha, A., K. Nakamura, et al. (2008). "Genetic analyses of roundabout (ROBO) axon guidance receptors in autism." Am J Med Genet B Neuropsychiatr Genet 147B(7): 1019-1027.

Azuma, T., W. Witke, et al. (1998). "Gelsolin is a downstream effector of rac for fibroblast motility." Embo J 17(5): 1362-1370.

Bar-Sagi, D. and A. Hall (2000). "Ras and Rho GTPases: A Family Reunion." Cell 103: 227-238.

Barzik, M., T. I. Kotova, et al. (2005). "Ena/VASP proteins enhance actin polymerization in the presence of barbed end capping proteins." J Biol Chem 280(31): 28653-28662.

Bashaw, G. J., T. Kidd, et al. (2000). "Repulsive axon guidance: Abelson and Enabled play opposing roles downstream of the roundabout receptor [In Process Citation]." Cell 101(7): 703-715.

Bedoyan, J. K., M. J. Friez, et al. (2009). "First case of deletion of the faciogenital dysplasia 1 (FGD1) gene in a patient with Aarskog-Scott syndrome." European journal of medical genetics 52(4): 262-264.

Bei, Y., J. Hogan, et al. (2002). "SRC-1 and Wnt signaling act together to specify endoderm and to control cleavage orientation in early C. elegans embryos." Dev Cell 3(1): 113-125.

Beltzner, C. C. and T. D. Pollard (2007). "Pathway of actin filament branch formation by Arp2/3 complex." J Biol Chem.

Besson, A., T. L. Wilson, et al. (2002). "The anchoring protein RACK1 links protein kinase Cepsilon to integrin beta chains. Requirements for adhesion and motility." J Biol Chem 277(24): 22073-22084.

Bishop, A. L. and A. Hall (2000). "Rho GTPases and their effector proteins." Biochem J 348 Pt 2: 241-255.

Biyasheva, A., T. Svitkina, et al. (2004). "Cascade pathway of filopodia formation downstream of SCAR." J Cell Sci 117(Pt 6): 837-848.

Bizat, N., J. M. Peyrin, et al. (2010). "Neuron dysfunction is induced by prion protein with an insertional mutation via a Fyn kinase and reversed by sirtuin activation in Caenorhabditis elegans." The Journal of

neuroscience : the official journal of the Society for Neuroscience 30(15): 5394-5403.

Borisy, G. G. and T. M. Svitkina (2000). "Actin machinery: pushing the envelope." Curr Opin Cell Biol 12(1): 104-112.

Brandt, D., M. Gimona, et al. (2002). "Protein kinase C induces actin reorganization via a Src- and Rho-dependent pathway." J Biol Chem 277(23): 20903-20910.

Brenner, S. (1974). "The genetics of *Caenorhabditis elegans*." Genetics 77(1): 71-94.

Brose, K., K. S. Bland, et al. (1999). "Slit proteins bind Robo receptors and have an evolutionarily conserved role in repulsive axon guidance." Cell 96(6): 795-806.

Buensuceso, C. S., D. Woodside, et al. (2001). "The WD protein Rack1 mediates protein kinase C and integrin-dependent cell migration." J Cell Sci 114(Pt 9): 1691-1698.

Chan, S. S., H. Zheng, et al. (1996). "UNC-40, a C. elegans homolog of DCC (Deleted in Colorectal Cancer), is required in motile cells responding to UNC-6 netrin cues." Cell 87(2): 187-195.

Chang, B. Y., K. B. Conroy, et al. (1998). "RACK1, a receptor for activated C kinase and a homolog of the beta subunit of G proteins, inhibits activity of src tyrosine kinases and growth of NIH 3T3 cells." Mol Cell Biol 18(6): 3245-3256.

Chang, B. Y., R. A. Harte, et al. (2002). "RACK1: a novel substrate for the Src protein-tyrosine kinase." Oncogene 21(50): 7619-7629.

Cheng, S., J. Mao, et al. (2000). "Filopodial behavior is dependent on the phosphorylation state of neuronal growth cones." Cell Motil Cytoskeleton 47(4): 337-350.

Chianale, F., E. Rainero, et al. "Diacylglycerol kinase alpha mediates HGF-induced Rac activation and membrane ruffling by regulating atypical PKC and RhoGDI." Proc Natl Acad Sci U S A 107(9): 4182-4187.

Ciani, L. and P. C. Salinas (2008). "From neuronal activity to the actin cytoskeleton: a role for CaMKKs and betaPIX in spine morphogenesis." Neuron 57(1): 3-4.

Collet, J., C. A. Spike, et al. (1998). "Analysis of osm-6, a gene that affects sensory cilium structure and sensory neuron function in Caenorhabditis elegans." Genetics 148(1): 187-200.

Coulson, A., J. Sulston, et al. (1986). "Toward a physical map of the genome of the nematode *Caenorhabditis elegans*." Proc. Natl. Acad. U.S.A. 83: 7821-7825.

Dan, C., A. Kelly, et al. (2001). "Cytoskeletal changes regulated by the PAK4 serine/threonine kinase are mediated by LIM kinase 1 and cofilin." J Biol Chem 276(34): 32115-32121.

Demarco, R. S. and E. A. Lundquist (2010). "RACK-1 acts with Rac GTPase signaling and UNC-115/abLIM in Caenorhabditis elegans axon pathfinding and cell migration." PLoS genetics 6(11): e1001215.

Dent, E. W. and F. B. Gertler (2003). "Cytoskeletal dynamics and transport in growth cone motility and axon guidance." Neuron 40(2): 209-227.

Dent, E. W. and K. Kalil (2001). "Axon branching requires interactions between dynamic microtubules and actin filaments." J Neurosci 21(24): 9757-9769.

Dickson, B. J. (2001). "Rho GTPases in growth cone guidance." Curr Opin Neurobiol 11(1): 103-110.

Dickson, B. J. (2002). "Molecular mechanisms of axon guidance." Science 298(5600): 1959-1964.

Dong, Y., D. Pruyne, et al. (2003). "Formin-dependent actin assembly is regulated by distinct modes of Rho signaling in yeast." J Cell Biol 161(6): 1081-1092.

Dyer, J. O., R. Demarco, et al. (2010). "Distinct roles of Rac GTPases and the UNC-73/Trio and PIX-1 Rac GTP exchange factors in neuroblast protrusion and migration in C. elegans." Small GTPases 1(1): 44-61.

Eden, S., R. Rohatgi, et al. (2002). "Mechanism of regulation of WAVE1-induced actin nucleation by Rac1 and Nck." Nature 418(6899): 790-793.

Epstein, H. F. and D. C. Shakes (1995). Caenorhabditis elegans: Modern Biological Analysis of an Organism. New York, Academic Press.

Evangelista, M., S. Zigmond, et al. (2003). "Formins: signaling effectors for assembly and polarization of actin filaments." Journal of cell science 116(Pt 13): 2603-2611.

Flanagan, J. G. and P. Vanderhaeghen (1998). "The ephrins and Eph receptors in neural development." Annu Rev Neurosci 21: 309-345.

Gallo, G. and P. C. Letourneau (2004). "Regulation of growth cone actin filaments by guidance cues." J Neurobiol 58(1): 92-102.

Gao, J., L. Estrada, et al. (2001). "The Caenorhabditis elegans homolog of FGD1, the human Cdc42 GEF gene responsible for faciogenital dysplasia, is critical for excretory cell morphogenesis." Hum Mol Genet 10(26): 3049-3062.

Garcia, M. C., M. Abbasi, et al. (2007). "Role of Drosophila gene dunc-115 in nervous system." Invert Neurosci 7(2): 119-128.

Gatlin, J. C., A. Estrada-Bernal, et al. (2006). "Myristoylated, alanine-rich C-kinase substrate phosphorylation regulates growth cone adhesion and pathfinding." Mol Biol Cell 17(12): 5115-5130.

Ghysen, A. (2003). "The origin and evolution of the nervous system." The International journal of developmental biology 47(7-8): 555-562.

Gitai, Z., T. W. Yu, et al. (2003). "The netrin receptor UNC-40/DCC stimulates axon attraction and outgrowth through enabled and, in parallel, Rac and UNC-115/AbLIM." Neuron 37(1): 53-65.

Hall, A. (1992). "Ras-related GTPases and the cytoskeleton." Molecular biology of the cell 3(5): 475-479.

Hall, A. (1998). "Rho GTPases and the actin cytoskeleton." Science 279(5350): 509-514.

Hannula-Jouppi, K., N. Kaminen-Ahola, et al. (2005). "The axon guidance receptor gene ROBO1 is a candidate gene for developmental dyslexia." PLoS Genet 1(4): e50.

Hao, J. C., T. W. Yu, et al. (2001). "C. elegans slit acts in midline, dorsal-ventral, and anterior-posterior guidance via the SAX-3/Robo receptor." Neuron 32(1): 25-38.

Hedgecock, E. M., J. G. Culotti, et al. (1990). "The *unc-5, unc-6,* and *unc-40* genes guide circumferential migrations of pioneer axons and mesodermal cells on the epidermis in *C. elegans.*" Neuron 4(1): 61-85.

Hikita, T., H. Qadota, et al. (2005). "Identification of a novel Cdc42 GEF that is localized to the PAT-3-mediated adhesive structure." Biochem Biophys Res Commun 335(1): 139-145.

Himmel, K. L., F. Bi, et al. (2002). "Activation of clg, a novel dbl family guanine nucleotide exchange factor gene, by proviral insertion at evi24, a common integration site in B cell and myeloid leukemias." J Biol Chem 277(16): 13463-13472.

Hoshino, M., M. Sone, et al. (1999). "Identification of the stef gene that encodes a novel guanine nucleotide exchange factor specific for Rac1." J Biol Chem 274(25): 17837-17844.

Huber, A. B., A. L. Kolodkin, et al. (2003). "Signaling at the growth cone: ligand-receptor complexes and the control of axon growth and guidance." Annu Rev Neurosci 26: 509-563.

Innocenti, M., A. Zucconi, et al. (2004). "Abi1 is essential for the formation and activation of a WAVE2 signalling complex." Nat Cell Biol 6(4): 319-327.

Itoh, B., T. Hirose, et al. (2005). "SRC-1, a non-receptor type of protein tyrosine kinase, controls the direction of cell and growth cone migration in C. elegans." Development 132(23): 5161-5172.

Jin, Y., E. Jorgensen, et al. (1999). "The Caenorhabditis elegans gene unc-25 encodes glutamic acid decarboxylase and is required for synaptic transmission but not synaptic development." J Neurosci 19(2): 539-548.

Kiely, P. A., G. S. Baillie, et al. (2009). "Phosphorylation of RACK1 on tyrosine 52 by c-Abl is required for insulin-like growth factor I-mediated regulation of focal adhesion kinase." J Biol Chem 284(30): 20263-20274.

Kikkawa, U., T. Kitano, et al. (1986). "Possible roles of protein kinase C in signal transduction in nervous tissues." Progress in brain research 69: 29-35.

Killeen, M. T. and S. S. Sybingco (2008). "Netrin, Slit and Wnt receptors allow axons to choose the axis of migration." Dev Biol 323(2): 143-151.

Kimble, J. and D. Hirsh (1979). "The postembryonic cell lineages of the hermaphrodite and male gonads in Caenorhabditis elegans." Dev Biol 70(2): 396-417.

Korobova, F. and T. Svitkina (2008). "Arp2/3 complex is important for filopodia formation, growth cone motility, and neuritogenesis in neuronal cells." Mol Biol Cell 19(4): 1561-1574.

Kubiseski, T. J., J. Culotti, et al. (2003). "Functional analysis of the Caenorhabditis elegans UNC-73B PH domain demonstrates a role in activation of the Rac GTPase in vitro and axon guidance in vivo." Mol Cell Biol 23(19): 6823-6835.

Lebrand, C., E. W. Dent, et al. (2004). "Critical role of Ena/VASP proteins for filopodia formation in neurons and in function downstream of netrin-1." Neuron 42(1): 37-49.

Li, W., J. Aurandt, et al. (2006). "FAK and Src kinases are required for netrin-induced tyrosine phosphorylation of UNC5." J Cell Sci 119(Pt 1): 47-55.

Li, W., J. Lee, et al. (2004). "Activation of FAK and Src are receptor-proximal events required for netrin signaling." Nat Neurosci 7(11): 1213-1221.

Liliental, J. and D. D. Chang (1998). "Rack1, a receptor for activated protein kinase C, interacts with integrin beta subunit." J Biol Chem 273(4): 2379-2383.

Lucanic, M. and H. J. Cheng (2008). "A RAC/CDC-42-independent GIT/PIX/PAK signaling pathway mediates cell migration in C. elegans." PLoS genetics 4(11): e1000269.

Lundquist, E. A. (2003). "Rac proteins and the control of axon development." Curr Opin Neurobiol 13(3): 384-390.

Lundquist, E. A., R. K. Herman, et al. (1998). "UNC-115, a conserved protein with predicted LIM and actin-binding domains, mediates axon guidance in C. elegans." Neuron 21(2): 385-392.

Lundquist, E. A., P. W. Reddien, et al. (2001). "Three C. elegans Rac proteins and several alternative Rac regulators control axon guidance, cell migration and apoptotic cell phagocytosis." Development 128(22): 4475-4488.

Machesky, L. M. and R. H. Insall (1998). "Scar1 and the related Wiskott-Aldrich syndrome protein, WASP, regulate the actin cytoskeleton through the Arp2/3 complex." Curr Biol 8(25): 1347-1356.

Marin, O., M. Valiente, et al. (2010). "Guiding neuronal cell migrations." Cold Spring Harbor perspectives in biology 2(2): a001834.

Matsuo, N., M. Hoshino, et al. (2002). "Characterization of STEF, a guanine nucleotide exchange factor for Rac1, required for neurite growth." J Biol Chem 277(4): 2860-2868.

Matsuo, N., M. Terao, et al. (2003). "Roles of STEF/Tiam1, guanine nucleotide exchange factors for Rac1, in regulation of growth cone morphology." Mol Cell Neurosci 24(1): 69-81.

Mattila, P. K. and P. Lappalainen (2008). "Filopodia: molecular architecture and cellular functions." Nature reviews. Molecular cell biology 9(6): 446-454.

Matusek, T., R. Gombos, et al. (2008). "Formin proteins of the DAAM subfamily play a role during axon growth." The Journal of

neuroscience : the official journal of the Society for Neuroscience 28(49): 13310-13319.
McIntire, S. L., E. Jorgensen, et al. (1993). "The GABAergic nervous system of Caenorhabditis elegans [see comments]." Nature 364(6435): 337-341.
Meighan, C. M. and J. E. Schwarzbauer (2007). "Control of C. elegans hermaphrodite gonad size and shape by vab-3/Pax6-mediated regulation of integrin receptors." Genes Dev 21(13): 1615-1620.
Mello, C. C., J. M. Kramer, et al. (1991). "Efficient gene transfer in *C. elegans*: extrachromosomal maintenance and intregration of transforming sequences." EMBO J. 10(12): 3959-3970.
Miki, H., S. Suetsugu, et al. (1998). "WAVE, a novel WASP-family protein involved in actin reorganization induced by Rac." EMBO J 17(23): 6932-6941.
Miki, H. and T. Takenawa (2003). "Regulation of actin dynamics by WASP family proteins." J Biochem 134(3): 309-313.
Miller, L. D., K. C. Lee, et al. (2004). "RACK1 regulates Src-mediated Sam68 and p190RhoGAP signaling." Oncogene 23(33): 5682-5686.
Mochly-Rosen, D., H. Khaner, et al. (1991). "Identification of intracellular receptor proteins for activated protein kinase C." Proc Natl Acad Sci U S A 88(9): 3997-4000.
Neer, E. J., C. J. Schmidt, et al. (1994). "The ancient regulatory-protein family of WD-repeat proteins." Nature 371(6495): 297-300.
Nishimura, T., T. Yamaguchi, et al. (2005). "PAR-6-PAR-3 mediates Cdc42-induced Rac activation through the Rac GEFs STEF/Tiam1." Nat Cell Biol 7(3): 270-277.
Nobes, C. D., Hall, A. (1995). "Rho, rac and cdc42 GTPases regulate the assembly of multimolecular focal complexes associated with actin stress fibers, lamalliposia and filopodia." Cell 81: 53-62.
Norris, A. D., J. O. Dyer, et al. (2009). "The Arp2/3 complex, UNC-115/abLIM, and UNC-34/Enabled regulate axon guidance and growth cone filopodia formation in Caenorhabditis elegans." Neural Dev 4: 38.
Pak, C. W., K. C. Flynn, et al. (2008). "Actin-binding proteins take the reins in growth cones." Nat Rev Neurosci 9(2): 136-147.
Pan, Y., G. Liu, et al. "Abnormal expression of netrin-G2 in temporal lobe epilepsy neurons in humans and a rat model." Exp Neurol 224(2): 340-346.
Pollard, T. D. and G. G. Borisy (2003). "Cellular motility driven by assembly and disassembly of actin filaments." Cell 112(4): 453-465.
Prasad, A. A. and R. J. Pasterkamp (2009). "Axon guidance in the dopamine system." Advances in experimental medicine and biology 651: 91-100.
Quinn, C. C., D. S. Pfeil, et al. (2008). "CED-10/Rac1 mediates axon guidance by regulating the asymmetric distribution of MIG-10/lamellipodin." Curr Biol 18(11): 808-813.

Robles, E., S. Woo, et al. (2005). "Src-dependent tyrosine phosphorylation at the tips of growth cone filopodia promotes extension." J Neurosci 25(33): 7669-7681.

Ron, D., C. H. Chen, et al. (1994). "Cloning of an intracellular receptor for protein kinase C: a homolog of the beta subunit of G proteins." Proc Natl Acad Sci U S A 91(3): 839-843.

Roof, D. J., A. Hayes, et al. (1997). "Molecular characterization of abLIM, a novel actin-binding and double zinc finger protein." J Cell Biol 138(3): 575-588.

Sambrook, J., Fritsch, E.F., Maniatis, T. (1989). Molecular cloning: a laboratory manual. Cold Spring Harbor, NY, Cold Spring Harbor Laboratory Press.

Schechtman, D. and D. Mochly-Rosen (2001). "Adaptor proteins in protein kinase C-mediated signal transduction." Oncogene 20(44): 6339-6347.

Schmidt, A. and A. Hall (2002). "Guanine nucleotide exchange factors for Rho GTPases: turning on the switch." Genes Dev 16(13): 1587-1609.

Seipel, K., Q. G. Medley, et al. (1999). "Trio amino-terminal guanine nucleotide exchange factor domain expression promotes actin cytoskeleton reorganization, cell migration and anchorage-independent cell growth." J Cell Sci 112(Pt 12): 1825-1834.

Shakir, M. A., J. S. Gill, et al. (2006). "Interactions of UNC-34 Enabled with Rac GTPases and the NIK kinase MIG-15 in Caenorhabditis elegans axon pathfinding and neuronal migration." Genetics 172(2): 893-913.

Shakir, M. A., K. Jiang, et al. (2008). "The Arp2/3 Activators WAVE and WASP Have Distinct Genetic Interactions With Rac GTPases in Caenorhabditis elegans Axon Guidance." Genetics 179(4): 1957-1971.

Shekarabi, M. and T. E. Kennedy (2002). "The netrin-1 receptor DCC promotes filopodia formation and cell spreading by activating Cdc42 and Rac1." Mol Cell Neurosci 19(1): 1-17.

Sklan, E. H., E. Podoly, et al. (2006). "RACK1 has the nerve to act: structure meets function in the nervous system." Prog Neurobiol 78(2): 117-134.

Small, J. V., T. Stradal, et al. (2002). "The lamellipodium: where motility begins." Trends in cell biology 12(3): 112-120.

Sondek, J., A. Bohm, et al. (1996). "Crystal structure of a G-protein beta gamma dimer at 2.1A resolution." Nature 379(6563): 369-374.

Steven, R., T. J. Kubiseski, et al. (1998). "UNC-73 activates the Rac GTPase and is required for cell and growth cone migrations in C. elegans." Cell 92: 785-795.

Struckhoff, E. C. and E. A. Lundquist (2003). "The actin-binding protein UNC-115 is an effector of Rac signaling during axon pathfinding in C. elegans." Development 130(4): 693-704.

Suetsugu, S., H. Miki, et al. (2002). "Spatial and temporal regulation of actin polymerization for cytoskeleton formation through Arp2/3 complex

and WASP/WAVE proteins." Cell motility and the cytoskeleton 51(3): 113-122.

Sulston, J. and J. Hodgkin (1988). Methods. The Nematode *Caenorhabditis elegans*. W. B. Wood. Cold Spring Harbor, New York, Cold Spring Harbor Laboratory Press: 587-606.

Sulston, J. E. and H. R. Horvitz (1977). "Post-embryonic cell lineages of the nematode, Caenorhabditis elegans." Dev Biol 56(1): 110-156.

Svitkina, T. M. and G. G. Borisy (1999). "Arp2/3 complex and actin depolymerizing factor/cofilin in dendritic organization and treadmilling of actin filament array in lamellipodia." J Cell Biol 145(5): 1009-1026.

Svitkina, T. M., E. A. Bulanova, et al. (2003). "Mechanism of filopodia initiation by reorganization of a dendritic network." J Cell Biol 160(3): 409-421.

Symons, M. (2000). "Adhesion signaling: PAK meets Rac on solid ground." Curr Biol 10(14): R535-537.

Tabuse, Y. (2002). "Protein kinase C isotypes in C. elegans." J Biochem 132(4): 519-522.

Tannoury, H., V. Rodriguez, et al. "CACN-1/Cactin interacts genetically with MIG-2 GTPase signaling to control distal tip cell migration in C. elegans." Dev Biol.

Welch, M. D., A. Mallavarapu, et al. (1997). "Actin dynamics in vivo." Curr Opin Cell Biol 9(1): 54-61.

Welch, M. D. and R. D. Mullins (2002). "Cellular control of actin nucleation." Annu Rev Cell Dev Biol 18: 247-288.

White, J. G., E. Southgate, et al. (1986). "The structure of the nervous system of the nematode *Caenorhabditis elegans*." Philos. Trans. R. Soc. Lond. 314: 1-340.

White, J. G., E. Southgate, et al. (1986). "The structure of the ventral nerve cord of *Caenorhabditis elegans*." Philos. Trans. R. Soc. Lond. [Biol] 275(938): 327-348.

Withee, J., B. Galligan, et al. (2004). "Caenorhabditis elegans WASP and Ena/VASP Proteins Play Compensatory Roles in Morphogenesis and Neuronal Cell Migration." Genetics 167(3): 1165-1176.

Wolf, A. M., A. I. Lyuksyutova, et al. (2008). "Phosphatidylinositol-3-kinase-atypical protein kinase C signaling is required for Wnt attraction and anterior-posterior axon guidance." The Journal of neuroscience : the official journal of the Society for Neuroscience 28(13): 3456-3467.

Worthylake, D. K., K. L. Rossman, et al. (2000). "Crystal structure of Rac1 in complex with the guanine nucleotide exchange region of Tiam1." Nature 408(6813): 682-688.

Wu, Y. C., T. W. Cheng, et al. (2002). "Distinct rac activation pathways control Caenorhabditis elegans cell migration and axon outgrowth." Dev Biol 250(1): 145-155.

Yang, Y., J. Lu, et al. (2006). "SWAN-1, a Caenorhabditis elegans WD repeat protein of the AN11 family, is a negative regulator of Rac GTPase function." Genetics 174(4): 1917-1932.

Yang, Y. and E. A. Lundquist (2005). "The actin-binding protein UNC-115/abLIM controls formation of lamellipodia and filopodia and neuronal morphogenesis in Caenorhabditis elegans." Mol Cell Biol 25(12): 5158-5170.

Zallen, J. A., S. A. Kirch, et al. (1999). "Genes required for axon pathfinding and extension in the C. elegans nerve ring." Development 126(16): 3679-3692.

Zallen, J. A., B. A. Yi, et al. (1998). "The conserved immunoglobulin superfamily member SAX-3/Robo directs multiple aspects of axon guidance in C. elegans." Cell 92(2): 217-227.

Zheng, Y., D. J. Fischer, et al. (1996). "The faciogenital dysplasia gene product FGD1 functions as a Cdc42Hs-specific guanine-nucleotide exchange factor." J Biol Chem 271(52): 33169-33172.

Zhong, W. and P. W. Sternberg (2006). "Genome-wide prediction of C. elegans genetic interactions." Science 311(5766): 1481-1484.

Zhou, F. Q. and C. S. Cohan (2004). "How actin filaments and microtubules steer growth cones to their targets." J Neurobiol 58(1): 84-91.